3-1-2002

An Analysis of Mutually Dispersive Brown Symbols for Non-Linear Ambiguity Suppression

Matthew J. Papaphotis

AN ANALYSIS OF MUTUALLY DISPERSIVE BROWN SYMBOLS FOR NON-LINEAR AMBIGUITY SUPPRESSION

THESIS

Matthew J. Papaphotis, Flight Lieutenant, RAAF

AFIT/GE/ENG/02M-19

DEPARTMENT OF THE AIR FORCE

AIR UNIVERSITY

AIR FORCE INSTITUTE OF TECHNOLOGY

Wright-Patterson Air Force Base, Ohio

Report Documentation Page

Report Date 15 Mar 02	Report Type Final	Dates Covered (from... to) Jun 2001 - Mar 2002

Title and Subtitle An Analysis of Mutually Dispersive Brown Symbols for Non-Linear Ambiguity Suppression	**Contract Number**
	Grant Number
	Program Element Number
Author(s) Flight LT Matthew J. Papaphotis, RAAF	**Project Number**
	Task Number
	Work Unit Number
Performing Organization Name(s) and Address(es) Air Force Institute of Technology Graduate School of Engineering and Management (AFIT/EN) 2950 P Street, Bldg 640 WPAFB OH 45433-7765	**Performing Organization Report Number** AFIT/GE/ENG/02M-19
Sponsoring/Monitoring Agency Name(s) and Address(es) AFRL/SN Attn: Dr. William M. Brown 2241 Avionics Circle WPAFB OH 45433-7765	**Sponsor/Monitor's Acronym(s)**
	Sponsor/Monitor's Report Number(s)

Distribution/Availability Statement
Approved for public release, distribution unlimited

Supplementary Notes

Abstract
This thesis significantly advances research towards the implementation of optimal Non-linear Ambiguity Suppression (NLS) waveforms by analyzing the Brown theorem. The Brown theorem is reintroduced with the use of simplified linear algebraic notation. A methodology for Brown symbol design and digitization is provided, and the concept of dispersive gain is introduced. Numerical methods are utilized to design, synthesize, and analyze Brown symbol performance. The theoretical performance in compression and dispersion of Brown symbols is demonstrated and is shown to exhibit significant improvement compared to discrete codes. As a result of this research a process is derived for the design of optimal mutually dispersive symbols for any sized family. In other words, the limitations imposed by conjugate LFM are overcome using NLS waveforms that provide an effective -fold increase in radar unambiguous range. This research effort has taken a theorem from its infancy, validated it analytically, simplified it algebraically, tested it for relizability, and now provides a means for the synthesis and digitization of pulse coded waveforms that generate an N-fold increase in radar effetive unambiguous range. Peripherally, this effort has motivated many avenues of future research.

Subject Terms	
: Non-linear Ambiguity Suppression, Mutually Dispersive, Brown Theorem, Radar, Ambiguous Range, Digital Signal Processing, Ambiguous Doppler, Pulse Coding, Ambiguity Mitigation.	
Report Classification unclassified	**Classification of this page** unclassified
Classification of Abstract unclassified	**Limitation of Abstract** UU
Number of Pages 126	

An Analysis of Mutually Dispersive Brown

Symbols for Non-linear Ambiguity Suppression

THESIS

Presented to the Faculty

Department of Electrical and Computer Engineering

Graduate School of Engineering and Management

Air Force Institute of Technology

Air University

Air Education and Training Command

in Partial Fulfillment of the Requirements for the

Degree of Master of Science in Electrical Engineering

Matthew J. Papaphotis, BE MSc *UNSW*

Flight Lieutenant, RAAF

March, 2002
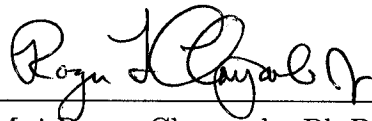
An Analysis of Mutually Dispersive Brown

Symbols for Non-linear Ambiguity Suppression

Matthew J. Papaphotis, BE MSc *UNSW*

Flight Lieutenant, RAAF

Approved:

_____   _____
Maj Roger Claypoole, Ph.D.   14 MAR 02
Thesis Advisor   Date

_____   _____
Dr Michael Temple, Ph.D.   13 Mor 02
Committee Member   Date

_____   _____
Dr Meir Pachter, Ph.D.   13 March 02
Committee Member   Date

Acknowledgements

Opportunity is missed by most people because it is dressed in overalls and looks like work.

<div align="right">Thomas A. Edison</div>

The opportunity to engage in a United States Air Force coordinated postgraduate program does not eventuate without considerable support and commitment from a large international contingent. For the joint efforts of the Royal Australian Air Force and United States Air Force in making this possible I am extremely indebted.

My sincerest thanks to my faculty advisor, Major Roger Claypoole, for providing an entertaining and highly informative approach to learning, for your counsel as an advisor, and for injecting an Australian flavour into your lectures. Dr Michael Temple, for the guidance you have given I am grateful, and Dr Meir Pachter thank you for your support. I would, also, like to thank Dr William Brown, from the Air Force Research Laboratories, for both the support and latitude provided to me in this endeavor. Finally, to all of the lecturers that facilitated my education along the way, thank you.

The knowledge I have gained from my sojourn to Dayton has not been of purely academic origin. To my fellow colleagues, and now good friends, thank you for your company and for showing me how to kick back "American Style." To the Nugget-clique, I will say to the new friends I make, with pride and fond memories of you all, "How you doin'?," you all rock! To Jay, your assistance as a translator was invaluable, thanks for helping me keep the important stuff in focus. Last, but by no means least, I would like to thank my extended family for being the keystone of all that I do.

<div align="right">Matthew J. Papaphotis</div>

Table of Contents

List of Figures

List of Tables

List of Abbreviations

AFIT/GE/ENG/02M-19

Abstract

Monostatic radars employ pulsed waveforms to achieve receiver/transmitter isolation. Pulsed waveforms, however, are intrinsically ambiguous in range and Doppler. The mitigation of these inherent ambiguities has been the focus of radar waveform designers for many decades. In 1962 Palermo used two conjugate linear frequency modulated (LFM) pulses to demonstrate a concept that reduces ambiguous energy in processed radar return signals. This approach, known as Non-linear Ambiguity Suppression (NLS), acts on the radar return for a pulse-coded waveform by compressing undesirable pulses and suppressing them using saturation thresholding. This process effectively reduces the energy contribution of undesirable pulses in the resultant radar return. In this way Palermo was able to provide a 2-fold improvement in range ambiguities, however the use of conjugate LFM pulses does not extend to larger symbol families, thus having severe limitations.

In order to overcome the limitation on symbol family size, NLS radar waveforms can comprise pseudo-random discrete codes, such as Gold codes, that exhibit strong mutual dispersion properties. However, no theorem exists that directly tackles the problem of designing optimal mutually dispersive symbols. This thesis analyzes the Brown theorem, a recent theorem devised in support of NLS. The Brown theorem utilizes a rms time duration metric to design, in the frequency domain, optimal mutually dispersive symbols for any sized pulse family. The Fourier transform of the rms time duration is considered because it neatly isolates the envelope and phase components of the NLS waveform thereby permitting the systematic design of mutually dispersive pulses. Optimality in compression is found from the solution to a constrained optimization problem, whilst mutuality in dispersion is ensured via a prudent selection of phase-rate functions.

This thesis significantly advances research towards the implementation of optimal NLS waveforms by analyzing the Brown theorem. The Brown theorem is reintroduced with the use of simplified linear algebraic notation. A methodology for Brown symbol design and digitization is provided, and the concept of dispersive gain is introduced. Numerical methods are utilized to design, synthesize, and analyze Brown symbol performance. The theoretical performance in compression and dispersion of Brown symbols is demonstrated and is shown to exhibit significant improvement compared to discrete codes. As a result of this research a process is presented for the design of optimal mutually dispersive symbols for any sized family. In other words, the limitations imposed by conjugate LFM are overcome using NLS waveforms that provide an effective N-fold increase in radar unambiguous range.

AN ANALYSIS OF MUTUALLY DISPERSIVE BROWN SYMBOLS FOR NON-LINEAR AMBIGUITY SUPPRESSION

I. Introduction

1.1 Research Motivation

The radar system is primarily employed for providing information about the presence of a target, and its associated parameters such as size, location and motion. This information is sought after in a hierarchy from *target detection* to *parameter estimation* with *waveform resolution* being the governing metric of precision [31]. Accordingly, radar waveforms are chosen based on application so that they deliver sufficient precision in resolution. With their origins in continuous wave systems, radars quickly evolved into pulsed systems before the end of World War II. Monostatic radars (collocated transmitter and receiver) utilize pulsed waveforms so that returns are received free of interference from radar transmissions. Originally extremely narrow pulses were used to achieve high resolution, however, due to hardware saturation limitations this resulted in low transmit power and was deemed ineffective. In 1960, Klauder et al. [17] introduced the linear frequency modulated (LFM), or chirp, pulse which exploited spectral content to achieve pulse compression; this marked the beginning of the era of pulse compression waveform design.

A pulsed radar transmits short pulses of electromagnetic energy at a rate known as the Pulse Repetition Frequency (PRF). This rate varies based on operational requirements but intrinsically leads to ambiguities in range (time delay) and Doppler (velocity) estimation. By changing the PRF these ambiguities may be controlled but not necessarily removed. A number of different methods exist for reducing the degree of ambiguity in radar returns. However, the previously transmitted pulse that

generated the return under consideration must be determined to entirely remove range ambiguities. The ability to identify a particular member of a set of uniquely coded pulses from all others in the set is known as *pulse discrimination*. This proves invaluable in many applications, such as pulsed-Doppler radar and wireless spread-spectrum communications [30]. Pulse compression and pulse discrimination are related through mutual dispersion. A set of symbols having crosscorrelation functions with equivalent dispersive characteristics are said to be *mutually dispersive*. If the same set of symbols exhibit good pulse compression, *i.e.*, have focused autocorrelation functions, then pulse discrimination becomes rudimentary. In the ideal case the matched output, or autocorrelation function, would be the dirac delta function (all energy concentrated at a single point). Clearly this is not realizable, therefore highly dispersive crosscorrelation functions are required to enable pulse discrimination using a filter and threshold detector.

Intent on improving unambiguous range, Palermo [28] discovered a means of combining pulse compression and pulse discrimination into one technique, known as Non-linear Suppression (NLS). NLS utilizes pulse discrimination to reduce ambiguous energy in a radar return with the added benefit of exploiting pulse compression to achieve high range resolution. Each channel of a NLS system is assigned a unique symbol; the radar return signal is passed through the channel producing an output indicating the presence of that symbol alone. Consequently, a series of suppression operators are employed in each channel to sequentially suppress the response of all undesirable symbols. These suppression operators are the kernel of NLS that exploit the pulse discrimination concept to suppress undesirable symbol responses.

Given a suitable mutually dispersive symbol set, Palermo's suppression kernel comprises three components: pre-filter, non-linearity, and post-filter. The pre-filter is matched for a particular undesirable symbol, resulting in a highly focused autocorrelation response, and dispersed crosscorrelation response for all other symbols. The pre-filtered signal then undergoes a saturating non-linearity that clips (limits) the

input above a prescribed threshold. This effectively removes a good deal of undesirable symbol energy without affecting other symbols. Finally, the suppressed signal is passed through a post-filter that inverts the pre-filter effect. Sequentially performing this NLS operation for all but the desired pulse reduces the ambiguous energy in the resultant signal. When the desired symbol is finally focused, or matched-filtered, the ambiguous energy present in the processed radar return is significantly reduced. Therefore, NLS is an interpulse coding scheme that exploits pulse discrimination to provide a means for reducing pulsed radar range ambiguities.

A fundamental prerequisite to employing NLS is having a set of mutually dispersive symbols. In [5] Brown[1] presents a theorem on optimal mutually dispersive symbols. As stated earlier, mutually dispersive symbols may be characterized by the dispersive characteristics of their correlation functions. By considering the Fourier transform of the rms time duration of the correlation functions, Brown devises a theory for the spectral design of optimal mutually dispersive symbols. In this fashion, the rms time duration neatly isolates the envelope and phase components of the correlation function thereby permitting the systematic design of mutually dispersive pulses. This formulation indicates that the optimal spectral envelope is the solution to a constrained optimization problem, and the optimal phase-rate functions are linear combinations of a weighted-orthonormal basis. The search for the optimal linear weighting of the basis functions spawns a problem, coined by Brown as the Hermit Problem. Brown states that the crosscorrelation dispersion of such symbols is independent of basis and proportional to the number of symbols, N, in the set via $2N/(N-1)$. However, the theory for the design of an optimal mutually dispersive set of symbols, known as *Brown symbols*, remains untested.

1.2 Research Goal

The goal of this research is to:

---

[1]Chief Scientist, Sensors Directorate of the Air Force Research Laboratory. Fellow of the IEEE.

1. Explain the formulation of Brown's theorem [5] whilst introducing a simplified linear algebraic notation;

2. Describe a systematic process for designing Brown symbols through an analysis of Brown's work and by theoretical extension;

3. Provide a theoretical analysis for the digitization of Brown symbols;

4. Evaluate performance of Brown symbols, comprising dispersive gain, through simulation and numerical approximation; and

5. Compare the performance of various Brown symbols with discrete codes through simulation.

1.3   Thesis Organization

Chapter II introduces background theory and presents a review of current literature. Due to the theoretical nature of this thesis, a functional analysis overview is provided defining nomenclature and metrics. Numerical approximation techniques and the role of the Discrete Fourier Transform (DFT) are discussed. The reference radar model and generic form for the radar return signal are defined. Bandpass systems and analytic notation are discussed, including consideration of optimal filtering in white noise. Pulsed waveform design is discussed in light of range and Doppler ambiguities of monostatic pulse Doppler radar, and metrics for signal characterization are defined, including rms time duration. Finally, ambiguity suppression is reviewed, consideration is given to PRF techniques, and the NLS concept is explained.

Chapter III explains Brown's theorem and introduces the symbol design methodology. A brief overview of the NLS concept is provided. The scope of the research is outlined as relating to the approach and associated synthesis constraints. The radar model is related to NLS by analytically defining, as in [5], the problem of designing a symbol set suited to NLS, and the Brown NLS system is illustrated. Brown's theorem is derived by tying together the optimal envelope, phase-rate functions, Hermit Prob-

lem solutions, dispersive gain and the theoretically optimal performance. Notation for biphase codes is defined relating the suitability of these codes to NLS. Finally, metrics used to characterize and contrast Brown symbols are discussed, providing an overview of the numerical approximation approach.

In Chapter IV, Brown symbols are devised analytically and then constructed, providing results from Matlab® simulations. The design requirements are considered for each Brown symbol components: the Hermit Problem solution, phase-rate basis function design, phase function calculation, and symbol synthesis. Results are provided demonstrating the sensitivity of Brown symbols to the choice of phase-rate basis functions and envelope; physical realizability is also discussed. Finally, the performance of Brown symbols is contrasted with that of biphase symbols suited to NLS.

Chapter V provides a summary of the significant research findings. The research goal is restated and the conclusive results summarized. The significance of this research is discussed and recommendations for future research provided.

II. Background

2.1 Introduction

This chapter introduces background theory and presents a review of current literature. Due to the theoretical nature of this thesis Section 2.2 provides a functional analysis overview, defines nomenclature and metrics, and discusses Numerical approximation techniques and the role of the Discrete Fourier Transform. Section 2.3 defines the reference radar model and generic form for the radar return signal, discusses bandpass systems and analytic notation and considers optimal filtering in white noise. Section 2.3.3 discusses pulsed waveform design in light of range and Doppler ambiguities of monostatic pulse Doppler radar, and defines signal associated metrics for characterizing radar signals. Finally, Section 2.4 reviews ambiguity suppression, considering Pulse Repetition Frequency (PRF) techniques and Non-linear Suppression (NLS).

2.2 Signal and Waveform Analysis

2.2.1 Signal Spaces. The construction and characterization of signal spaces is fundamental to this thesis. A signal is defined as "a quantity which, in some manner, conveys information about the state of a physical system [11:1]." A *signal space*, therefore, is the space in which a given signal can be considered a single point or entity. The signals considered in this thesis are associated with the radar system depicted in Figure 2.2, and are denoted as functions of either time, $x(t)$, or frequency, $X(f)$. With the constraint of physical realizability enforced, these signals are constrained to exist within the union of the sets of energy-limited and band-limited signals, that is $\{x : x \in S_E(K) \bigcup S_B(\Phi)\}$ [11:5] where,

Energy-limited signals:

$$S_E(K) = \left\{ x : \int_{-\infty}^{\infty} |x(t)|^2 dt \leq K < \infty \right\}. \tag{2.1}$$

Band-limited signals:

$$S_B(\Phi) = \left\{ x : X(f) = \int_{-\infty}^{\infty} x(t) \mathrm{e}^{-j2\pi ft} dt = 0 \text{ for all } |f| \geq \frac{\Phi}{2} \right\}. \tag{2.2}$$

The populous of physically realizable signals is considerable and therefore requires a means of characterizing the different elements for comparison. Any functional that maps elements or pairs of elements onto the real line provides a means of characterization. A measure, defined as *distance* [11:20], is used to produce a real positive number. Provided that the functional, $d : \{x, y\} \rightarrow \mathcal{R}$, exhibits the normal properties of distance then it is commonly known as a *metric*, and when combined with a set of elements results in a *metric space* [11].

Of all possible metrics, the analysis undertaken in this thesis requires only an understanding of the *Euclidean metric*, *norm*, and *inner product*. When considering vectors in N-dimensional space, or $\mathcal{R}^N$, with vectors $\mathbf{x} = [\mathrm{x}_0 \ \mathrm{x}_1 \ \ldots \ \mathrm{x}_{N-1}]^T$ and $\mathbf{y} = [\mathrm{y}_0 \ \mathrm{y}_1 \ \ldots \ \mathrm{y}_{N-1}]^T$, the *Euclidean metric* $d_2(\mathbf{x},\mathbf{y})$ is defined as [11]

$$
\begin{aligned}
d_2(\mathbf{x},\mathbf{y}) &= \|\mathbf{x} \text{ - } \mathbf{y}\| \\
&= \left[\sum_{k=0}^{N-1} |\mathrm{x}_k - \mathrm{y}_k|^2 \right]^{\frac{1}{2}}.
\end{aligned}
\tag{2.3}
$$

When considering the set of real or complex time functions, $x(t)$ and $y(t)$, defined over the interval $\{t : a \leq t < b\}$, the Euclidean metric becomes [11]

$$d_2(x, y) = \left[\int_a^b |x(t) - y(t)|^2 dt \right]^{\frac{1}{2}}. \tag{2.4}$$

The *norm* determines the "size" of a particular element in a set and therefore is a particularly useful variant of the Euclidean metric. This metric $d_2(\mathbf{x},0) = \|\mathbf{x}\|$ is defined for real or complex vectors as

$$\|\mathbf{x}\| = \left[\sum_{k=0}^{N-1} |x_k|^2 \right]^{\frac{1}{2}}, \tag{2.5}$$

and for arbitrary time functions as

$$\|x\| = \left[\int_a^b |x(t)|^2 dt \right]^{\frac{1}{2}}. \tag{2.6}$$

Any complex or real time function with finite size belongs to the set of finite energy signals, $S_E(K)$, defined in Eq (2.1). To complete the discussion of signal spaces, a metric describing the relationship between pairs of vectors is defined in the form of an *inner product*. The inner product of a pair of real or complex vectors, and arbitrary time functions is defined in Eq (2.7) and Eq (2.8), respectively:

$$(\mathbf{x},\mathbf{y}) = \sum_{k=0}^{N-1} x_k \, y_k^*, \tag{2.7}$$

$$(x, y) = \int_a^b x(t) \, y^*(t) dt. \tag{2.8}$$

In some applications it may be beneficial to emphasize a certain time, or frequency, *window* in calculating element pair relationships. The *weighted inner product* is designed to provide this utility and is described by [11]

$$(x, y)_w = \int_a^b w(t)x(t)y^*(t)dt. \tag{2.9}$$

The *norm* metric, described earlier, in conjunction with a linear space forms a *normed linear space* with $\|\mathbf{x}\| = (\mathbf{x},\mathbf{x})^{\frac{1}{2}}$. Also, describing an inner product in this way leads to the concept of *orthogonality*. The inner product between two vectors is

related to the norm squared of the vector $\mathbf{x}+\mathbf{y}$ as follows:

$$\|\mathbf{x} + \mathbf{y}\|^2 = \|\mathbf{x}\|^2 + \|\mathbf{y}\|^2 + 2\mathbf{x}^T\mathbf{y}. \tag{2.10}$$

The vector $\mathbf{x}+\mathbf{y}$ is a vector completing a triangle having sides $\mathbf{x}$ and $\mathbf{y}$. The Pythagorean Theorem states that if the square of the hypotenuse equals the sum of the square of the sides, then the sides are orthogonal. From the equality described above, this implies that if $\mathbf{x}^T\mathbf{y} = 0$, then $\mathbf{x}$ is orthogonal to $\mathbf{y}$.

Not surprisingly, a signal space may be represented by far fewer elements than are contained in the entire space. The signal space described by all *linear combina-tions* of any N elements $\mathbf{u}_k$ is called a *linear subspace*, denoted $S_N(\mathbf{x})$ and defined as [11]

$$S_N(\mathbf{x}) = \left\{ \mathbf{x} : \sum_{k=0}^{N-1} c_k\mathbf{u}_k = \mathbf{x} \right\}. \tag{2.11}$$

Any set of elements from a signal space are said to be *linearly independent* if the equality $\sum_{k=0}^{N-1} c_k\mathbf{u}_k = 0$ can only be satisfied when $c_k = 0$ for all k, *i.e.*, any $\mathbf{u}_k$ cannot be written as a linear combination of the other elements. When this is the case, $\{\mathbf{u}_k\}$ is known as a *basis* for the N-dimensional subspace $S_N(\mathbf{x})$, and $S_N(\mathbf{x})$ is said to be *spanned* by $\{\mathbf{u}_k\}$. Therefore, any N-linearly independent elements in $S_N(\mathbf{x})$ can form a basis, implying that a basis is by no means unique.

Any vector by this construction, $\mathbf{x} \in S_N(\mathbf{x})$, can be represented by a linear combination of basis elements. The weighting of the lth basis element is determined by taking the inner product of $\mathbf{x}$ with a vector that is orthogonal to all other basis elements, and that normalizes the lth basis element as detailed below.

$$c_l = (\mathbf{x}, \mathbf{v}_l) = \sum_{k=0}^{N-1} c_k(\mathbf{u}_k, \mathbf{v}_l) \tag{2.12}$$

This process is simplified greatly by choosing an orthonormal basis $\{\mathbf{q}_k\}$. That is $\{\mathbf{q}_k : (\mathbf{q}_k, \mathbf{q}_l) = \delta_{kl}\}$, where δ_{kl} is the Kronecker delta, which equals unity only when $k = l$ and zero otherwise. In other words, $\mathbf{q}_k$ has unit size and is orthogonal to all other elements in the basis. In this way, the weighting of the lth basis element is determined by simply taking the inner product of $\mathbf{x}$ with the lth basis element.

A basis may be *orthonormalized* using the Gram-Schmidt orthonormalization procedure. Given a set of N-linearly independent vectors $\{\mathbf{u}_k\}$, the orthonormal set $\{\mathbf{q}_k\}$ is calculated by normalizing the set $\{\mathbf{w}_k\}$ obtained by [18:279]:

$$
\begin{aligned}
\mathbf{w}_0 &= \mathbf{u}_0 \\
\mathbf{w}_1 &= \mathbf{u}_1 - (\mathbf{u}_1, \mathbf{q}_0)\mathbf{q}_0 \\
\mathbf{w}_2 &= \mathbf{u}_2 - (\mathbf{u}_2, \mathbf{q}_1)\mathbf{q}_1 - (\mathbf{u}_2, \mathbf{q}_0)\mathbf{q}_0 \\
&\ \ \vdots \\
\mathbf{w}_k &= \mathbf{u}_k - \sum_{l=0}^{k-1}(\mathbf{u}_k, \mathbf{q}_l)\mathbf{q}_l
\end{aligned}
\tag{2.13}
$$

where

$$
\mathbf{q}_k = \frac{\mathbf{w}_k}{\|\mathbf{w}_k\|}
\tag{2.14}
$$

2.2.2 Integral Transforms. Section 2.2.1 discussed signal spaces and metrics that are commonly used to characterize signals that exist as elements within them. This section explores the relationship of these concepts to Integral transforms.

As discussed in section 2.2.1, linear subspaces may be described by a linear combination of a set of basis elements as illustrated in Eq (2.11). The study of continuous time functions, in $S_E(K)$, can be considered analogous by viewing an N-dimensional vector as a discrete approximation to a continuous time function whose approximation error decreases as the sampling interval approaches zero. In this way

Eq (2.11) can be redefined for continuous signals by the functional

$$x(t) = \int_\Xi c(\xi)\varphi(t,\xi)d\xi, \tag{2.15}$$

where Ξ is the range of ξ. Note that $c(\xi)$ is analogous to c_k in Eq (2.11) and that $\varphi(t,\xi)$, called the *basis kernel*, is the time continuous basis function parameterized by ξ. In order to complete this analogy $c(\xi)$ is described as

$$c(\xi) = \int_T x(t)\vartheta(\xi,t)dt, \tag{2.16}$$

where T is the range of t. This equation is the inner product of $x(t)$ with $\vartheta(\xi,t)$, known as the *reciprocal basis kernel*. For linear subspaces this is the set of basis elements that enables the recovery of the original basis weighting due to the imposed orthogonality relationship.

When a complex sinusoid is used as the basis kernel the well known Fourier transform with the Fourier transform pair is described here:

$$\mathcal{F}\{x(t)\} : X(f) \triangleq \int_{-\infty}^{\infty} x(t)e^{-j2\pi ft}dt, \tag{2.17}$$

$$\mathcal{F}^{-1}\{X(f)\} : x(t) \triangleq \int_{-\infty}^{\infty} X(f)e^{j2\pi ft}df. \tag{2.18}$$

The frequency content in a continuous time function is divined from this transform.

There are, however, properties of the Fourier transform that should be discussed in order to relate this concept to an analysis of a radar system. For $x(t)$ a real-valued function, the complex conjugate of Eq (2.17) shows that $X^*(f) = X(-f)$. This is significant as it illustrates a symmetry in the frequency content of real time functions, and therefore a redundancy. That is, only one-half of the spectrum is required to define a real-valued signal. Consequently, an analysis of real signals is simplified by representing them with a one-sided spectral signal, or *analytic signal.*

One approach is to define a complex valued signal, $\psi(t) \in \mathcal{C}$, that has a one-sided spectrum equivalent to that of the real-valued signal, $\Psi(f) = X(f)$ for $f \geq 0$, and whose real part is equal to the signal, $\Re\{\psi(t)\} = x(t)$. For example:

$$\psi(t) = x(t) + \jmath\hat{x}(t) \tag{2.19}$$

$$\Psi(f) = X(f) + \jmath\hat{X}(f). \tag{2.20}$$

$\Psi(f)$ is to be one-sided, and has arbitrarily been assumed non-negative for positive frequencies. Therefore, the spectrum of the imaginary part of the analytic signal, $\hat{X}(f)$, must cancel the spectrum of $X(f)$ for negative frequencies and as such is defined as

$$\hat{X}(f) = \left\{ \begin{array}{ll} -jX(f) & f \geq 0 \\ jX(f) & f < 0 \end{array} \right\} = -jX(f)\,\mathrm{sgn}(f), \tag{2.21}$$

where $\mathrm{sgn}(f)$ is 1 for $f \geq 0$ and -1 for $f < 0$. Therefore, from Eq (2.20) and Eq (2.21) the spectral density of the analytic signal becomes one-sided and is of the form

$$\Psi(f) = \left\{ \begin{array}{ll} 2X(f) & f \geq 0 \\ 0 & f < 0 \end{array} \right. \tag{2.22}$$

The time function, $\hat{x}(t)$, can be determined by taking the inverse Fourier transform of $\hat{X}(f)$ defined in Eq (2.21). For $\mathcal{F}^{-1}\{-\jmath\,\mathrm{sgn}(f)\} = 1/\pi t$, by the convolution property of the Fourier transform, $\hat{x}(t)$ is given by

$$\mathcal{H}\{x(t)\} : \hat{x}(t) \overset{\triangle}{=} x(t) \star \frac{1}{\pi t}$$
$$= \frac{1}{\pi} \int_{-\infty}^{\infty} \frac{x(s)}{t - s} \, ds. \tag{2.23}$$

Eq (2.23) introduces the *Hilbert transform* definition, another integral transform as defined in Eq (2.15). In this case, however, $1/(t - s)$ is the basis kernel and exhibits

2-7

a singularity at $s = t$, therefore, define

$$\int_{-\infty}^{\infty} \Rightarrow \lim_{\varepsilon \to 0^+} \left(\int_{-\infty}^{t-\varepsilon} + \int_{t-\varepsilon}^{\infty} \right).$$

2.2.3 Discrete Signal Approximations. Although much of the later discussions in this thesis are related to an optimization approach regarding continuous time signals, a physical implementation is likely to require some manner of digitization. Therefore, this section provides the digital signal processing background necessary to facilitate this transition and to introduce some numerical approximation fundamentals.

The use of a complex exponential as a basis kernel, as seen in the Fourier transform introduced in Section 2.2.2, is commonly considered for various forms of discrete signals. Signals are typically taken to be either continuous or sampled approximations, therefore an appropriate revision of the Fourier transform is required. The transform pair for continuous signals in time and frequency is described in Eq (2.17); signals that are continuous and periodic in time may be represented by a Fourier series [25], *i.e.*, having discrete or sampled frequency spectra. The duality of frequency and time signals, as related via the Fourier transform, ensures the spectra of a time sampled signal is continuous and periodic; being related via the Discrete-Time Fourier Transform (DTFT) [25]. The majority of digital systems that exploit the spectral content of a signal, however, sample the signal and then by processing it appropriately generate a frequency representation that is also discrete. This transform is called the Discrete Fourier Transform (DFT) and is defined in Eq (2.24) and Eq (2.25). Recall that x_k denotes the kth element of the vector $\mathbf{x}$ [25].

$$X_k = \sum_{l=0}^{N_s-1} x_l \, e^{-j2\pi kl/N_s} \tag{2.24}$$

$$x_l = \frac{1}{N_s} \sum_{k=0}^{N_s-1} X_k \, e^{j2\pi lk/N_s}, \tag{2.25}$$

where N_s is the total number of samples. In this case, however, the elements of $\mathbf{x}$ are samples of the continuous time function $x(t)$ taken at a sampling interval t_0, as such $\mathrm{x}_k = t_0\, x(kt_0)$. The Shannon Sampling Theorem describes the circumstances in which $\mathbf{x}$ completely represents $x(t)$. Sampling a continuous time signal, at t_0, results in a periodic frequency spectrum. The DTFT of the sampled signal is [25]

$$\sum_{k=-\infty}^{\infty} t_0\, x(kt_0)\mathrm{e}^{-j2\pi fkt_0} = \sum_{k=-\infty}^{\infty} X(f + k\Phi_0). \tag{2.26}$$

Therefore, by sampling at an interval t_0 the spectrum of the signal becomes periodic at $\Phi_0 = 1/t_0$. Effective reconstruction of the original signal is attained if the spectral copies created by sampling are removed. Therefore, two things are required to be able to reconstruct $x(t)$, firstly the spectral copies must not interfere with each other, and secondly each of the copies for $k \neq 0$ must be removed. The first of these is achieved by ensuring that $x(t)$ is band-limited, that is $x(t) \in S_B(2f_{max})$, and t_0 must be chosen such that $\Phi_0 = 1/t_0 \geq 2f_{max}$, *i.e.*, to avoid aliasing the Nyquist rate must be achieved [25:129]. Secondly, removal of the spectral copies of the sampled signal is accomplished by passing only those frequencies $|f| \leq f_{max} \leq \Phi_0/2$. When $\Phi_0 = 2f_{max}$ an ideal low-pass filter is required, defined in Eq (2.27), with impulse response $h(t)$ described as

$$\begin{aligned}
H(f) &= \mathrm{rect}(f/\Phi_0) & (2.27)\\
h(t) &= \int_{-\frac{\Phi_0}{2}}^{\frac{\Phi_0}{2}} \mathrm{e}^{j2\pi ft} df \\
&= \frac{1}{t_0}\mathrm{sinc}(\Phi_0 t), & (2.28)
\end{aligned}$$

where

$$\mathrm{rect}(\xi) = \begin{cases} 1 & \xi \leq 1/2 \\ 0 & \text{else} \end{cases}, \tag{2.29}$$

and

$$\text{sinc}(\xi) \;\; = \;\; \frac{\sin(\pi\xi)}{\pi\xi}. \tag{2.30}$$

Therefore reconstruction of $x(t)$ is possible via the convolution of the sampled signal with the impulse response function $h(t)$:

$$
\begin{aligned}
x(t) \;\; &= \;\; t_0\, x(kt_0) \star h(t) \\
&= \;\; \sum_{k=-\infty}^{\infty} t_0 x(kt_0)\, h(t - kt_0) \\
&= \;\; \sum_{k=-\infty}^{\infty} x(kt_0)\, \text{sinc}(\Phi_0[t - kt_0]).
\end{aligned} \tag{2.31}
$$

In reality, $h(t)$ is not a time-limited signal, therefore this type of reconstruction is not realizable. In practice t_0 is chosen so that $\Phi_0 \gg 2f_{max}$ enabling the use of cheap filters with smooth pass-band characteristics, $i.e.$, $\tilde{H}(f) \approx \text{rect}(f/2f_{max})$.

The transition to sampled signals from continuous time is therefore permissable provided the Nyquist sample rate is achieved. In numerically approximating the Fourier Transform of a sampled signal, however, further constraints are encountered. Beginning by defining the *rectangle-rule* approximation to the Fourier transform consider signals sampled in both time, sample interval t_0, and frequency, sample interval f_0.

$$
\begin{aligned}
x(t) \;\; &= \;\; \int_{-\infty}^{\infty} X(f)\mathrm{e}^{j2\pi ft} df \\
&\approx \;\; \sum_{l=0}^{N_s-1} X(lf_0)\, \mathrm{e}^{j2\pi lf_0 t} f_0 \;\; \stackrel{\triangle}{=} \;\; \tilde{x}(t)
\end{aligned} \tag{2.32}
$$

This approximation leads to the mapping of discrete-frequency signals to discrete-time signals. Having N_s samples in frequency leads to a transform that calculates the corresponding N_s-sample time signal, $t_0\, \tilde{x}(kt_0)$. From Eq (2.26) $\Phi_0\, t_0 = 1$, and

since there are N_s samples in frequency at f_0, $\Phi_0 = N_s f_0 \Rightarrow t_0 f_0 = 1/N_s$. The sampled time signal is therefore represented by

$$
\begin{aligned}
t_0 \, \tilde{x}(kt_0) &= t_0 \sum_{l=0}^{N_s-1} X(lf_0) \, e^{j2\pi lk/N_s} f_0 \\
&= \frac{1}{N_s} \sum_{l=0}^{N_s-1} X(lf_0) \, e^{j2\pi lk/N_s},
\end{aligned}
\tag{2.33}
$$

which is the DFT as defined in Eq (2.24). The choice of N_s and the associated sample intervals defines the resolution of the transform and extent of aliasing. As shown earlier, to prevent aliasing $1/t_0 \geq 2f_{max}$. The sample interval and rate, t_0 and f_0, are related via $t_0 f_0 = 1/N_s$. Since t_0 must be chosen to prevent aliasing, the spectral sample interval, f_0, can only be shortened by increasing the number of samples N_s, a technique known as zero padding.

2.3   Pulse Doppler Radar Fundamentals

2.3.1   Radar and Communications Model.   This section defines the radar model that is assumed in this thesis. In defining the model composition an arbitrary radar signal is considered and the environmental range map that it generates is analyzed. Radar and communications systems are constrained to transmit real signals. However, the transmission of complex waveforms may be considered possible through quadrature receiver design [6]. An arbitrary signal $x_m(t) = a(t) \cos[2\pi f_c t + \phi(t)]$, has envelope $a(t)$, phase modulation $\phi(t)$ and is modulated with carrier frequency f_c Hz. When this signal is processed, as illustrated in Figure 2.1, via mixing with an in-phase signal $2\cos(2\pi f_c t)$ then low-pass filtered the signal $a(t)\cos[\phi(t)]$ is obtained. Likewise, when the signal is quadrature mixed with $-2\sin(2\pi f_c t)$, then filtered, the result is $a(t)\sin[\phi(t)]$.

The output, or low-pass signal corresponding to $x_m(t)$, may now be described in terms of an ordered pair $\{a(t)\cos[\phi(t)], a(t)\sin[\phi(t)]\}$, and represented in complex
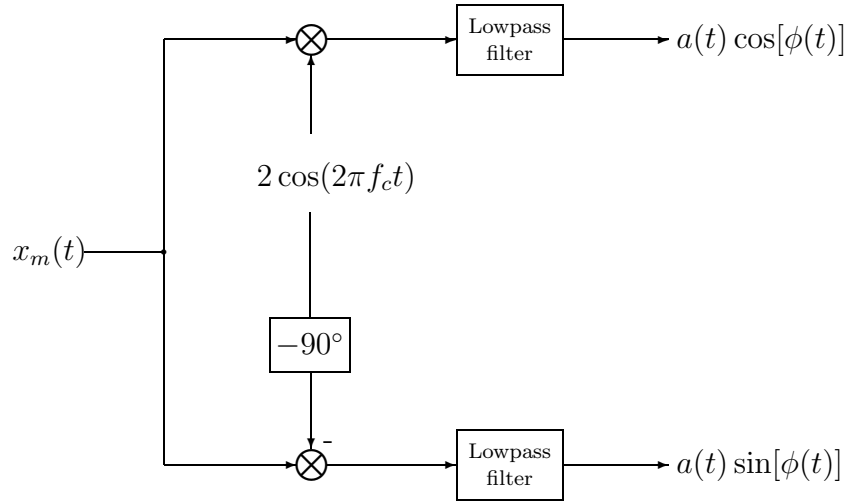
Figure 2.1. In-phase and Quadrature signal processing. The component labelled $-90°$ effects a phase shift on the passed signal.

notation as shown in Eq (2.34) [6]:

$$
\begin{aligned}
x(t) &= \mathrm{LPF}[x_m(t)2\cos(2\pi f_c t)] + \jmath\,\mathrm{LPF}[-x_m(t)2\sin(2\pi f_c t)] \\
&= a(t)\cos[\phi(t)] + \jmath\,a(t)\sin[\phi(t)] \\
&= a(t)\mathrm{e}^{\jmath\,\phi(t)}.
\end{aligned}
\tag{2.34}
$$

Accordingly, this notation is employed to represent the signal's, $x_m(t)$, low-pass in-phase and quadrature (IQ) components, denoted the *complex low-pass video signal* [6:131]. This means of modulation is a form of quadrature multiplexing and is known to suffer performance degradation from a loss of phase lock. The degradation occurs in the form of undesirable cross-talk in the output IQ channels. Radar systems that employ complex low-pass video signals, therefore require coherent receiver and transmitter coupling. Assuming that the reference radar system is capable of coherent processing and immobile, a single sweep of the range channel is analyzed.

The electromagnetic energy returned to a radar at any given time is determined by the spectral reflectivity of a spherical range shell about the emitting radar

2-12

antenna [6:136]. The reflectivity of the environment is modelled with a function, $u(s)$, representing the *radial reflectivity density* defined by

$$u(s) = u_0(s)e^{\jmath\varphi(s)}. \tag{2.35}$$

Subsequently, the incremental radar return in the range channel due to signal $x_m(t)$, illuminating a shell at range s and thickness ds, is represented by:

$$u_0(s)ds\, a\left(t - \frac{2s}{c}\right)\cos\left[2\pi f_c\left(t - \frac{2s}{c}\right) + \phi\left(t - \frac{2s}{c}\right) + \varphi(s)\right], \tag{2.36}$$

where c is the speed of light, and $2s/c$ represents the round-trip time delay between transmission and reception of $x_m(t)$ from a reflector at range s. The coherent superposition of these returns describes the radar return in the range channel, calculated here as [6]:

$$r_m(t) = \int_{-\infty}^{\infty} u_0(s)\, a\left(t - \frac{2s}{c}\right)\cos\left[2\pi f_c\left(t - \frac{2s}{c}\right) + \phi\left(t - \frac{2s}{c}\right) + \varphi(s)\right]ds. \tag{2.37}$$

The previous analysis of IQ demodulation of $x_m(t)$ lead to the compact complex low-pass video notation $x(t)$. Therefore, when $r_m(t)$ is coherently IQ demodulated Eq (2.37) becomes

$$r(t) = \int_{-\infty}^{\infty} u(s)\, a\left(t - \frac{2s}{c}\right) e^{\jmath\left[2\pi f_c \frac{2s}{c} + \phi\left(t - \frac{2s}{c}\right)\right]}ds. \tag{2.38}$$

With a simple change of variables, the delay term is redefined as $2s/c = \tau$ and the form of a convolution becomes more readily apparent. Finally, Eq (2.38) becomes

$$
\begin{aligned}
r(t) &= \int_{-\infty}^{\infty} \underbrace{u\left(\frac{c\tau}{2}\right) e^{\jmath\frac{4\pi}{\lambda}\frac{c\tau}{2}}}_{u_m(t)} \quad \underbrace{a(t-\tau)\, e^{\jmath\phi(t-\tau)}\frac{c}{2}}_{x(t)}\, d\tau \\
&= \qquad\qquad u_m(t) \quad \star \qquad x(t).
\end{aligned}
\tag{2.39}
$$

The radar range channel can therefore be represented by the convolution of the modulated radial reflectivity density with the complex low-pass video of the transmitted signal. This model is illustrated in Figure 2.2. To more accurately capture the effects of environmental interference the range cell is combined with additive noise. The final component of the model is the receiver filter.
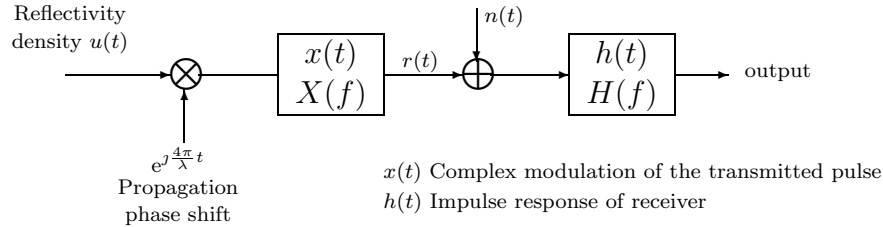
Figure 2.2.   Radar model [6:138] relating spectral reflectivity density $u(s)$, the complex modulation of the transmitted pulse $x(t)$ and radar return.

Note that the true reflectivity density is effected by the radar waveform selection, modulation frequency, and the receiver filter design. These aspects of the model are discussed in the following section.

2.3.2   Bandpass Signals and Systems.   This section revisits some of the characteristics of bandpass signals and systems that are key to the development of this thesis. Due to platform size limitations and antenna gain characteristics[1] radar signals are typically modulated at high frequencies. Also, due to power constraints and spectrum utilization these signals are bandlimited. Subsequently, the transmitted radar signal is described as *narrowband*, meaning the carrier frequency is much greater than the signal bandwidth, *i.e.*, $\{x(t) : x(t) \in S_B(\Phi)\}$, with $f_0 \gg \Phi$. Primarily, this permits two things that are discussed in this section: firstly, the simplified use of analytic notation, and secondly optimization of receiver filter design to eliminate noise.

---

[1]For example, the gain of a parabolic antenna is inversely proportional to the square of the wavelength of the transmitted signal, recall $G \approx \frac{4\pi A_e}{\lambda^2}$ [35].

The analytic representation of a signal $\psi(t) = x(t) + \jmath \hat{x}(t)$, from Eq (2.19), describes a signal having only a positive-sided spectrum and real component $x(t)$, however the calculation of the Hilbert transform can generate unwieldy functions. Notably, if $x(t)$ is modulated with a complex carrier, its entire spectrum is shifted from baseband to f_c, so

$$
\begin{aligned}
x_a(t) &= x(t)e^{\jmath 2\pi f_c t} \\
&= a(t)\cos[2\pi f_c t + \phi(t)] + \jmath \sin[2\pi f_c t + \phi(t)].
\end{aligned}
\tag{2.40}
$$

If the shifted spectrum has only positive frequency content then it approximately meets the criteria for the analytic form for $x_m(t)$. For this to be analytic in the strict sense, however, the imaginary part of $x_a(t)$ must be the Hilbert transform of its real part. A detailed analysis of the Hilbert transform of $x_m(t)$ shows that provided $\Re\{x(t)\} = a(t)\cos[\phi(t)]$ and $\Im\{x(t)\} = a(t)\sin[\phi(t)]$ are bandlimited below f_c, then $x_a(t)$, from Eq (2.40), is the correct analytic signal representation of $x_m(t)$ [4].

Figure 2.3 shows the effect of modulating a signal on a complex carrier. Figure 2.3(b) illustrates the spectrum modulated insufficiently, subsequently containing negative frequencies and therefore failing as an analytic approximation. In Figure 2.3(c) the modulation frequency is chosen such that it is greater than the half-bandwidth of the signal. Radar signals are typically considered narrowband, and are therefore able to utilize Eq (2.40) as a valid analytic representation of $x_m(t)$.

The receiver design for narrowband signals is next discussed by considering the detection of a single target in stationary white Gaussian noise. Although optimality in this scenario depends on noise parameters and costs associated with detection threshold selection, the following investigation considers receiver optimization in terms of maximizing only the Signal-to-Noise Ratio ($\mathcal{SNR}$). Figure 2.2 provides the model in this case, by considering a signal in additive noise $y = r + n$. The system output, therefore, is $z = y \star h = r \star h + n \star h$. The $\mathcal{SNR}$ under consideration is
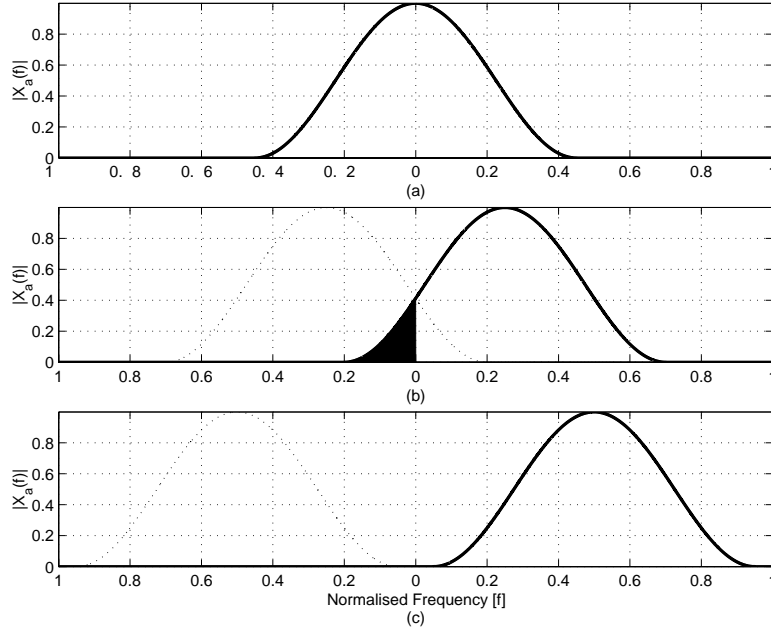
Figure 2.3.   Spectral modulation of a bandlimited signal. A bandlimited signal, (a), can be represented using analytic signal notion provided its modulated spectrum, (b), exists in only one hemisphere, (c).

defined as the ratio of peak signal power to average noise power:

$$\mathcal{SNR} \;=\; \frac{|\int_{-\infty}^{\infty} R(f)H(f)e^{j2\pi f\tau}df|^2}{\int_{-\infty}^{\infty} S_n(f)|H(f)|^2 df}, \tag{2.41}$$

where $S_n(f)$ is the power spectral density of $n(t)$. By the Schwartz inequality the numerator can be bounded as

$$\left|\int_{-\infty}^{\infty} R(f)H(f)e^{j2\pi f\tau}df\right|^2 \;\leq\; \int_{-\infty}^{\infty}|R(f)|^2df \int_{-\infty}^{\infty}|H(f)e^{j2\pi f\tau}|^2df$$

$$=\; \int_{-\infty}^{\infty}|R(f)|^2df \int_{-\infty}^{\infty}|H(f)|^2df, \tag{2.42}$$

assuming $n(t)$ is white Gaussian noise with power spectral density $S_n(f) = \eta/2$. Combining this with Eq (2.41) and Eq (2.42) the $\mathcal{SNR}$ becomes

$$
\begin{aligned}
\mathcal{SNR} &\leq \frac{2 \int_{-\infty}^{\infty} |R(f)|^2 df \int_{-\infty}^{\infty} |H(f)|^2 df}{\eta \int_{-\infty}^{\infty} |H(f)|^2 df} \\
&= \frac{2}{\eta} \int_{-\infty}^{\infty} |R(f)|^2 df \\
&= \frac{2\mathcal{E}}{\eta}.
\end{aligned}
\tag{2.43}
$$

Equality holds in Eq (2.43), if $H(f) = kR^*(f)e^{-j2\pi f\tau}$. Therefore the optimal filter in white Gaussian noise is the matched filter, so named because the spectrum of the receiver is matched to that of the noise free signal. Consequently, the impulse response function of $H(f)$ is $h(t) = kr^*(\tau - t)$, a time delayed and flipped conjugate of the noise free signal.

A single point-target at range R and with radial velocity v_r has a two-fold effect on the returned constant carrier, f_c, pulse. The range of the target contributes to a round trip delay of $\tau = 2R/c$, and the radial velocity results in a Doppler shift, $\nu = 2v_r f_c/c$. The output of the matched filter can then be approximated for a single-target response as a function of Doppler and delay, as detailed in Eq (2.44):

$$
\begin{aligned}
\chi(\tau, \nu) &= \int_{-\infty}^{\infty} x(t)x^*(t - \tau)e^{j2\pi\nu t} dt \\
&= \int_{-\infty}^{\infty} X^*(f)X(f - \nu)e^{j2\pi f\tau} df.
\end{aligned}
\tag{2.44}
$$

This function was formulated by Ville [40] and introduced to radar by Woodward [41] and is commonly known as the *Ambiguity Function* [31]. Though modelling a moving target as a spectral shift is over simplified, this function serves as a good estimate in describing the ambiguities that exist for a given transmitted waveform. When normalized, this surface provides a quasi-joint density for describing the probability of a target's range and velocity. Appendix A provides ambiguity surfaces for a

single pulse at Appendix A.1.1, a pulse train at Appendix A.1.2 and a LFM pulse at Appendix A.1.3.

2.3.3 Radar Waveform Design. The previous sections describes the signal characteristics and radar model, as shown in Figure 2.2. This naturally leads to the topic of signal design. The constraints limiting the antenna size also restrict the number of antennae. Typically, a single antenna is used in the majority of airborne platforms, which logically constrains the analysis to monostatic systems, *i.e.*, collocated transmitter and receiver. Such systems must use pulsed waveforms to provide a listening interval to detect radar returns. This section explores desirable properties of radar waveforms and the design trade-offs associated with inherent ambiguities and resolution.

2.3.3.1 Pulse Doppler Radar Ambiguities. A radar is primarily employed for determining information about target presence, and associated parameters such as size, location and motion. This information is delivered in a hierarchy from *target detection* to *parameter estimation* with the governing metric of precision a function of *resolution* [31]. To improve a radar's performance in target detection, the $\mathcal{SNR}$ is maximized using a matched filter as described in Section 2.3.2. For parameter estimation, a target's range and velocity is considered via analyzing the matched filter output.

By dividing the radar range channel into *bins*, an estimate of range is given by detecting the presence of a pulse return in a given bin. If a pulse $x(t) = \text{rect}(t/\tau)$, as shown in Figure 2.4(a), were to be transmitted then the matched filter output would be a triangular pulse with width 2τ as shown in Figure 2.4(b). Using the half-power point as a measure of pulse width, the range bins become τ wide and provide a range resolution of $c\tau$. Target velocity, on the other hand, is determined as the range rate and can be calculated from the Doppler shift of the return signal [35]. The original spectrum of the pulse is a sinc($\cdot$) waveform, but the spectrum of the matched filter
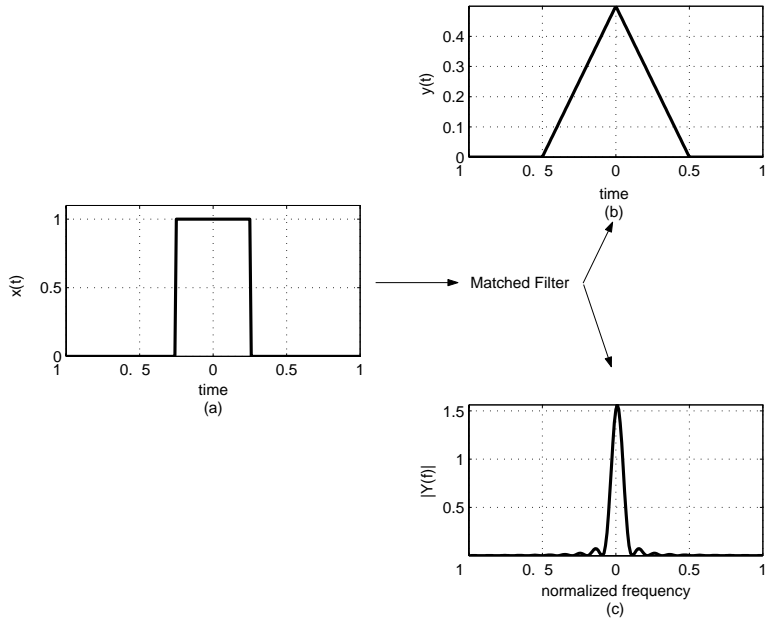
Figure 2.4.   Matched filter output of (a) in time, (b), and frequency, (c). The matched filtering of a rect-pulse results in a decrease in time resolution but an increase in the frequency resolution.

output is a $\text{sinc}^2(\cdot)$ waveform, as shown in Figure 2.4(c). Consequently, the matched filter output is narrower in frequency than the original signal providing better frequency resolution, illustrating a clear relationship between detection, estimation and resolution.

However, pulses are transmitted periodically, therefore the transmitted signal is described in Eq (2.45), where T is the Pulse Repetition Interval (PRI) and τ is the pulse width:

$$x(t) = \sum_{n=-\infty}^{\infty} \text{rect}\left(\frac{t - nT}{\tau}\right).$$

(2.45)

This leads to two significant observations. Firstly, if the radar power is such that the maximum detection range is greater than $cT/2$, then the range returns are ambiguous. Figure 2.5 illustrates this showing that if two targets, at ranges $R1$ and $R2$, are being illuminated by a pulsed radar then the returns from targets in the ambiguous range region, $R \geq R_u = cT/2$, fold-over and generate misleading range indications.

Secondly, the periodicity of the signal results in a sampling of the signal spectra[2]. The spectrum of a T-periodic pulse train is simply that of a single pulse sampled at an interval $1/T$. Therefore, if a pulse train is processed over what is termed a Coherent Processing Interval (CPI), then a comb-like spectra is generated resulting in better Doppler resolution. However, because the spectra is evenly spaced at $1/T$, ambiguities in the measurement of spectral shifts, or Doppler, are introduced. The unambiguous radial velocity of a target is $|v| \leq |v_u| = \lambda/4T$. Therefore, unambiguous radar operation requires $R|v| < c\lambda/8$.
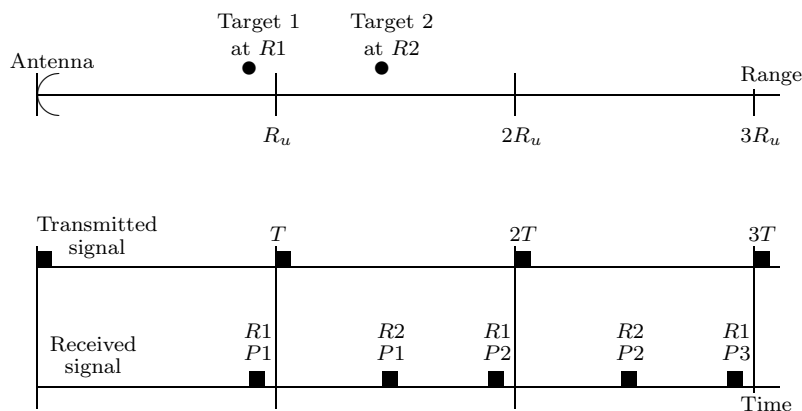
Figure 2.5.   Ambiguous pulsed radar returns [1:1-3]. The target at $R2$ is located in the ambiguous range interval, subsequently the first pulse, $P1$, is processed in the second CPI as a return from pulse $P2$.

Obviously, a better estimate of target parameters is attained with the removal of all types of ambiguities, and increased resolution in both time and frequency. Notably, by increasing the PRI, the unambiguous range is increased. However, the increase in PRI conversely decreases unambiguous velocity. Clearly, simultaneous removal of ambiguities in both range and Doppler cannot be achieved by solely altering the PRI. A technique, know as Non-linear Ambiguity Suppression (NLS), solves this problem to a considerable extent and will be discussed in Section 2.4.

---

[2]Recall from a Fourier series analysis that if a signal is T periodic then it can be represented by $x_T(t) = \sum_{k=-\infty}^{\infty} X_n e^{j2\pi n f_0 t}$, where $f_0 = 1/T$ and $X_n = f_0 X(n f_0)$. Therefore, the spectrum of $x_T(t)$ becomes $\mathcal{F}\{x_T(t)\} = \sum_{k=-\infty}^{\infty} f_0 X(n f_0)\delta(f - n f_0)$ [39].

2.3.3.2 Pulse Compression.   Previously, the resolution of the radar pulse was arbitrarily defined as the half-power region of a signal; a more rigorous analysis of resolution is now presented. A metric is required that operates on a signal and provides a real number describing the resolution of that signal, $\sigma : \{x\} \rightarrow \mathcal{R}$. Three such metrics are: total duration (σ_T), equivalent rectangle (σ_E), and root mean squared (rms) signal duration (σ). **Total duration** is defined in time and frequency respectively as:

$$\sigma_T = \left[\frac{\int_{-\infty}^{\infty} |x(t)|^2 dt}{|\int_{-\infty}^{\infty} x(t) dt|^2} \right]^{\frac{1}{2}}$$

$$\Sigma_T = \left[\frac{\int_{-\infty}^{\infty} |X(f)|^2 df}{|\int_{-\infty}^{\infty} X(f) df|^2} \right]^{\frac{1}{2}}.$$

(2.46)

The **equivalent rectangle** metric aims to describe the width required to define a rect($\cdot$) pulse of equivalent height to the signal at its center such that the rect($\cdot$) contains the same amount of energy as the signal. This is defined in time and frequency respectively as:

$$\sigma_E = \left[\frac{\int_{-\infty}^{\infty} |x(t)|^2 dt}{|x(t_c)|^2} \right]^{\frac{1}{2}}$$

$$\Sigma_E = \left[\frac{\int_{-\infty}^{\infty} |X(f)|^2 df}{|X(f_c)|^2} \right]^{\frac{1}{2}}.$$

(2.47)

Finally the **rms signal duration** is defined. The moments of statistical densities provide information about spread and location and are therefore used to characterize random variables. Analogously, these moments are often used to characterize signal precision and resolution performance [31]. The first moments are used to describe a

signal's center of mass and are defined in time and frequency respectively as:

$$t_c = \frac{\int_{-\infty}^{\infty} t|x(t)|^2 dt}{\int_{-\infty}^{\infty} |x(t)|^2 dt}$$

$$f_c = \frac{\int_{-\infty}^{\infty} f|X(f)|^2 df}{\int_{-\infty}^{\infty} |X(f)|^2 df}.$$

(2.48)

The centered second moment, denoted here as rms signal duration, is a measure of spread and is defined in time and frequency respectively in Eq (2.49). These metrics are used most predominantly throughout this thesis.

$$\sigma = \left[\frac{\int_{-\infty}^{\infty} (t - t_c)^2 |x(t)|^2 dt}{\int_{-\infty}^{\infty} |x(t)|^2 dt}\right]^{\frac{1}{2}}$$

$$\Sigma = \left[\frac{\int_{-\infty}^{\infty} (f - f_c)^2 |X(f)|^2 df}{\int_{-\infty}^{\infty} |X(f)|^2 df}\right]^{\frac{1}{2}}$$

(2.49)

By invoking Schwartz inequality on the product of the time and frequency rms signal durations of Eq (2.49), a time-bandwidth product is derived and bounded by Gabor [12] so that

$$\sigma\Sigma \geq 1,$$

(2.50)

where equality is achieved when $x(t) = -\mathrm{e}^{-\mu t^2/2}$ [31:55]. As an initial observation, this indicates that by increasing signal bandwidth the rms time duration reduces and therefore range resolution improves proportionately, with a LFM pulse providing the best performance.

This indicates that the range resolution of a signal is, at the very least, inversely proportional to its bandwidth, providing an upper bound. By exploiting this property and making the time-bandwidth product as large as the system can sustain, the greatest resolution for a given bandwidth is achieved. For uniform pulsed signals, a popular means of doing this is through LFM. Such pulses are generated by either

directly modulating a constant frequency signal with a variable-frequency oscillator, or passing a constant frequency signal through a dispersive filter [17]. These signals are known as either LFM or quadratic phase signals having the form described in Eq (2.51):

$$x_{\text{LFM}}(t) = \text{rect}\left(\frac{t}{\tau}\right) e^{j\pi\mu t^2}, \text{ where } \mu = \Phi/\tau. \tag{2.51}$$

The matched filter output of this signal is

$$z_{\text{LFM}}(t) = \text{rect}\left(\frac{t}{2\tau}\right) \frac{\sin \pi[\mu t\tau - \mu t^2]}{\pi\mu t}, \tag{2.52}$$

characterized by quadratic phase and with its maximum at $t = 0$.

An understanding of how bandwidth affects the resolution of this function is obtained by considering the null-null width, $\tilde{\sigma}$, of the mainlobe:

$$\tilde{\sigma} = \frac{\sqrt{\mu\tau^2 + 4} - \sqrt{\mu\tau^2 - 4}}{2\sqrt{\mu}}. \tag{2.53}$$

When the pulse width τ is fixed, the bandwidth Φ increases linearly with μ. Therefore as μ is increased, and thus the bandwidth of the signal increased, the numerator approaches zero, $i.e.$, $\sqrt{\mu\tau^2 + 4} \approx \sqrt{\mu\tau^2 - 4}$, and the denominator increases, causing $\tilde{\sigma}$ to become very small. LFM is a means of improving the resolution of a matched filter output by increasing the spectral content and bandwidth of a fixed duration single pulse.

In general, a waveform that has a time-bandwidth product much greater than unity is said to exhibit properties of pulse compression [31]. There are many waveforms that have been designed, aside from LFM, exhibiting these properties such as Barker codes [35], polyphase codes [21] [22], Costas codes [8], and maximal length pseudo-random noise sequences [23], such as Gold codes [7].

2.4   Ambiguity Suppression

The ambiguities detailed in Section 2.3.3.1 are inherent for any pulsed radar system. This section discusses approaches to mitigate these ambiguities, discussing a multiple PRF approach and a pulse discrimination process known as Non-linear Ambiguity Suppression (NLS) [28].

2.4.1   Pulse Repetition Frequency Approaches.   Ambiguities can be mitigated to some extent through the choice of the PRI, however, as this section shows, these tend to be application specific leading to a search for other alternatives. Section 2.3.3.1 discusses the origins of range and velocity ambiguities illustrating that the selection of the PRI T jointly effects velocity ambiguity and range ambiguity, motivating an analysis of PRI selection.
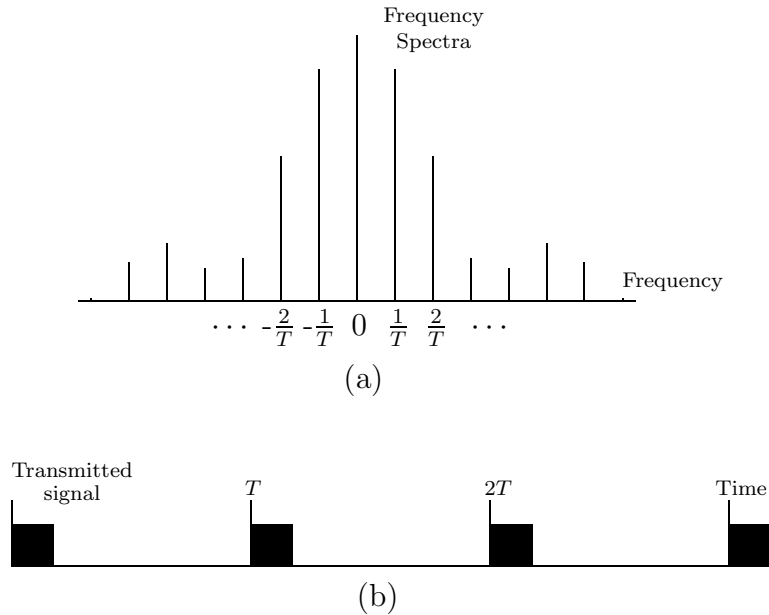
Figure 2.6.   Pulse train spectra and PRI. An infinite length pulse train with PRI T, (b), will have a comb-like spectra with harmonics separated by $1/T$, (a).

Typically, pulse doppler radars operate at one of three PRI rates: High, Medium, or Low. The PRI rate is also known as the Pulse Repetition Frequency

(PRF) and is defined as $f_p = 1/T$. High PRF radars have greater spectral separation and therefore are better suited for avoiding velocity ambiguities, but due to the associated small PRI suffer greatly from range ambiguities. Low PRF radars, on the other hand, have an unambiguous range near the maximum detection range of the radar system, but have a densely packed spectra exacerbating velocity ambiguities. Figure 2.6(a) illustrates the spectrum resulting from an infinite train of pulses, shown in Figure 2.6(b). The aforementioned accordion effect that PRI changes have on the spectral separation is clearly represented in this figure.

By utilizing multiple PRF's, these ambiguities can be significantly reduced. This technique may be conceptualized as the transmission of two or more pulsed waveforms from the same antenna, with each waveform having a unique PRF. The PRF's are typically related via

$$\text{PRF}_n = \frac{\text{a}_n}{T_u},\tag{2.54}$$

where PRF_n is the nth PRF, a_n is an integer, and T_u is a common sub-multiple of a prescribed PRI [1:1-18] [24:273]. A radar return from a target has a true range R_t described by $R_t = \gamma R_u + R_i$, where R_i is the indicated range and γR_u is an integer multiple of the unambiguous range. The unknowns are γ and R_t; therefore, by changing the PRF (and thereby R_u and R_i,) a second simultaneous equation is generated and a solution for the true range is found. Alternatively, the true range can be determined by identifying where the radar returns for the different PRFs coincide. However, the multiple PRF returns from this technique cannot be processed coherently, resulting in a less energy efficient implementation. Also, an environment that has multiple targets is likely to generate further ambiguous returns from *ghosting* [1:1-18].

2.4.2 Non-linear Suppression System Model. Non-linear Ambiguity Suppression (NLS) combines pulse compression and pulse discrimination techniques to

deliver a means of improving radar ambiguities in pulsed radar. The concept was introduced by Palermo in 1962 [28] utilizing a conjugate LFM coded pulse pair. The fundamental building block of the NLS technique is the *suppression kernel* Λ_k shown in Figure 2.7. This unit operates on the radar return to suppress a particular pulse response by first pre-filtering the entire signal to discriminate that pulse in some way from all other pulses. Once the presence of that pulse is emphasized in the radar return, the pulse is suppressed by a *suppression operator*, which ideally has no effect on all other pulses. After this suppression operation, the radar return is passed through a post-filtering process to remove the effect of pre-filtering. The pre-filter $h_k(t)$ and post-filter $g_k(t)$ condition the waveform to maximize the effect of the suppression operation on the kth pulse without impacting the other pulses. Therefore, the suppression operation determines the filter and pulse design criteria.
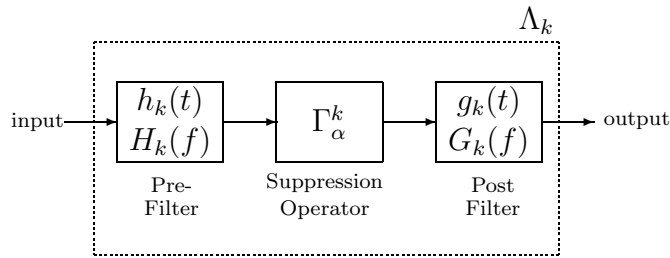
Figure 2.7.   General NLS kernel [1:2-11].

Two examples of *thresholding* suppression operators are illustrated in Figure 2.8(a) and (b). Although various suppression operators may be devised, this thesis focuses only on the use of thresholding suppression operators as these are the most common. The implications that thresholding has on formulation of a pulse design criteria is two-fold. To remove energy from a signal, the focused pulse response must have an amplitude greater than the threshold, consequently the pre-filtering process should project as much of the undesirable pulse energy above the threshold as possible whilst spreading all other pulses below it. When only thresholding suppression operators are considered, the suppression is dependent on the ability of the

2-26
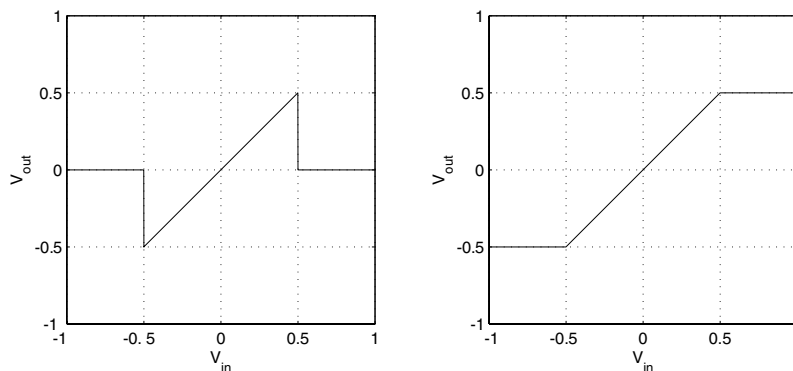
Figure 2.8.   Threshold suppression operators (Γ_α). Hole-punch (a), and saturation limiter (b), with $\alpha = 0.5V_{in}$ [1:1-23].

pre-filter to compress the intended pulse whilst spreading, or dispersing, all other pulses.

A common means of pulse compression exists through the matched filtering of certain waveforms. To utilize the NLS technique, a series of pulses must be designed in such a way that as a result of matched filtering for the kth pulse (causing it to become compressed) each of the remaining pulses are dispersed. This concept is known as mutual dispersion and is utilized in spread-spectrum applications such as direct sequence Code Division Multiple Access (CDMA) [30]. When thresholding NLS is employed, the components of the suppression kernel, in Figure 2.7, become: matched filter, threshold operator, and conjugate reflection filter.

A NLS system with N pulses utilizes as many channels to disinter each pulse from the radar return. The nth channel contains N–1 suppression kernels, $\Lambda_k \forall k \neq n$, aimed at suppressing all but the nth pulse from the pulse train as detailed in Figure 2.9. The final stage of each channel is a matched filter operation for the sought-after pulse. In other words, the nth channel extracts the nth pulse from a radar return whilst suppressing all others. As a result, the pulse repetition interval effectively increases N-fold. This extends the effective unambiguous range to $NcT/2$ and considerably alleviates the range ambiguities discussed in Section 2.3.3.
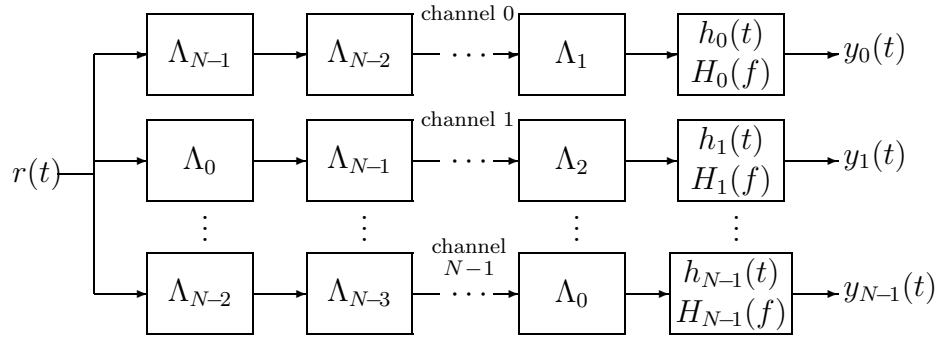
Figure 2.9. NLS system illustrating N individual channels each comprising $N-1$ suppression operations [1:2-15].

To illustrate this approach consider a pulse family comprised of two conjugate LFM waveforms $f_1(t) = e^{j2\pi\mu t^2}$, and $f_2(t) = e^{-j2\pi\mu t^2}$, for $|t| < 1$ and $\mu = 5$. The radar range channel is arbitrarily constructed over a CPI to contain these pulses, $r(t) = f_1(t - t_1) + f_2(t - t_2) + n(t)$, delayed in time and affected by Gaussian white noise, as detailed in Figure 2.10(a). Notice that the pulse returns overlap; this phenomena is known as self-clutter due to the interference each pulse contributes to the other. In attempting to disinter $f_2(t)$ from this signal it is passed through a matched filter, $F_2^*(f)$, resulting in the plot in Figure 2.10(b). On the other hand suppressing $f_1(t)$ with a thresholding non-linearity removes a good deal of its energy, and therefore interference contribution, as shown in 2.10(c). Because of the dispersive effect that matched filtering for $f_2(t)$ has on $f_1(t)$, both approaches provide good results, however the contribution to self-clutter is significantly reduced due to the suppression operation as shown in Figures 2.10(b) and (c).

2.5 Summary

This chapter introduced the background theory used throughout the remainder of this thesis, and in so doing presents a cross-section of the literature pertinent to this field. Section 2.2.1 introduced the concept of realizability and some signal theory basics and metrics. This analysis naturally lead to a discussion on integral transforms, the most prevalent being the Fourier and Hilbert transform, and to sub-
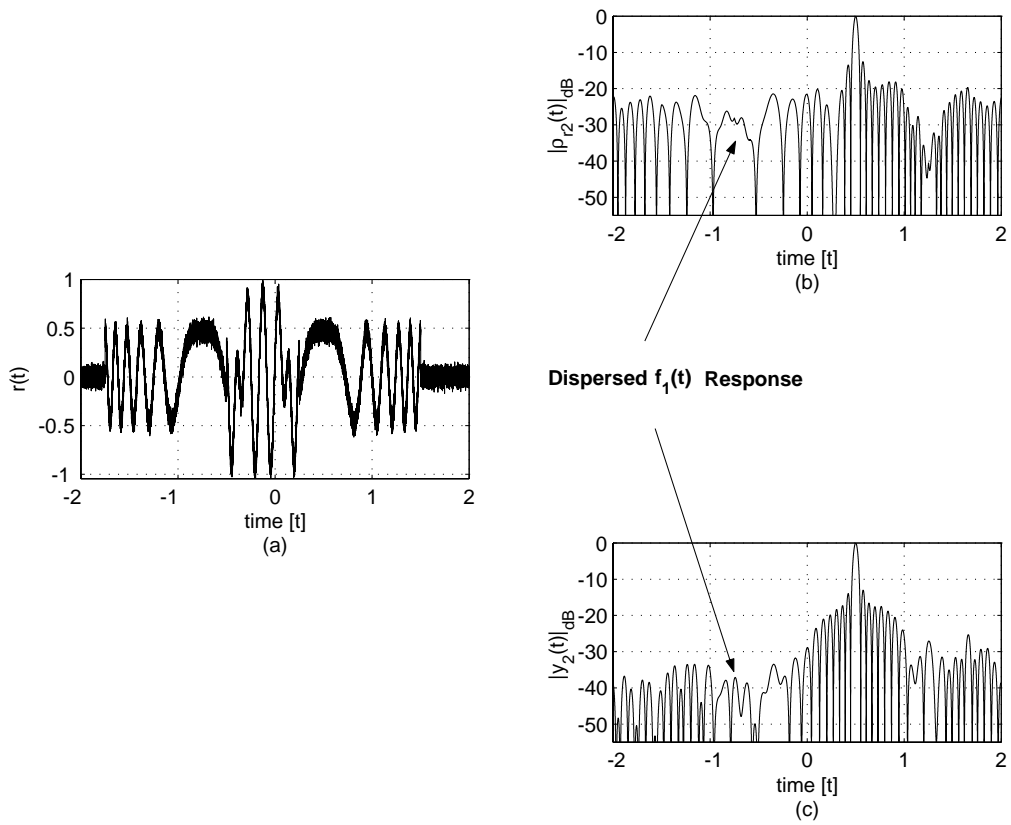
Figure 2.10.   NLS processing of conjugate LFM pulses. A radar return comprising a pair of conjugate LFM pulse responses is simulated, (a). The return is matched filtered for pulse 2 (right), compressing it and dispersing pulse 1 (left), (b). Pulse 1 is suppressed prior to matched filtering for pulse 2, (c).

sequent consideration given to numerical approximations. Section 2.3 introduced radar signals as a subset of realizable signals, narrowband in nature, permitting compact analytic notation. This section also provided the model for the radar system. Section 2.3 concluded with a discussion on radar waveform design describing ambiguities inherent to pulsed radar systems and defining metrics for measuring resolution. The core topic of this chapter was introduced in Section 2.4.2 where the NLS approach was explained. The NLS model was provided and NLS's superior ambiguity suppression performance was demonstrated.

III. NLS Symbol Design and Modelling

3.1   Introduction

The effectiveness of a thresholding NLS system hinges on the selection of symbols that exhibit good compression in autocorrelation and dispersion in crosscorrelation. Section 2.4.2 provided an example using conjugate linear FM symbols, unfortunately the use of these symbols is limited to only one pair, therefore to expand the symbol set a more detailed analysis of NLS is required. This chapter describes an approach conceived by Brown [5] that is optimal in rms time duration for generating a family of mutually dispersive symbols of any size. Section 3.2 provides a brief overview of the NLS concept. Section 3.3 discusses the scope of the research, relating the approach and associated synthesis constraints. Section 3.4 relates the radar model to NLS by defining analytically, as in [5], the problem of designing a symbol set suited to NLS, and illustrates the Brown NLS system. Section 3.5 derives Brown's theorem with the optimal envelope and phase-rate functions, introduces the Hermit Problem and dispersive gain, and provides an expression for theoretically optimal performance. Section 3.6 defines notation for biphase codes relating the suitability of these codes to NLS. Finally, Section 3.7 discusses the metrics used to characterize and contrast Brown symbols, providing an overview of the approach to numerical approximation.

3.2   Non-linear Ambiguity Suppression Overview

Radar systems are employed to detect targets and to facilitate parameter estimation. Within this construct, the pulse-like nature of pulse Doppler radar systems leads to radar returns containing range and velocity ambiguities degrading the overall system performance. The ambiguities may be eliminated should the attitude of

the target in question be such that the range velocity product is [35]

$$R|v| < \frac{1}{8}c\lambda, \tag{3.1}$$

where c is the speed of light and λ is the wavelength of the transmitted radar signal. Although a profile of the target's range and velocity characteristics may be constructed, typically they cannot be controlled, requiring an alternative means of eliminating ambiguities.

Non-linear Ambiguity Suppression (NLS) is a means of transmitting a pulse-train comprised of N pulses, each of which exhibit specific characteristics derived from the choice of suppression operator. When considering thresholding suppression operators the pre-filtering the pulse train must provide a two-fold affect. The filter must compress the intended pulse and spread, or disperse, all remaining pulses. This is the key design criteria for NLS symbol design.

By concatenating a chain of suppression kernels, each suppressing a different pulse as detailed in Figure 2.9, a series of non-linearities are effected on the radar return reducing the self-clutter. Figure 3.1 shows a time slice series for a LFM signal passed through a single suppression kernel. Figure 3.1(a) is the original linear FM pulse. This signal is passed through a matched filter; the response is shown as a dashed line in Figure 3.1(b), while the solid line indicates the resultant signal after hole-punch suppression. Finally, the suppressed signal is passed through a conjugate reflection filter where the output, displayed in Figure 3.1(c), exhibits a significant reduction in signal energy.

The suppression kernel, Λ_k, considered in this thesis takes the form illustrated in Figure 3.2 [1:2-11]. The pre-filtering is performed by a matched filter, compressing the kth pulse and spreading all others. The suppression operation is accomplished with a thresholding non-linearity, and finally the post-filtering is performed by a conjugate reflection filter. Using this kernel constrains the search for optimality.

3-2
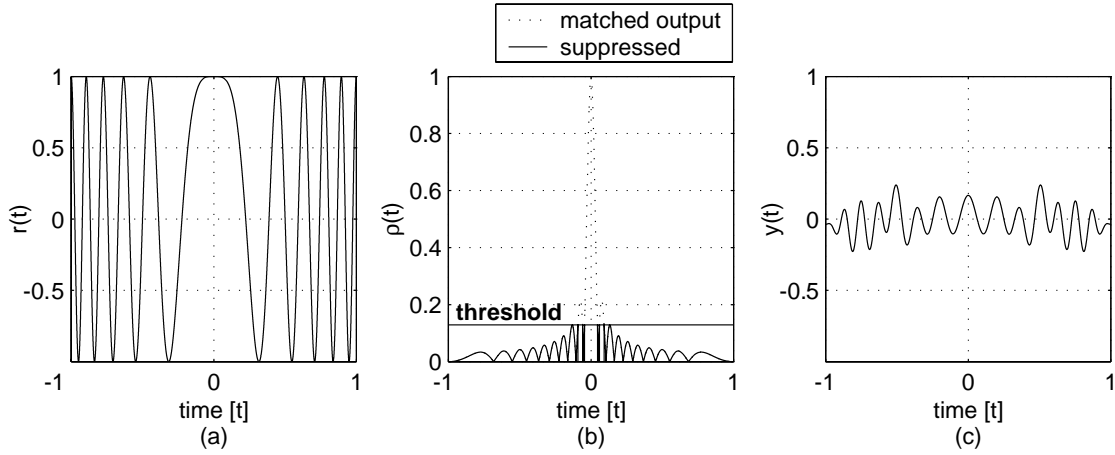
Figure 3.1.   Thresholding example with LFM (a) original signal, (b) thresholding comparison, and (c) suppressed signal.
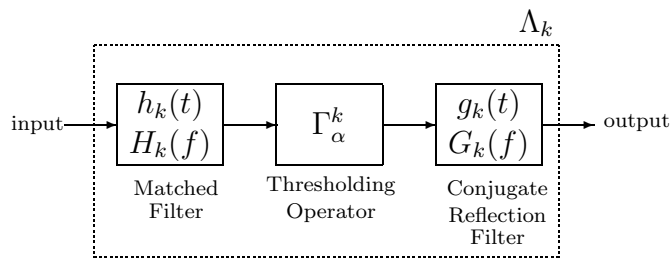
Figure 3.2.   Threshold NLS kernel [1:2-11].

Brown has devised a theorem that poses an optimal solution to pulse design for this configuration of NLS system [5]. Brown [5] describes, in terms of rms duration, the optimal correlation waveform introducing an elegant notation simplification. Brown considers the design of phase functions such that a set of codes may be devised with optimal mutually dispersive properties. This step leads to a problem, coined by Brown as the *Hermit Problem*, in which an N-dimensional solution is determined by choosing N vectors in N-space that are each maximally equidistant from each other.

3.3 Scope of Research

As stated in Section 1.2, the goals of this thesis are to:

1. Explain the formulation of Brown's theorem [5] whilst introducing a simplified linear algebraic notation;

2. Describe a systematic process for designing Brown symbols through an analysis of Brown's work and by theoretical extension;

3. Provide a theoretical analysis for the digitization of Brown symbols;

4. Evaluate performance of Brown symbols, comprising dispersive gain, through simulation and numerical approximation; and

5. Compare the performance of various Brown symbols with discrete codes through simulation.

The simulations conducted in generating and characterizing Brown symbols utilized Matlab®. This approach constrains the simulation to purely digital analysis, providing the theoretical background required to analyze Brown symbols for digitization and obtaining results using numerical approximation techniques. Analytic derivations of closed-form spectral definitions of Brown symbols are determined and synthesized as frequency sampled signals, the respective sampled time functions are de-

termined with the rectangle-rule approximation technique. Finally, the time-sampled correlation functions are calculated and analyzed.

3.4 Brown Theorem Motivation

Pulsed radar systems are challenged to divine the nature of their environment by processing radar returns amidst self-clutter and ambiguities. Section 2.3.3.1 highlighted the causes of ambiguities, concluding that it is not possible to entirely remove ambiguities using only the PRF as a control variable. Alternatively, NLS provides a powerful technique to overcome these challenges, however it poses different problems such as symbol selection, and difficulties in *optimal* symbol design.

The discovery of symbol families that are well-suited to NLS is not by any means a recent achievement. CDMA schemes are an example of the use of discrete codes that exhibit the very properties desired in NLS [2]. Instead, the search for *optimal* symbols has historically been relegated to the search for optimal discrete codes; an avenue of research that has encompassed a vast array of techniques from heuristic approaches to neural networks but that has not fully unveiled a solution to optimality in NLS. By considering the rms time duration of the correlation functions, Brown proposes an elegant theorem for the design of optimally mutual dispersive codes leading to an expression for the optimal performance of such codes.

This section presents Brown's theorem by first constructing the environmental model and presenting relevant assumptions as necessary. The problem definition is then stated and the theorem is explained. Finally, the resultant theoretical optimal performance in rms time duration is presented.

3.4.1 Environment Construction. Pulse Doppler radars are employed on a vast array of sensor platforms. Of course, platform specifics determine the particular performance profile and associated catalysts to system degradation. However, the problem of self-clutter and range and velocity ambiguities appears somewhat

ubiquitous. This derivation utilizes analytic notation and the radar model described in Section 2.3 and illustrated in Figure 2.2. Accordingly, the pulsed radar signal is defined as

$$x(t) = \sum_{k=0}^{N-1} f_k(t - kT), \tag{3.2}$$

where

$$f_k(t) = a_k(t) e^{j\phi_k(t)} \mathrm{rect}\left(\frac{t}{\tau_p}\right). \tag{3.3}$$

In other words, the radar waveform is comprised of N distinct pulses separated by a uniform interval T and of uniform width τ_p. Subsequently, when the kth pulse is modulated onto a carrier it can be denoted by the real part of the analytic signal

$$f_{m_k}(t) = a_k(t) \cos(2\pi f_c t + \phi_k(t)). \tag{3.4}$$

Using the radar model, Figure 2.2, the radar range channel $r(t)$ is constructed. Assuming the transmitted signal is received and processed with coherent IQ channels, the analytic notation may be retained. Recall that, in the IQ representation, the real part describes the output from the in-phase channel, whilst the quadrature channel output generates the imaginary part. Substituting $f_k(t)$ for $x(t)$ into Eq (2.39) describes the radar return of the kth pulse,

$$
\begin{aligned}
r(t) &= u_m(t) \star f_k(t) \\
&= \int_{-\infty}^{\infty} \frac{c}{2} u\left(\frac{c\tau}{2}\right) e^{j2\pi f_c \tau} a_k(t - \tau) e^{j\phi_k(t-\tau)} d\tau,
\end{aligned} \tag{3.5}
$$

taking the Fourier transform of both sides illustrates that the frequency response of the radar range channel is related to the transmitted pulse by

$$R(f) = F_k(f) U_m(f), \tag{3.6}$$

where

$$
\begin{aligned}
U_m(f) &= \mathcal{F}\left\{\frac{c}{2}u\left(\frac{ct}{2}\right)e^{j2\pi f_c t}\right\} \\
&= U\left(\frac{2f}{c}\right) \star \delta(f - f_c) \\
&= U\left(\frac{2[f - f_c]}{c}\right),
\end{aligned}
\tag{3.7}
$$

which is the spectral reflectivity density of the environment, colored in response to an incident wave at frequency f_c. Therefore, the frequency response of the radar range channel is

$$
R(f) = F_k(f)U\left(\frac{2[f - f_c]}{c}\right).
\tag{3.8}
$$

The spectrum of the transmitted pulse has a filtering effect on the spectral reflectivity density. High compression ratios from the matched output predicates a requirement for signals having large time-bandwidth products. Eq (3.8) illustrates that large bandwidth signals also pass more energy from the environment. The search for optimal signals in the Fourier domain then provides a more immediate relationship between the signal, the radar return, and the environment.

3.4.2 Problem Definition. Due to the temporal and spatial dynamics of the spectral reflectivity density function and sensor motion, each pulse return contains different information about the environment. The goal is to extract this information from a radar range channel with the highest fidelity, or minimal degradation. Section 2.3.3.1 covers the nature of range and velocity ambiguities and Section 2.4 discusses the benefits provided by NLS. By removing self-clutter and ambiguities, radar system performance is improved and although there are many approaches to ambiguity reduction the focus of this thesis centers on the use of a NLS technique.

Brown looks in the Fourier domain to divine an optimal solution which leads to an improved implementation of the NLS system [5:18]. Firstly, complex notation is used to describe the spectrum of each of the N pulses in the symbol set. Eq (3.9) defines the Fourier transform pair of the kth pulse

$$F_k(\omega) = A^{\frac{1}{2}}(\omega)e^{J\Phi_k(\omega)} \tag{3.9}$$

where $\omega = 2\pi f$ and the envelope $A(\omega)$ and phase $\Phi_k(\omega)$ functions of $F_k(\omega)$ are both real and bandlimited, *i.e.*, $A(\omega), \Phi_k(\omega) \in \Re$, with $A(\omega) = 0$ for all $|\omega| > \Omega_0/2$. However, whilst the signal $F_k(\omega) \stackrel{\mathcal{F}}{\Longleftrightarrow} f_k(t)$, this is not true of the individual envelope and phase function components, *i.e.*, $A(\omega) \stackrel{\mathcal{F}}{\Longleftrightarrow\!\!\!\!/} a_k(t)$ and $\Phi_k(\omega) \stackrel{\mathcal{F}}{\Longleftrightarrow\!\!\!\!/} \phi_k(t)$. The components of the NLS kernel, in Figure 3.2, are now redefined using this notation. The matched filtering operation for the kth pulse is $H_k(\omega) = F_k^*(\omega) = A^{\frac{1}{2}}(\omega)e^{-J\Phi_k(\omega)}$, whilst the conjugate reflection filter is $G_k(\omega) = [F_k^*(\omega)]^{-1} = A^{-\frac{1}{2}}(\omega)e^{J\Phi_k(\omega)}$. The conjugate reflection filter from Λ^k and its neighboring matched filter, from Λ^{k-1}, have reciprocal envelopes that are independent of k. These filters may be combined to form the equivalent filter $G_k(\omega)H_{k-1}(\omega) = e^{J[\Phi_k(\omega)-\Phi_{k-1}(\omega)]}$. This filter effectively refocuses the radar return, emphasizing the next pulse, and as such is denoted the *refocusing filter*. The resultant suppression kernel, denoted the Brown kernel Υ_k, is defined as illustrated in Figure 3.3.
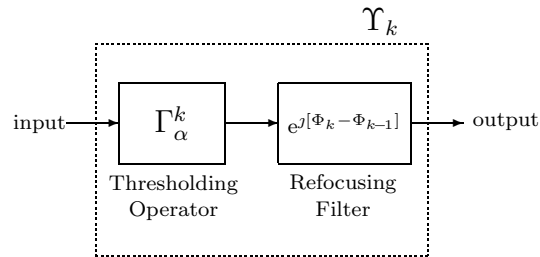
Figure 3.3.   Brown threshold NLS kernel.

Note, also, that the first stage of matched filters share the envelope $A^{\frac{1}{2}}(\omega)$. Subsequently, the implementation of the NLS system may be further simplified by

moving the envelope component $A^{\frac{1}{2}}(\omega)$ to the front of the suppression bank. When a NLS system is constructed with the aforementioned simplifications it may be re-described as shown in Figure 3.4. This implementation is similar in structure to the implementation shown in Figure 2.9 but is more compact in terms of notation and avoids singularities in the refocusing filter design. Therefore, this is the refer-
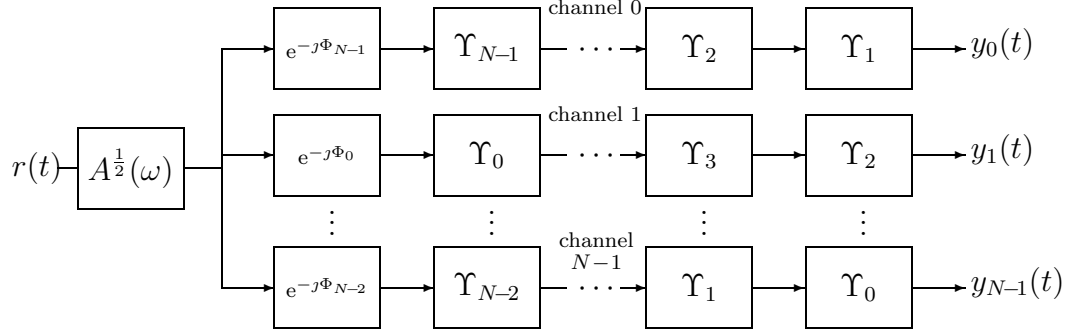
Figure 3.4.   Brown NLS system [5].

ence model used in this thesis for implementation of Brown symbols. With the NLS system defined, the problem becomes that of designing envelope $A(\omega)$ and N phase functions $\Phi_k(\omega)$ yielding an optimal set of symbols. The following section describes Brown's approach to the problem.

3.5   Brown's Optimally Mutual Dispersive Symbols

3.5.1   Optimality Design Criteria.   To provide a rigid mathematical frame-work, compression and dispersion measurements are calculated using the appropriate metrics described in Section 2.3.3.2. Recall from Eq (2.49) that the *rms time dura-tion* of a signal centered at $t = 0$ and having unit energy is given by

$$\sigma^2 = \int_{-\infty}^{\infty} t^2 |x(t)|^2 dt. \tag{3.10}$$

Because of Fourier transform duality, this equation may be rewritten in terms of a Fourier pair for time function $f(t)$. In this case, using the Fourier properties

$$\mathcal{F}\{tx(t)\} \ = \ \jmath\frac{d}{d\omega}X(\omega) \ = \ \jmath\dot{X}(\omega) \tag{3.11}$$

$$\int_{-\infty}^{\infty}|x(t)|^2dt \ = \ \frac{1}{2\pi}\int_{-\infty}^{\infty}|X(\omega)|^2d\omega \tag{3.12}$$

leads to the equivalent expression for the rms time duration of a signal in terms of frequency,

$$\sigma^2 = \frac{1}{2\pi}\int_{-\infty}^{\infty}\left|\jmath\dot{X}(\omega)\right|^2 d\omega. \tag{3.13}$$

By defining the spectral waveform as an arbitrary complex analytic signal, $i.e.$, $X(\omega) = \beta(\omega)e^{\jmath\mu(\omega)}$, a useful formulation of the rms time duration is developed:

$$
\begin{aligned}
\sigma^2 \ &= \ \frac{1}{2\pi}\int_{-\infty}^{\infty}\left|\jmath\frac{d}{d\omega}\beta(\omega)e^{\jmath\mu(\omega)}\right|^2 d\omega \\
&= \ \frac{1}{2\pi}\int_{-\infty}^{\infty}\left|\jmath\dot{\beta}(\omega)e^{\jmath\mu(\omega)} - \beta(\omega)\dot{\mu}(\omega)e^{\jmath\mu(\omega)}\right|^2 d\omega \\
&= \ \frac{1}{2\pi}\int_{-\infty}^{\infty}\dot{\beta}^2(\omega)d\omega + \frac{1}{2\pi}\int_{-\infty}^{\infty}\dot{\mu}^2(\omega)\beta^2(\omega)d\omega. \tag{3.14}
\end{aligned}
$$

This is a useful way of describing the rms time duration because it partially isolates the phase function, actually the phase-rate function, from the envelope. The NLS kernel performs thresholding on the correlation functions. Consequently, should the lth pulse of the symbol set defined in Eq (3.9) arrive at Υ_k, then the correlation function suppressed by the thresholding operator is defined as

$$
\begin{aligned}
F_l(\omega)H_k(\omega) \ &= \ F_l(\omega)F_k^*(\omega) \ \triangleq \ P_{lk}(\omega) \\
&= \ A(\omega)e^{\jmath[\Phi_l(\omega) - \Phi_k(\omega)]} \tag{3.15}
\end{aligned}
$$

where $P_{lk}(\omega) \overset{\mathcal{F}}{\Longleftrightarrow} \rho_{lk}(t)$ denotes the crosscorrelation function and $P_{kk}(\omega) \overset{\mathcal{F}}{\Longleftrightarrow} \rho_{kk}(t)$ denotes the autocorrelation function. Since Υ_k aims to suppress only the kth pulse response the autocorrelation function, $\rho_{kk}(t)$, should be maximally compressed (fo-

cused) whilst all crosscorrelation functions, $\rho_{lk}(t)$, should be maximally dispersed. The rms time duration is small for compressed signals and large for dispersed signals thereby providing a useful metric for comparing correlation functions. From Eq (3.14), the correlation functions that arrive at Υ_k have the following rms time duration

$$\sigma_{lk}^2 = \frac{1}{2\pi} \int_{-\infty}^{\infty} \dot{A}^2(\omega)d\omega + \frac{1}{2\pi} \int_{-\infty}^{\infty} [\dot{\Phi}_l(\omega) - \dot{\Phi}_k(\omega)]^2 A^2(\omega)d\omega. \tag{3.16}$$

Where $\dot{\Phi}_k(\omega)$ and $\dot{A}(\omega)$ denotes the first derivative with respect to ω. The elegance of Brown's solution becomes no more apparent than is shown here. For $l = k$ the rms time duration of the autocorrelation function has no phase component, leaving only the first term of Eq 3.16. The rms time duration of the autocorrelation function is therefore independent of phase, decoupling the design of envelope $A(\omega)$, to optimize autocorrelation compression, from the phase functions $\Phi_k(\omega)$, to optimize crosscorrelation dispersion. In other words, rms time duration as a metric of optimization provides a means of designing mutually dispersive symbols.

3.5.1.1   Optimal Envelope Design.   Brown pursues the choice of an envelope that optimizes the compression of a matched filtered bandlimited signal [5:7]. The design of the optimal envelope, $A(\omega)$, such that σ_{kk}^2 is minimized requires a solution to the following constrained optimization problem:

$$\text{Minimize} \quad \frac{1}{2\pi} \int_{-\infty}^{\infty} \dot{A}^2(\omega)d\omega,$$

$$\text{Such that} \quad \frac{1}{2\pi} \int_{-\infty}^{\infty} A^2(\omega)d\omega = 1.$$

The function achieving this is the cosine taper described in Eq (3.17) [5:8].

$$A(\omega) = \begin{cases} \sqrt{\frac{4\pi}{\Omega_0}} \cos\left(\frac{\pi\omega}{\Omega_0}\right) & , |\omega| < \frac{\Omega_0}{2} \\ 0 & , \text{else} \end{cases} \tag{3.17}$$

The cosine taper, therefore, provides the optimal performance in rms time duration
of the autocorrelation function as illustrated:

$$
\begin{aligned}
\sigma_{kk}^2 &= \frac{1}{2\pi} \int_{-\infty}^{\infty} \dot{A}^2(\omega) d\omega \\
&= \frac{2\pi^2}{\Omega_0^3} \int_{-\frac{\Omega_0}{2}}^{\frac{\Omega_0}{2}} \sin^2\left(\frac{\pi\omega}{\Omega_0}\right) d\omega \\
&= \frac{\pi^2}{\Omega_0^2}.
\end{aligned}
\tag{3.18}
$$

The cosine taper is the optimal spectral envelope ensuring minimal rms time
duration for a matched filtered, finite bandwidth signal. The next step, therefore,
is to design phase-rate functions providing the highest degree of dispersion in the
crosscorrelation response.

3.5.1.2   Optimal Phase-Rate Functions.   The design of optimal phase-
rate functions begins by noticing that the second term is of Eq (3.16) can be expanded
into components of the form

$$
(x, y)_w = \int_a^b x(t) y^*(t) w(t) dt.
\tag{3.19}
$$

This function was first introduced in Eq (2.9) as the weighted inner product of two
functions. To utilize this expression, Brown defines the phase-rate functions as points
in a Hilbert space, $\dot{\Phi}_k(\omega) \in \mathcal{H}$. Each of the phase-rate functions is then defined as a
linear combination of basis functions, $\varphi_n(\omega)$, as shown

$$
\begin{aligned}
\dot{\Phi}_k(\omega) &= \sum_{n=0}^{N-1} c_{kn}\, \varphi_n(\omega) \\
&= \mathbf{c}_k^T\, \boldsymbol{\varphi}(\omega),
\end{aligned}
\tag{3.20}
$$

where

$$\mathbf{c}_k = \begin{bmatrix} c_{k0} \ c_{k1} \ c_{k2} \ \ldots \ c_{kN-1} \end{bmatrix}^T$$

$$\boldsymbol{\varphi}(\omega) = \begin{bmatrix} \varphi_0(\omega) \ \varphi_1(\omega) \ \varphi_2(\omega) \ \ldots \ \varphi_{N-1}(\omega) \end{bmatrix}^T$$

$$\varphi_k(\omega) \in \mathcal{H} \ \forall \ k.$$

These basis functions are chosen as odd functions of ω and are orthonormal within the weighted inner product space incorporating $A^2(\omega)$. The last of these characteristics may be expressed mathematically as

$$(\varphi_k, \varphi_l)_{A^2} = \frac{1}{2\pi} \int_{-\infty}^{\infty} \varphi_k(\omega)\varphi_l(\omega)A^2(\omega)d\omega = \delta_{kl} \tag{3.21}$$

By incorporating Eqs (3.20) and (3.21), the second term of Eq (3.16), describing the dispersion the crosscorrelation function, is expanded as follows

$$\sigma_{lk}^2 - \sigma_{kk}^2 = \frac{1}{2\pi} \int_{-\infty}^{\infty} [\mathbf{c}_l^T \boldsymbol{\varphi}(\omega) - \mathbf{c}_k^T \boldsymbol{\varphi}(\omega)]^2 A^2(\omega)d\omega$$

$$\text{sub: } \mathbf{d}_{lk} \overset{\triangle}{=} \mathbf{c}_l - \mathbf{c}_k$$

$$= \frac{1}{2\pi} \int_{-\infty}^{\infty} \sum_{n=0}^{N-1} d_{lk,n} \varphi_n(\omega) \sum_{m=0}^{N-1} d_{lk,m} \varphi_m(\omega) A^2(\omega)d\omega$$

$$= \frac{1}{2\pi} \sum_{n=0}^{N-1} \sum_{m=0}^{N-1} d_{lk,n} \, d_{lk,m} \int_{-\infty}^{\infty} \varphi_n(\omega) \, \varphi_m(\omega) A^2(\omega)d\omega$$

$$= \|\mathbf{d}_{lk}\|^2. \tag{3.22}$$

Subsequently, the dispersive term in the rms time duration can be reduced in this manner to the norm squared of $\mathbf{d}_{lk}$, *i.e.*, the square of the Euclidean distance between vectors $\mathbf{c}_l$ and $\mathbf{c}_k$, which is $d_2^2(\mathbf{c}_l, \mathbf{c}_k)$ as defined at Eq (2.3). Notably, by selecting a satisfactory basis set performance is no longer dependant on the choice of phase-rate functions. Instead, the problem becomes one of selecting optimal coefficient weighting vectors, *i.e.*, N vectors in N-dimensional space having the greatest equiv-

alent Euclidean distance. This problem has been coined by Brown as "The Hermit Problem" [5:9].

3.5.2   The Hermit Problem.   This problem is so named in reference to a scenario, wherein N-hermits living on a unit sphere in N-dimensional space jostle for a position that provides the greatest solitude. The vectors addressing each hermit in the steady state solution to this competitive relocation, being maximally equidistant, describe a solution to the problem. This solution, however, is not unique. Brown begins his analysis of this problem in 2-dimensional space [5:9], eventually providing a generic analysis for the more conceptually challenging higher dimensions.

Brown provides that in 2-dimensions the hermits will clearly reside at the opposite ends of a line. In 3-dimensional space they will reside within the same plane, each hermit separated by an arc of 120°. Conceptualization of a solution is confounded when considering 4-dimensional space, however Brown presents the following generic process for obtaining a solution [5:10]. Begin with the length N vector $\boldsymbol{\alpha} = [\cos\xi \ \cos\xi \ \cos\xi \ \ldots \ \cos\xi]^T$, where $\cos\xi = 1/\sqrt{N}$. This vector is of unit length and contains an equal contribution from each of the orthogonal axes. Brown visualizes this vector as the handle of an umbrella with N spokes. As the umbrella opens, the spokes move outward through the respective axes until they all become perpendicular to the umbrella handle, $\boldsymbol{\alpha}$. Figure 3.5 illustrates a particular solution to the Hermit Problem for $N = 2$ and $N = 3$. Notably, a different solution is achieved for each different rotation of $\boldsymbol{\alpha}$. However, this has no impact on the performance of symbols coded with Brown's approach.

Brown provides the following observations. The solution to the hermit problem is $(N-1)$-dimensional; in 2-dimensions the solutions exist on a line and in 3-dimensions within a plane, and so on. Also, the sum of the resultant vectors is zero, $\sum_k \mathbf{c}_k = 0$. Brown continues, providing an expression for optimal performance of these symbols using a trigonometric proof. The results in Chapter IV illustrate
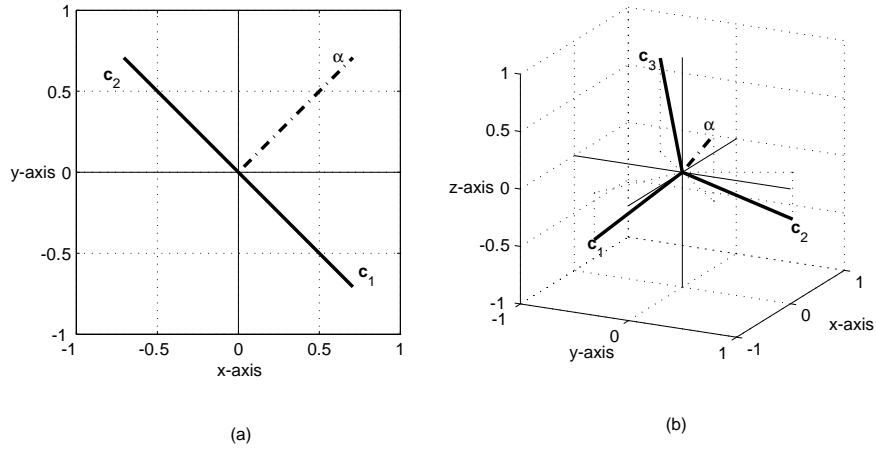
Figure 3.5.   A solution to the Hermit Problem for (a)
$N = 2$, and (b) $N = 3$.

an implementation utilizing a linear algebraic approach, by digressing here from Brown's approach the solution is obtained using a linear algebraic methodology.

The umbrella analysis leads into the following proof by emphasizing the requirement for orthogonality. Each of the solution vectors, $\mathbf{c}_k$, must be orthogonal to the umbrella handle and as such exist in an orthogonal $(N{-}1)$-dimensional space. Subsequently, the N-dimensional space may be decomposed into two orthogonal subspaces. The subspace containing the solution vectors is denoted the *hermit subspace*, $\langle \mathbf{C} \rangle$, and the subspace containing the umbrella handle is called the *orthogonal subspace*, $\langle \mathbf{A} \rangle$, where

$$\mathbf{C} \;=\; [\mathbf{c}_0\ \mathbf{c}_1\ \mathbf{c}_2 \ldots \mathbf{c}_{N-1}], \tag{3.23}$$

$$\mathbf{A} \;=\; \boldsymbol{\alpha}. \tag{3.24}$$

The orthogonal projection operator that projects onto $\langle \mathbf{A} \rangle$ is defined as [34:47]

$$
\begin{aligned}
\mathbf{P}_A \;&=\; \mathbf{A}\left(\mathbf{A}^T \mathbf{A}\right)^{-1} \mathbf{A}^T \\
&=\; \boldsymbol{\alpha}\left(\boldsymbol{\alpha}^T \boldsymbol{\alpha}\right)^{-1} \boldsymbol{\alpha}^T \\
&=\; \frac{1}{N}\mathbf{1},
\end{aligned}
\tag{3.25}
$$

where

$$\mathbf{1} = \begin{bmatrix} 1 & 1 & 1 & \dots & 1 \\ 1 & 1 & 1 & \dots & 1 \\ 1 & 1 & 1 & \dots & 1 \\ \vdots & \vdots & \vdots & \ddots & \vdots \\ 1 & 1 & 1 & \dots & 1 \end{bmatrix}_{N \times N.} \quad (3.26)$$

$\langle \mathbf{C} \rangle$ is an orthogonal subspace to $\langle \mathbf{A} \rangle$ therefore the projection matrix for $\langle \mathbf{C} \rangle$ is defined as

$$
\begin{aligned}
\mathbf{P}_C &= \mathbf{I}_N - \mathbf{P}_A \\
&= \mathbf{I}_N - \frac{1}{N}\mathbf{1} \\
&= \frac{1}{N} \begin{bmatrix} N-1 & -1 & -1 & \dots & -1 \\ -1 & N-1 & -1 & \dots & -1 \\ -1 & -1 & N-1 & \dots & -1 \\ \vdots & \vdots & \vdots & \ddots & \vdots \\ -1 & -1 & -1 & \dots & N-1 \end{bmatrix}_{N \times N,}
\end{aligned}
\quad (3.27)
$$

where $\mathbf{I}_N$ is the $N \times N$ identity matrix. Each of the N vectors in $\mathbf{P}_C$ is orthogonal to $\boldsymbol{\alpha}$, also being evenly separated in $\langle \mathbf{C} \rangle$. Subsequently, a solution to the Hermit Problem exists as the normalized column vectors of $\mathbf{P}_C$. Projection matrices are *idempotent*[1] therefore by observation the diagonal elements of $\mathbf{P}_C$ describe the norm of the column vectors. Normalizing the projection matrix $\mathbf{P}_C$ by dividing by the

---

[1]An idempotent matrix when multiplied with itself results in the original matrix, that is $\mathbf{P}_C^2 = \mathbf{P}_C$.

square root of this value generates a solution to the Hermit Problem $\mathbf{C}$ defined as

$$\mathbf{C} = \frac{1}{\sqrt{N^2 - N}} \begin{bmatrix} N-1 & -1 & -1 & \cdots & -1 \\ -1 & N-1 & -1 & \cdots & -1 \\ -1 & -1 & N-1 & \cdots & -1 \\ \vdots & \vdots & \vdots & \ddots & \vdots \\ -1 & -1 & -1 & \cdots & N-1 \end{bmatrix}_{N \times N}. \tag{3.28}$$

The metric describing dispersion for Brown's approach is the Euclidean distance. This squared distance, between any vector pair $\mathbf{c}_l$, $\mathbf{c}_k$ where $l \neq k$, is defined as

$$
\begin{aligned}
d_2^2(\mathbf{c}_l, \mathbf{c}_k) &= \mathbf{d}_{lk}^T \, \mathbf{d}_{lk} \\
&= (\mathbf{c}_l - \mathbf{c}_k)^T (\mathbf{c}_l - \mathbf{c}_k) \\
&= \frac{2N}{N-1}.
\end{aligned}
\tag{3.29}
$$

Also, the angle that is subtended between any pair of vectors is given by

$$
\begin{aligned}
\cos \xi_N &= \mathbf{c}_l^T \, \mathbf{c}_k \\
&= \frac{1}{1-N}.
\end{aligned}
\tag{3.30}
$$

Eq (3.22) illustrates that the rms time duration for non-matched, or crosscorrelated, symbols is governed by the Euclidean distance between the Hermits. Accordingly, the performance of Brown's approach is provided by Eq (3.29). This expression, however, is given under the constraint that each vector has unit length. Notably, a uniform increase in the length of the vectors will provide a direct increase in the Euclidean distance without compromising mutuality and therefore produce an improvement in the dispersive properties of the crosscorrelated symbols.

In the following chapter *dispersive gain* (G_D), is introduced to uniformly increase the length of the vector solutions to the Hermit Problem, such that

$$\mathbf{c}_k \quad \Rightarrow \quad \sqrt{G_D}\mathbf{c}_k,$$

therefore

$$
\begin{aligned}
d_2^2(\mathbf{c}_l, \mathbf{c}_k) &= G_D(\mathbf{c}_l - \mathbf{c}_k)^T(\mathbf{c}_l - \mathbf{c}_k) \\
&= \left(\frac{2N}{N-1}\right)G_D.
\end{aligned}
\tag{3.31}
$$

The achievable performance of symbols augmented by G_D is constrained only by hardware limitations.

3.6 Discrete NLS Signals

3.6.1 Desirable Signal Properties. Waveforms utilized for NLS are required, due to the nature of the threshold suppression operator, to compress on autocorrelation and disperse on crosscorrelation. Typically, the search for NLS codes has leveraged off scientific and technical advances in the field of communications, particularly spread-spectrum communications, resulting in a range of literature on the uses of biphase and polyphase codes. Such codes are typically comprised of a sequence of chips, or discrete phase coded intervals, that concatenate to describe the symbol, or code. The general form of a complex phase coded signal is provided in Eq (3.32) [20:152]:

$$x(t) = \frac{1}{\sqrt{M\tau}}\sum_{m=0}^{M-1}\mathrm{x}_m \,\mathrm{rect}\left(\frac{t + \left(\frac{M-1}{2} - m\right)\tau}{\tau}\right),\tag{3.32}$$

where

$$\mathrm{x}_m = \begin{cases} \mathrm{e}^{\jmath\phi_m}, & 0 \leq t \leq \tau \\ 0, & \text{elsewhere.} \end{cases}\tag{3.33}$$

There are a number of techniques used in phase-coding a sequence to achieve compression, such as Barker codes [3] and Pseudo-Random Noise (PRN)-sequences. Optimally, these codes must be mutually dispersive to be of any practical use in NLS.

3.6.2 Biphase Codes. Biphase codes are so named because the phase-code is limited to being one of two possible values, $\phi_m \in \{0, \pi\}$. Subsequently, the resultant code is a real valued signal having a chip value of $x_m = \pm 1$. These codes, therefore, are represented using an M-length sequence $\mathbf{x} = e^{j\phi}$.

Barker sequences generate two-valued autocorrelation functions, being either 1 or $1/M$ [35] and thus have desirable autocorrelation compression properties. However, only a limited number of Barker codes exist and they do not have desirable crosscorrelation properties. Maximal-length PRN-sequences, known as m-sequences, are usually generated via a Linear Feedback Shift Register (LFSR) [30]. For m-sequences, the LFSR is configured to generate maximal-length sequences that exhibit two-valued autocorrelation functions, as per the Barker sequences. A Gold code family is a set of *preferred pairs* of m-sequences, having crosscorrelation functions with three-values. Due to the mutually dispersive nature of Gold codes, they have been employed in DS-CDMA and spread-spectrum communications applications. Recently, these codes were demonstrated to provide an effective symbol set for NLS [2]. Gold codes are discrete codes that are well suited to NLS and are evaluated in Section 4.4.

3.7 Numerical Estimation of NLS Symbols Performance

3.7.1 Performance Metrics. The performance of the symbols, analyzed in the following chapter, is measured in terms of the rms time duration of the correlation function, defined in Eq (3.34). The correlation function was optimized, in terms of

rms time duration, for Brown symbols in Eq (3.15).

$$\rho_{lk}(t) = \int_{-\infty}^{\infty} f_l(s) f_k^*(s+t) ds \qquad (3.34)$$

$$P_{lk}(\omega) = F_l(\omega) F_k^*(\omega) \qquad (3.35)$$

The calculation of the periodic correlation function for discrete codes can be represented as shown in Eq (3.36) [33:594].

$$\theta_n(\mathbf{x}, \mathbf{y}) = \lambda \sum_{m=0}^{M-1} \mathrm{x}_m \mathrm{y}_{m+n}^* \ \ \forall \, n = 1-M, -M, \ldots, M-1, \qquad (3.36)$$

where

$$\lambda = \int_{-\frac{\tau}{2}}^{\frac{\tau}{2}} \mathrm{rect}^2\left(\frac{t}{\tau}\right) dt. \qquad (3.37)$$

There are three metrics that are commonly used to compare the correlation functions for discrete codes [2:3-2]. These metrics are: the Peak Autocorrelation Sidelobe Level (PSL); Integrated Autocorrelation Sidelobe Level (ISL); and Peak Crosscorrelation Level (PCCL), defined in Eqs (3.38), (3.39), and (3.40) respectively [26:537].

$$\mathrm{PSL} = 10\log\left[\frac{\displaystyle\max_{\substack{n \\ n\neq 0}} |\theta_n(\mathbf{x},\mathbf{x})|^2}{|\theta_0(\mathbf{x},\mathbf{x})|^2}\right] \qquad (3.38)$$

$$\mathrm{ISL} = 10\log\left[\frac{\sum_{\substack{m=1-M \\ m\neq 0}}^{M-1} |\theta_m(\mathbf{x},\mathbf{x})|^2}{|\theta_0(\mathbf{x},\mathbf{x})|^2}\right] \qquad (3.39)$$

$$\mathrm{PCCL} = 10\log\left[\frac{\displaystyle\max_{n} |\theta_n(\mathbf{x},\mathbf{y})|^2}{\mathbf{max}\{|\theta_0(\mathbf{x},\mathbf{x})|^2, |\theta_0(\mathbf{y},\mathbf{y})|^2\}}\right] \qquad (3.40)$$

The PSL metric provides a measure of the disparity in the peak power of the auto-correlation function compared with the power of the most prominent sidelobe. ISL measures the total power in the sidelobes compared to the mainlobe. PCCL measures the disparity in the peak power of the autocorrelation function compared with

the power of the most prominent sidelobe in the crosscorrelation function. There-
fore, small sidelobes will produce a small PSL, high compression ratios will produce a
small ISL and high crosscorrelation dispersion will result in a small PCCL. In short,
the smaller these values the more suited the codes will be to NLS implementation.

Unfortunately, these metrics are not defined for continuous signals. Therefore,
the following adjustment is made to accommodate the calculation of these param-
eters for a continuous signal. Firstly, the times $\tilde{t}$ at which the extremum for the
autocorrelation function occur must be determined, denoted

$$\tilde{t} = \left\{ t : \frac{d}{dt} |\rho_{kk}(t)| = 0 \right\}. \tag{3.41}$$

The set, $\tilde{t}$, is then used to generate a discrete sampling of the autocorrelation func-
tion, at the extremum, which in turn leads to the construction of the discrete auto-
correlation function

$$\tilde{\theta}_n(f_k, f_k) = \rho_{kk}(\tilde{t}_n), \tag{3.42}$$

where $\tilde{t}_n$ is the nth ordered element of the set $\tilde{t}$. This ordered set is then used for
generating the discrete crosscorrelation sequences $\tilde{\boldsymbol{\theta}}(f_k, f_l)$. With discrete sequences
defined in this way the metric set is expanded to incorporate continuous waveforms.

3.7.2 Process Overview. Chapter IV provides simulation results for vari-
ous forms of Brown symbols. The design process divined from Section 3.5 may be
summarized as follows, for $k = 0,\ 1,\ \ldots,\ N{-}1$:

1. Choose any set of N unit-vectors in N-dimensional space that solves The Her-
   mit Problem. $\mathbf{C} = [\mathbf{c}_0\ \mathbf{c}_1\ \ldots\ \mathbf{c}_{N-1}]$;

2. Choose any set of N odd functions. $\boldsymbol{\varphi}(\omega) = [\varphi_0(\omega)\ \varphi_1(\omega)\ \ldots\ \varphi_{N-1}(\omega)]^T$, such
   that $\frac{1}{2\pi} \int_{-\infty}^{\infty} \varphi_k(\omega)\varphi_l(\omega)A^2(\omega)d\omega = \delta_{kl}$;

3. Describe the resultant N phase-rate functions $\dot{\Phi}_k(\omega) = \sqrt{G_D}\mathbf{c}_k^T\,\boldsymbol{\varphi}(\omega)$;

4. Describe the resultant N phase functions $\Phi_k(\omega) = \sqrt{G_D}\mathbf{c}_k^T\int_\omega\boldsymbol{\varphi}(\omega)d\omega$;

5. The resultant N mutually dispersive codes expressed in the frequency domain are then $F_k(\omega) = A^{\frac{1}{2}}(\omega)\mathrm{e}^{\jmath\Phi_k(\omega)}$; and

6. The resultant N mutually dispersive codes expressed in the time domain are $f_k(t) = \frac{1}{2\pi}\int_{-\infty}^\infty A^{\frac{1}{2}}(\omega)\mathrm{e}^{\jmath[\Phi_k(\omega)+\omega t]}d\omega$.

This process is demonstrated in the following chapter.

3.8 Assumptions

To meet the research goals and stay within time and resource constraints, some assumptions are necessary. As explained in Section 3.3, this research seeks to simplify the notation of Brown's approach, provide the theoretical extension for digitization of Brown symbols, validate the theoretical expressions of rms time duration, and analyze the resultant correlation waveforms. As such the following assumptions have been made:

1. The Brown symbols being modelled are individual radar returns from stationary single point targets;

2. The environment and radar system do not distort the phase information of the Brown symbols;

3. There is no system or environmental noise; and

4. The hardware specifications are such that the sample frequency and bandwidth chosen for numerical simulation are attainable.

3.9 Summary

This chapter described Brown's approach, which is optimal in rms time duration, for generating a family of mutually dispersive symbols of any size. Section 3.2

provided a brief overview of the NLS concept. Section 3.3 discussed the scope of the research, relating the approach and associated synthesis constraints. Section 3.4 related the radar model to NLS and analytically defined, as in [5], the problem of designing a symbol set suited to NLS. Section 3.5 derived Brown's theorem divining the optimal envelope, phase-rate functions and solutions to the Hermit Problem, and also introduced dispersive gain and provided expressions for optimal performance. Section 3.6 defined notation for biphase codes relating the suitability of these codes to NLS. Finally, Section 3.7 discussed the metrics used to characterize and contrast Brown symbols, providing an overview of the numerical approximation approach undertaken.

IV. Analysis and Results

4.1 Introduction

In this chapter, Brown symbols are devised analytically, using the process outlined in Section 3.7.2, and then constructed and simulated in Matlab®. Section 4.2 considers the design of each of the Brown symbol components, being the Hermit Problem solution, phase-rate basis function design, phase function calculation, and symbol synthesis. Section 4.3 demonstrates the invariance of Brown symbols to the choice of phase-rate basis functions and envelope, and considers physical realizability. Finally, Section 4.4 contrasts the performance of Brown symbols with that of extant biphase symbols.

4.2 Brown Symbol Design

Section 3.5.1.1 devised the optimal envelope for Brown symbols. This section describes the process of generating Brown symbols by solving the Hermit Problem and designing phase functions.

4.2.1 Hermit Problem Solution.

Section 3.5.2 outlined a methodology for solving the Hermit Problem by using a linear algebraic technique. Given the starting vector α described in Section 3.5.2, this approach provides a simple means of generating the solution matrix, $\mathbf{C}$, as detailed in Eq (4.1).

$$\mathbf{C} = \frac{N\mathbf{I}_N - \mathbf{1}}{\sqrt{N^2 - N}},\tag{4.1}$$

where $\mathbf{I}_N$ is an $N \times N$ identity matrix, and

$$\mathbf{1} = \begin{bmatrix} 1 & 1 & 1 & \dots & 1 \\ 1 & 1 & 1 & \dots & 1 \\ 1 & 1 & 1 & \dots & 1 \\ \vdots & \vdots & \vdots & \ddots & \vdots \\ 1 & 1 & 1 & \dots & 1 \end{bmatrix}_{N \times N}. \tag{4.2}$$

Alternative solutions to the Hermit Problem can be attained by reworking the derivation using a different vector for the umbrella handel, $\boldsymbol{\alpha}$, or by operating on the solution provided here with an N-dimensional rotation matrix. Once a solution has been calculated, the next step of generating Brown symbols is to determine the phase functions.

4.2.2 Phase Function Design. Section 3.5.1.2 provided a methodology for the design of optimal phase-rate functions and indicated that N basis functions are required. These functions must be odd functions of ω and orthonormal within the weighted inner product space incorporating $A^2(\omega)$. A generic four-step process for generating these basis functions follows:

1. Choose any set of N odd and linearly independent functions.
   $\boldsymbol{\vartheta}(\omega) = [\vartheta_0(\omega)\ \vartheta_1(\omega)\ \dots\ \vartheta_{N-1}(\omega)]^T$.

2. Using any orthonormalization procedure with the weighted inner-product, generate a set of orthonormal basis functions $\boldsymbol{\varphi}(\omega) = [\varphi_0(\omega)\ \varphi_1(\omega)\ \dots\ \varphi_{N-1}(\omega)]^T$.

3. Describe the resultant N phase-rate functions $\dot{\Phi}_k(\omega) = \sqrt{G_D}\mathbf{c}_k^T\ \boldsymbol{\varphi}(\omega)$, where G_D is the dispersive gain factor and $\mathbf{c}_k$ is the kth solution to the Hermit Problem.

4. Calculate the resultant N phase functions $\Phi_k(\omega) = \sqrt{G_D}\mathbf{c}_k^T \int_\omega \boldsymbol{\varphi}(\omega)d\omega$.

This process can be very involved but permits the widest selection of basis functions for implementation in Brown symbols. Once the phase functions are calculated the Brown symbols can be compiled.

4.2.3 Symbol Synthesis. The phase functions are the key element in designing strong mutually dispersive symbols. Once the N phase functions have been calculated the Brown symbols maybe compiled. The resultant N-symbol family is represented, for $k = 0, 1, \ldots, N$, as

$$F_k(\omega) = \sqrt[4]{\frac{4\pi}{\Omega_0}} \cos^{\frac{1}{2}}\left(\frac{\pi\omega}{\Omega_0}\right) e^{J\Phi_k(\omega)} \mathrm{rect}\left(\frac{\omega}{\Omega_0}\right) \tag{4.3}$$

$$f_k(t) = \frac{1}{2\pi} \int_{-\frac{\Omega_0}{2}}^{\frac{\Omega_0}{2}} \sqrt[4]{\frac{4\pi}{\Omega_0}} \cos^{\frac{1}{2}}\left(\frac{\pi\omega}{\Omega_0}\right) e^{J[\Phi_k(\omega)+\omega t]} d\omega. \tag{4.4}$$

The phase functions are sampled and reconstructed as vectors in Matlab®. Care is taken to ensure that the frequency sample interval is chosen to avoid time-aliasing. The nth element of the kth sampled phase function is described as $\tilde{\Phi}_{kn} = \Phi_k(n\omega_0)$; the tilde notation is used to denote the sampled approximation to the continuous frequency or time function . Due to sampling in the frequency domain the corresponding time function will be periodic with period $T_0 = 2\pi/\omega_0$, therefore ω_0 is chosen to avoid aliasing such that $\omega_0 \leq 2\pi/T_0$. This is simply the converse to the time sampled analysis provided in Section 2.2.3. Each of the phase functions and the envelope $\tilde{A}_n = A(n\omega_0)$ are sampled in this manner to synthesize the spectral Brown symbols. The nth element of the kth Brown symbol, in frequency, is therefore defined as

$$\tilde{F}_{kn} = \tilde{A}_n e^{J\tilde{\Phi}_{kn}}. \tag{4.5}$$

As mentioned earlier, these symbols are constructed in Matlab®. Matlab® is a discrete simulation application that constrains further analysis to a numerical approximation. The corresponding time domain signal for each of the Brown symbols is

calculated using the rectangular-rule approximation to the Fourier transform, which is the DFT as shown in Eq (2.33). The resultant vector has an equivalent number of samples (N_s) and a time sample interval $t_0 = 2\pi/N_s\omega_0$. The nth element of the kth Brown symbol, in time, is defined as

$$
\begin{aligned}
\tilde{\text{f}}_{kn} &= \frac{1}{N_s} \sum_{l=0}^{N_s-1} \tilde{\text{F}}_{kl} \, e^{j2\pi ln/N_s} \\
&= \frac{1}{N_s} \sum_{l=0}^{N_s-1} \tilde{\text{A}}_l \, e^{j[\tilde{\Phi}_{kl}+2\pi ln/N_s]}.
\end{aligned}
\tag{4.6}
$$

Consequently, the results provided in this chapter are parameterized by the following: choice of basis $\varphi_k(\omega)$; number of symbols (N); bandwidth (Ω_0); and dispersive gain (G_D). The last of these, dispersive gain, was introduced in Section 3.5.2 as a factor that uniformly increases the length of the vectors that solve the Hermit Problem, thereby controlling the dispersion induced in the crosscorrelation functions.

4.3 Brown Symbol Sensitivity

Brown's theorem indicates that the resultant symbols exhibit properties that are insensitive to changes in basis. However, this is only in consideration of the rms time duration of the correlation functions. This section considers a number of different bases illustrating that although the theoretical results are achieved independent of basis, the form of the correlation functions vary.

Unless otherwise stipulated, the results provided in this section are generated using a bandwidth of $\Omega_0 = 8\pi$. Under this condition the theoretical rms time duration for the autocorrelation function is $\sigma_{kk}^2 = \pi^2/\Omega_0^2 = 0.0156$, and for the crosscorrelation functions is $\sigma_{lk}^2 = \pi^2/\Omega_0^2 + (2G_D N)/(N-1)$, which for a symbol family of $N = 3$, and $G_D = 0$ dB, is 3.0156.

4.3.1 Sinusoidal Basis. Sinusoids are an obvious choice as basis functions due to their orthogonality properties. Appendix B.1 derives the generation of an N-dimensional set of sinusoidal basis functions that retain orthonormality within the weighted inner product space. The general form for each element in this set of basis functions is described in Eq (4.7).

$$\varphi_n(\omega) \triangleq \sqrt{2}\sin(a_n\omega), \tag{4.7}$$

therefore

$$\Phi_k(\omega) = \sum_{n=0}^{N-1} -\frac{\sqrt{2G_D}c_{kn}}{a_n}\cos(a_n\omega), \tag{4.8}$$

where a_n is an arbitrary positive integer and c_{kn} is the nth element of the kth solution to the Hermit Problem. As indicated in Appendix B.1, for orthogonality to be exactly met, this basis requires the bandwidth to be an even integer multiple of π, *i.e.*, $\Omega_0 = 2m\pi$, $m \in \mathcal{Z}$. The synthesized Brown symbols are then of the form

$$F_k(\omega) = \sqrt[4]{\frac{4\pi}{\Omega_0}}\cos^{\frac{1}{2}}\left(\frac{\pi\omega}{\Omega_0}\right)e^{-j\left[\sum_{n=0}^{N-1}\frac{\sqrt{2G_D}c_{kn}}{a_n}\cos(a_n\omega)\right]}\text{rect}\left(\frac{\omega}{\Omega_0}\right) \tag{4.9}$$

$$f_k(t) = \frac{1}{2\pi}\int_{-\frac{\Omega_0}{2}}^{\frac{\Omega_0}{2}}\sqrt[4]{\frac{4\pi}{\Omega_0}}\cos^{\frac{1}{2}}\left(\frac{\pi\omega}{\Omega_0}\right)e^{j\left[\omega t-\sum_{n=0}^{N-1}\frac{\sqrt{2G_D}c_{kn}}{a_n}\cos(a_n\omega)\right]}d\omega. \tag{4.10}$$

A closed form solution to Eq (4.10) is unlikely to exist, however, a numerical approximation to this function provides a means of analysis. This approach does not detract from the end result of physical implementation as the sampled form of $f_k(t) \Rightarrow t_0 f_k(nt_0) = \tilde{f}_{kn}$ is the code that a digital radar system would utilize, with parameters such as sample interval governed by hardware specifics.

These symbols are synthesized, as detailed in Section 4.2.3, for a code family of $N = 3$ symbols. A dB plot of the autocorrelation function, which is the same for each symbol, is displayed in Figure 4.1. The x-axis describes the time lag and the

y-axis describes the amplitude, in decibels. The metrics described in Table 4.1 have

Figure 4.1.   Autocorrelation function for a sinusoidal basis with $N = 3$, $G_D = 0$ dB, and $\mathbf{a} = [13\ 18\ 23]^T$.

been calculated from these crosscorrelation functions.

Table 4.1.   Autocorrelation metrics for a sinusoidal basis with $N = 3$, $G_D = 0$ dB, and $\mathbf{a} = [13\ 18\ 23]^T$.

$\rho_{lk}(t)$	PSL [dB]	ISL [dB]	σ_{kk}^2
$\rho_{00}(t)$	-23.000	-18.931	0.016
$\rho_{11}(t)$	-23.000	-18.931	0.016
$\rho_{22}(t)$	-23.000	-18.931	0.016

A dB plot of the crosscorrelation functions is displayed in Figure 4.2. The x-axis describes the time lag and the y-axis describes the amplitude, in decibels. The metrics described in Table 4.2 have been calculated from these crosscorrelation functions. Although the theoretical results for σ_{kk}^2 and σ_{kl}^2 are achieved the cross-correlation plots do not show strong dispersive properties resulting in undesirably small values of PCCL and dominant sidelobes. By increasing the dispersive gain
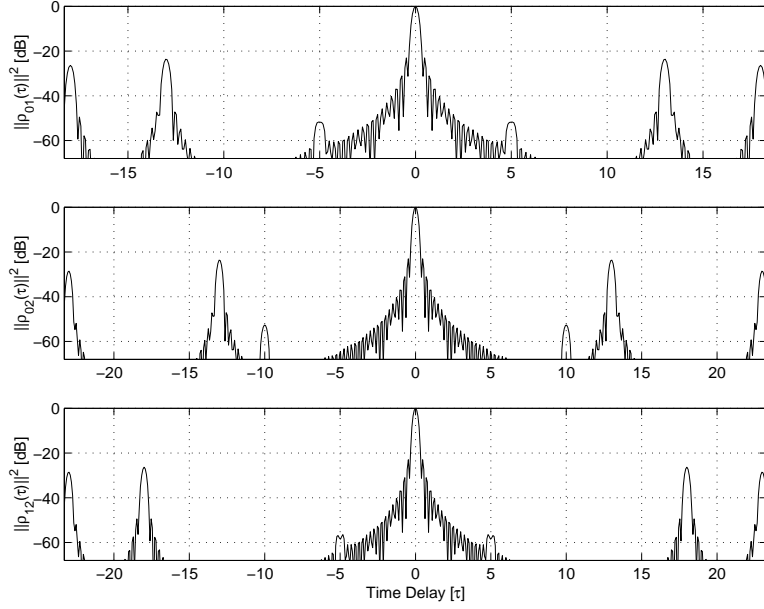
Figure 4.2. Crosscorrelation functions for a sinusoidal basis with $N = 3$, $G_D = 0$ dB, and $\mathbf{a} = [13 \ 18 \ 23]^T$.

Table 4.2. Crosscorrelation metrics for a sinusoidal basis with $N = 3$, $G_D = 0$ dB, and $\mathbf{a} = [13 \ 18 \ 23]^T$.

$\rho_{lk}(t)$	PCCL [dB]	σ_{kl}^2
$\rho_{01}(t)$	-0.059	3.016
$\rho_{02}(t)$	-0.051	3.016
$\rho_{12}(t)$	-0.032	3.016

the amount of spread is controlled. Figures 4.3 and 4.4 illustrate the effect on the crosscorrelation functions of increasing G_D to 20 and 40 dB respectively.   The

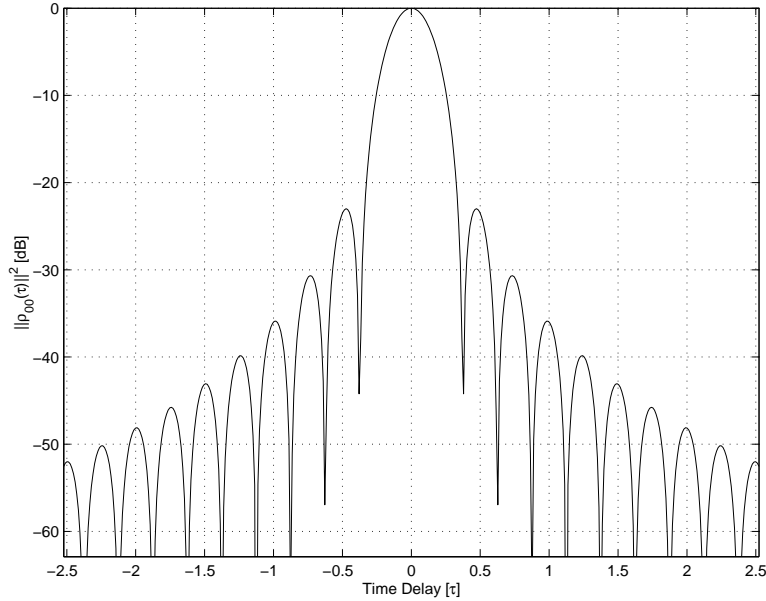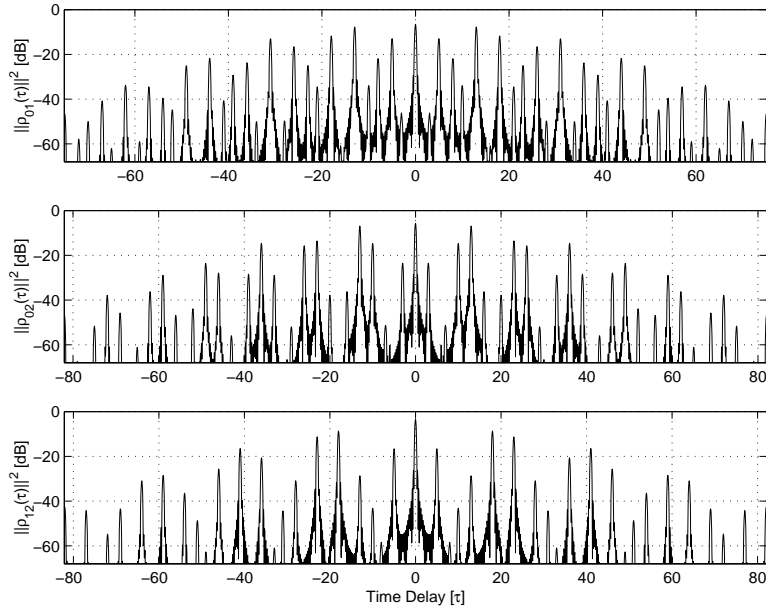
Figure 4.3.   Crosscorrelation functions for a sinusoidal basis with $N = 3$, $G_D = 20$ dB, and $\mathbf{a} = [13\ 18\ 23]^T$.

Table 4.3.   Crosscorrelation metrics for a sinusoidal basis with $N = 3$, $G_D = 20$ dB, and $\mathbf{a} = [13\ 18\ 23]^T$.

$\rho_{lk}(t)$	PCCL [dB]	σ_{kl}^2
$\rho_{01}(t)$	-6.537	300.016
$\rho_{02}(t)$	-5.670	300.016
$\rho_{12}(t)$	-3.420	300.016

metrics described in Tables 4.3 and 4.4 have been calculated from these correlation functions shown in Figures 4.3 and 4.4 respectively.

Increasing the dispersive gain, G_D, has the effect of improving the dispersive properties of the crosscorrelation functions without affecting the autocorrelation functions. To improve the compression of the autocorrelation function the bandwidth must be increased as illustrated (for a sinusoidal basis) in Figure 4.5. This
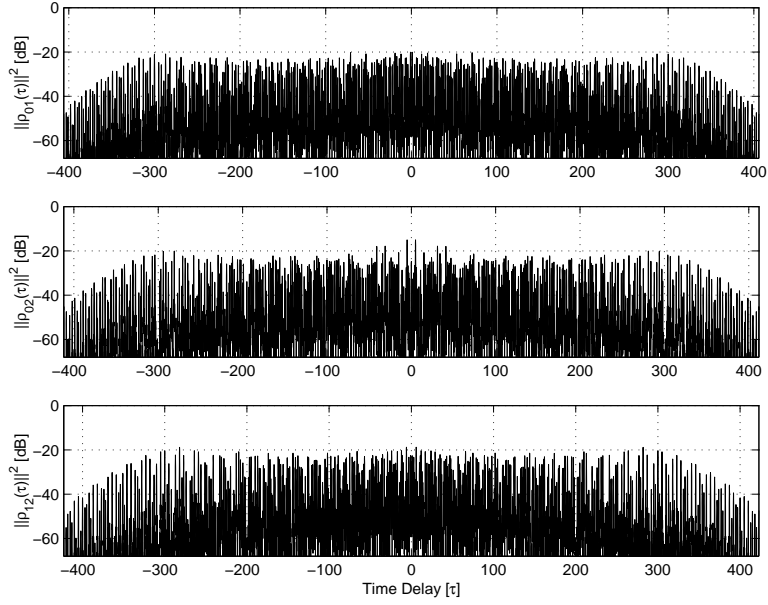
Figure 4.4.   Crosscorrelation functions for a sinusoidal basis with $N = 3$, $G_D = 40$ dB, and $\mathbf{a} = \begin{bmatrix} 13 \ 18 \ 23 \end{bmatrix}^T$.

Table 4.4.   Crosscorrelation metrics for a sinusoidal basis with $N = 3$, $G_D = 40$ dB, and $\mathbf{a} = \begin{bmatrix} 13 \ 18 \ 23 \end{bmatrix}^T$.

$\rho_{lk}(t)$	PCCL [dB]	σ_{kl}^2
$\rho_{01}(t)$	-19.985	30000.016
$\rho_{02}(t)$	-14.925	30000.016
$\rho_{12}(t)$	-18.789	30000.016

basis achieves the theoretical Brown autocorrelation performance, as a function of bandwidth.
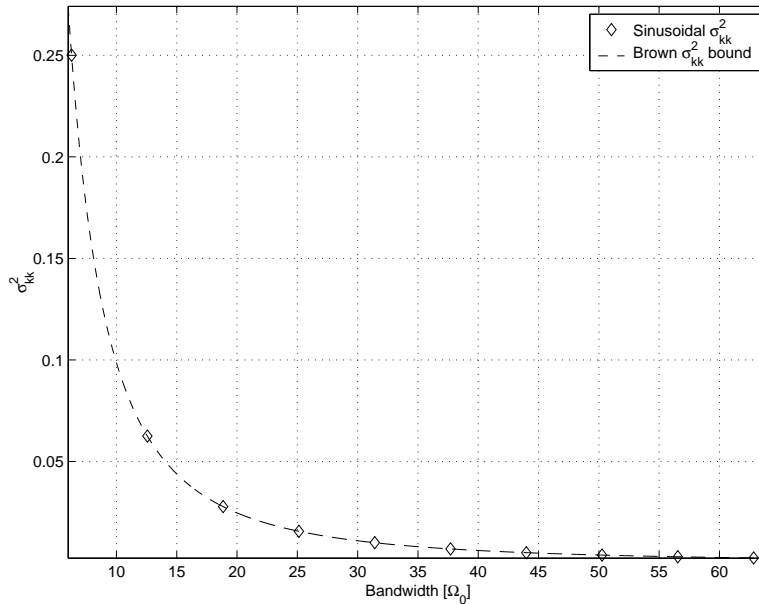
Figure 4.5. σ_{kk}^2 for a sinusoidal basis with $G_D = 0$ dB and $\mathbf{a} = [13\ 18\ 23]^T$.

The performance of the crosscorrelation in terms of rms time duration is considered in relation to the number of symbols (N). Figure 4.6 indicates that the theoretical Brown crosscorrelation result, for symbol families with $N = 2,\ 3,\ \ldots,\ 7$, is also achieved with the sinusoidal basis. Although the crosscorrelation dispersion decreases with an increase in the number of symbols, increasing the dispersive gain offsets this effect.

This section demonstrated that the sinusoidal basis is a valid basis for any size symbol family, achieving the theoretical Brown results in each case. This, however, says nothing of the suitability of these symbols for physical implementation or their comparative performance. These aspects are now considered.

4.3.1.1   Realizable Brown Symbols.   Brown symbols are bandlimited and therefore unlimited in time. However, a physical implementation of these sym-
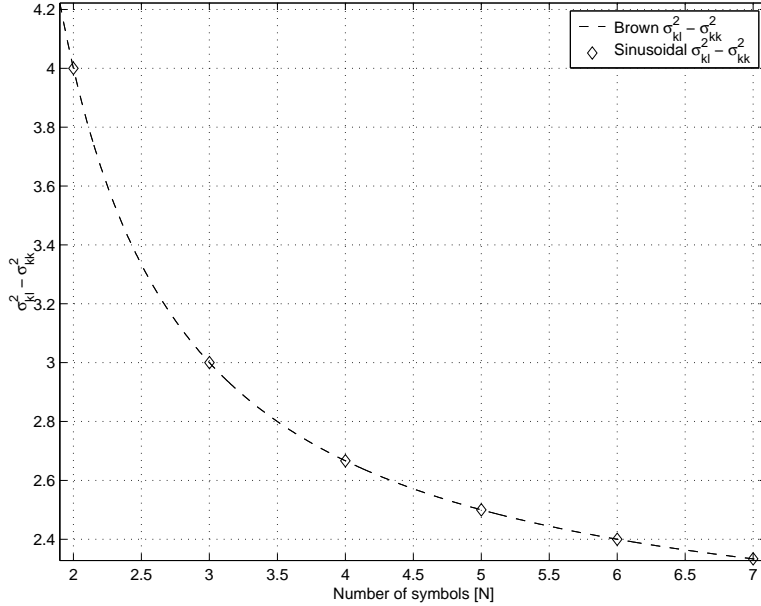
Figure 4.6. $\sigma_{kl}^2 - \sigma_{kk}^2$ for a sinusoidal basis with $G_D = 0$ dB and $\mathbf{a} = [13\ 18\ 23]^T$.

bols requires them to be time-limited. Consequently, an analysis of windowed Brown symbols is provided. Following this a comparison is made between the performance of a pair of sinusoidal Brown symbols and the conjugate LFM symbols used in the initial demonstration by Palermo [28].

The requirement to transmit time-limited symbols leads to an analysis of windowed Brown symbols. In this analysis a rectangular window, $w(t)$, of unit height is employed to create a time-limited Brown symbol,

$$w(t) = \text{rect}\left(\frac{t}{T_w}\right), \tag{4.11}$$

where T_w is the width of the window. The window will zero the tails of the Brown symbols for $f_k(t)$, $|t| \geq T_w/2$. Figure 4.7 illustrates, for Brown symbols generated with various dispersive gains, that the signal energy becomes more concentrated as the dispersive gain is increased. The x-axis describes the dispersive gain, in decibels,

4-11

and the y-axis describes the relative half-window width $T_w/2$ as a fraction of the rms time duration of the Brown symbol σ_k.
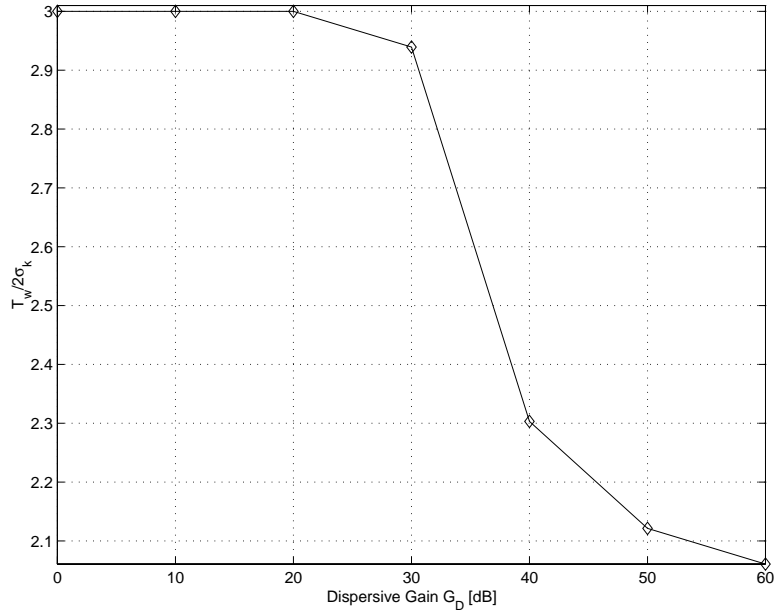
Figure 4.7.   Relative window duration $T_w/2\sigma_k$ required to capture 99.9% of signal energy as a function of dispersive gain G_D.

Accordingly, Brown symbols generated using a large dispersive gain are more compact and are therefore better suited to windowing. Figure 4.8 displays the effect that shortening the window width has on the properties of the crosscorrelation function. Notably, the effect of windowing Brown symbols becomes insignificant for $T_w/2 \approx 2.5\ \sigma_k$. Therefore the performance of Brown symbols is not significantly degraded due to windowing, for large dispersive gain, suggesting that these symbols are easily modified for physical implementation.

Originally Palermo utilized conjugate LFM pulses to demonstrate the effectiveness of NLS. Unfortunately the number of conjugate LFM is limited to $N = 2$. Having demonstrated that Brown symbols may be windowed for physical implementation a comparison is now provided between the characteristics of sinusoidal Brown symbols and conjugate LFM. In this comparison symbols are generated hav-
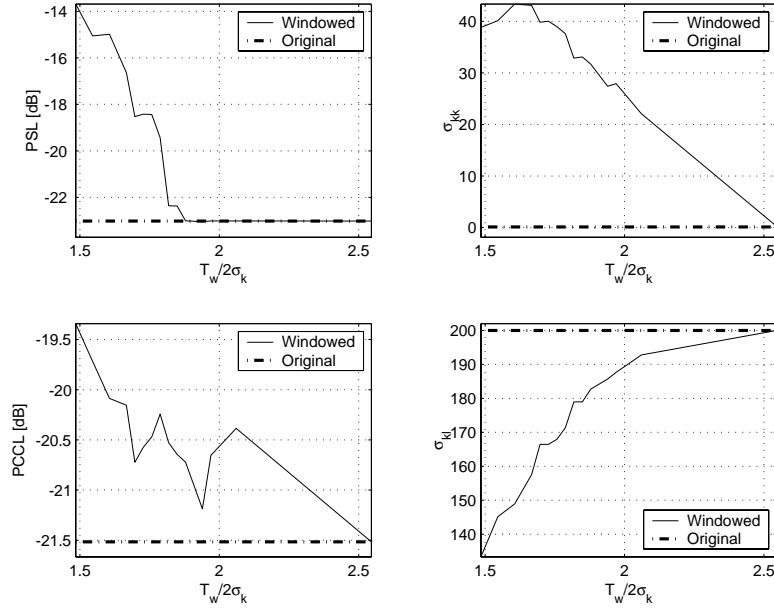
Figure 4.8. Correlation function statistics for windowed Brown sym-
bols with sinusoidal basis for $N = 2$, $G_D = 40$ dB, and
$\mathbf{a} = [13\ 18]^T$. (a) PSL, (b) σ_{kk}, (c) PCCL, and (d) σ_{kl}.

ing equivalent rms time duration and energy. The results, in Figure 4.9, illustrate
the comparative performance. Brown symbols, being optimized for rms time dura-
tion of the correlation function, show equivalent or better performance in all areas
except the peak crosscorrelation level (PCCL). Figure 4.9 (c) shows that the Brown
symbols exhibit approximately 10 dB worse PCCL than conjugate LFM. However,
Brown symbols exhibit consistent performance when compared with conjugate LFM,
and unlike conjugate LFM, Brown symbols are not limited in symbol family size.

4.3.2 Polynomial Basis.   Polynomials have been shown in various applica-
tions to exhibit strong orthogonality properties, as illustrated by the set of Chebyshev
polynomials, Hermite functions, Legendre polynomials and so on [36:136-160] [16:25-
36]. Unfortunately, these specific sets are orthogonal only within a unity weighted
inner product space requiring further analysis for adaptation to optimal Brown sym-
bols. The design of polynomial basis for use in Brown codes is explored in this
section.
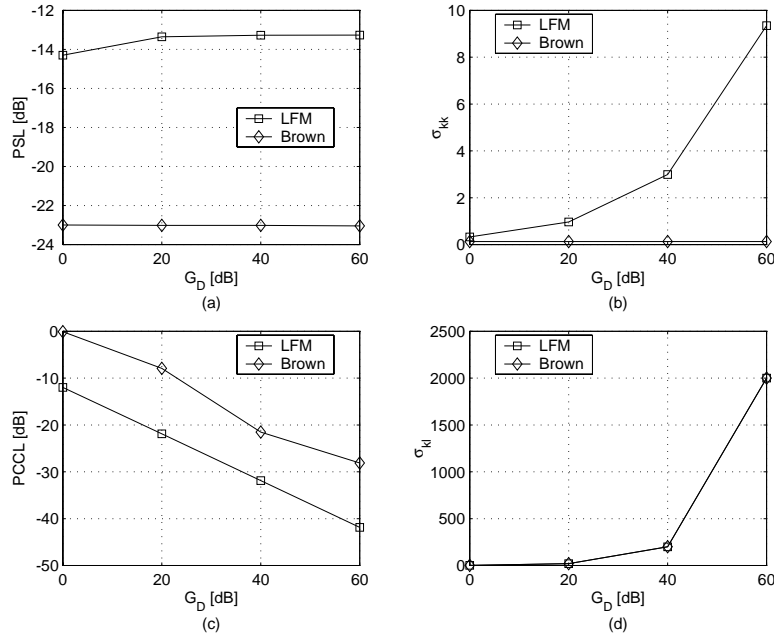
Figure 4.9.   Correlation function statistics for conjugate LFM and Brown symbols with sinusoidal basis for $N = 2$ and $\mathbf{a} = [13\ 18]^T$. (a) PSL, (b) σ_{kk}, (c) PCCL, and (d) σ_{kl}.

Appendix B.2 shows that an N-dimensional set of polynomial basis functions, which retain orthonormality within the weighted inner product space, can be generated. The general form for each element in this set of basis functions, is described in Eq (4.12). Each basis element $\varphi_n(\omega)$, of order $2p - 1$, is a weighted set of odd polynomials:

$$\varphi_n(\omega) \triangleq \sum_{m=0}^{p-1} \mathrm{b}_{nm}\omega^{2m+1}. \tag{4.12}$$

where b_{nm} is the element in the mth row of the nth column of the matrix $\mathbf{B}$ defined in Eq (B.12). Therefore

$$\begin{aligned}
\Phi_k(\omega) &= \sum_{n=0}^{N-1} \sqrt{G_D}\mathrm{c}_{kn} \sum_{m=0}^{p-1} \mathrm{b}_{nm}\frac{\omega^{2m+2}}{2m+2} \\
&= \sqrt{G_D}\mathbf{c}_k^T\mathbf{B}^T \int_\omega \boldsymbol{\varphi}(\omega)d\omega, \tag{4.13}
\end{aligned}$$

4-14

where $\mathbf{c}_k$ is the kth solution to the Hermit Problem. The synthesized Brown symbols are therefore

$$F_k(\omega) = \sqrt[4]{\frac{4\pi}{\Omega_0}} \cos^{\frac{1}{2}}\left(\frac{\pi\omega}{\Omega_0}\right) e^{\jmath\left[\sqrt{G_D}\mathbf{c}_k^T\mathbf{B}^T \int_\omega \boldsymbol{\varphi}(\omega)d\omega\right]} \text{rect}\left(\frac{\omega}{\Omega_0}\right) \qquad (4.14)$$

$$f_k(t) = \frac{1}{2\pi} \int_{-\frac{\Omega_0}{2}}^{\frac{\Omega_0}{2}} \sqrt[4]{\frac{4\pi}{\Omega_0}} \cos^{\frac{1}{2}}\left(\frac{\pi\omega}{\Omega_0}\right) e^{\jmath\left[\omega t + \sqrt{G_D}\mathbf{c}_k^T\mathbf{B}^T \int_\omega \boldsymbol{\varphi}(\omega)d\omega\right]} d\omega. \qquad (4.15)$$

As was the case with Eq (4.10), a closed form solution to Eq (4.15) is unlikely to exist, however, a numerical approximation to this function again provides a means of analysis.

These symbols are synthesized, as detailed in Section 4.2.3, for a code family of $N = 3$ symbols. A dB plot of the autocorrelation function, which is the same for each symbol, is displayed in Figure 4.10. The x-axis describes the time lag and the y-axis describes the amplitude, in decibels. The metrics described in Table 4.5 have
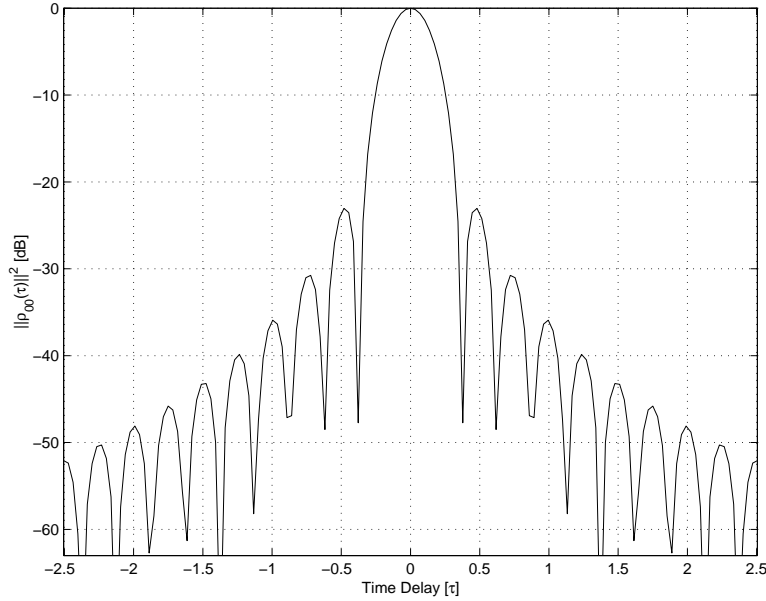
Figure 4.10.   Autocorrelation function for a polynomial basis with $N = 3$ and $G_D = 0$ dB.

been calculated from these crosscorrelation functions.

Table 4.5.   Autocorrelation metrics for a polynomial basis with $N = 3$
and $G_D = 0$ dB.

$\rho_{lk}(t)$	PSL [dB]	ISL [dB]	σ^2_{kk}
$\rho_{00}(t)$	-23.048	-18.975	0.016
$\rho_{11}(t)$	-23.048	-18.975	0.016
$\rho_{22}(t)$	-23.048	-18.975	0.016

A dB plot of the crosscorrelation functions is displayed in Figure 4.11. The x-axis describes the time lag and the y-axis describes the amplitude, in decibels. The
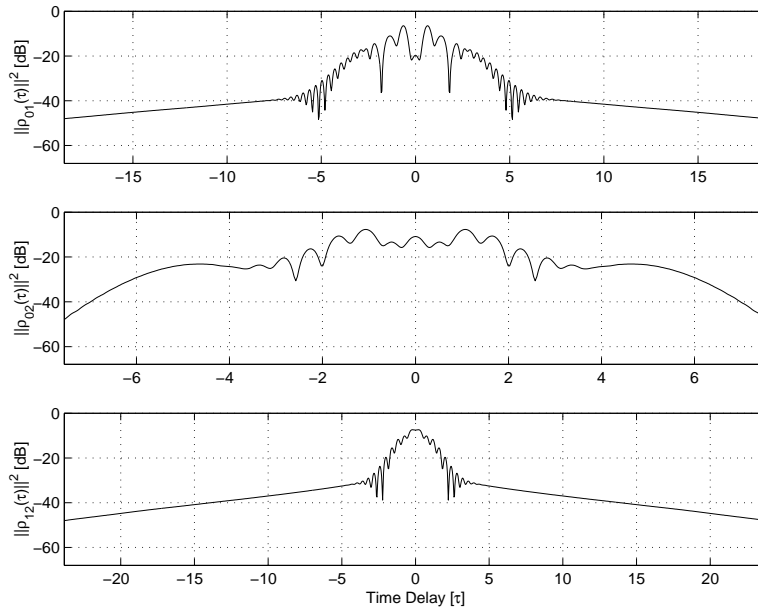
Figure 4.11.   Crosscorrelation functions for a polynomial basis with
$N = 3$ and $G_D = 0$ dB.

metrics described in Table 4.6 have been calculated from these correlation functions.

Again, although the polynomial basis has achieved the theoretical results for σ^2_{kk} and σ^2_{kl}, these crosscorrelation plots also fail to show strong dispersive properties. By increasing the dispersive gain the amount of spread is controlled. Figures 4.12 and 4.13 illustrate the effect on the crosscorrelation functions of increasing G_D to

Table 4.6. Crosscorrelation metrics for a polynomial basis with $N = 3$
and $G_D = 0$ dB.

$\rho_{lk}(t)$	PCCL [dB]	σ_{kl}^2
$\rho_{01}(t)$	-6.482	3.016
$\rho_{02}(t)$	-7.690	3.016
$\rho_{12}(t)$	-7.382	3.016

20 and 40 dB respectively. The metrics described in Tables 4.7 and 4.8 have
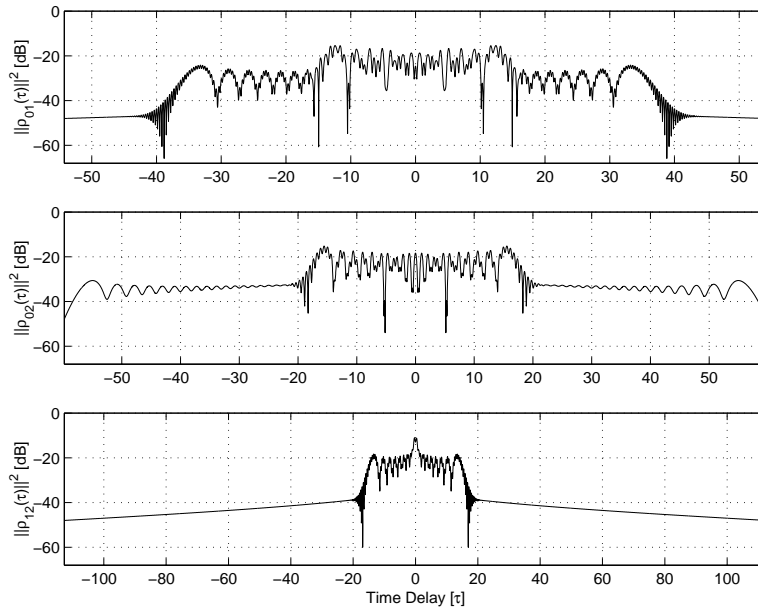
Figure 4.12. Crosscorrelation functions for a polynomial basis with
$N = 3$ and $G_D = 20$ dB.

been calculated from the crosscorrelation functions shown in Figures 4.12 and 4.13
respectively. This section demonstrated that the polynomial basis is a valid basis
for any size symbol family, achieving the theoretical results in each case.

4.3.3 Chebyshev Basis. Appendix B.3 shows that an N-dimensional set
of Chebyshev basis functions can be generated when a non-ideal uniform spectral
envelope is employed. Under this condition the nth element in the set of Chebyshev
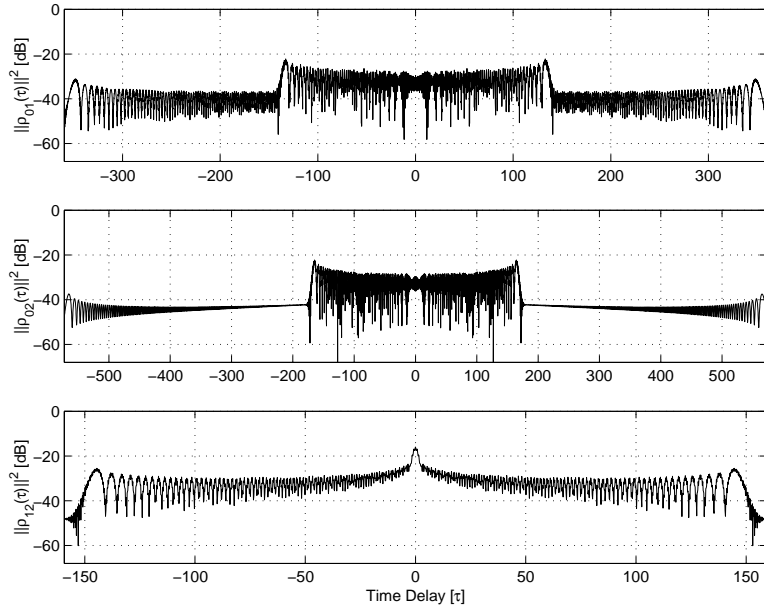
Figure 4.13.   Crosscorrelation functions for a polynomial basis with
                 $N = 3$ and $G_D = 40$ dB.

Table 4.7.   Crosscorrelation metrics for a polynomial basis with $N = 3$
               and $G_D = 20$ dB.

$\rho_{lk}(t)$	PCCL [dB]	σ_{kl}^2
$\rho_{01}(t)$	-15.407	300.016
$\rho_{02}(t)$	-15.187	300.016
$\rho_{12}(t)$	-11.159	300.016

Table 4.8.   Crosscorrelation metrics for a polynomial basis with $N = 3$
               and $G_D = 40$ dB.

$\rho_{lk}(t)$	PCCL [dB]	σ_{kl}^2
$\rho_{01}(t)$	-22.189	30000.016
$\rho_{02}(t)$	-22.264	30000.016
$\rho_{12}(t)$	-15.978	30000.016

4-18

basis functions is described in Eq (4.16)

$$\varphi_n(\omega) \triangleq \frac{\sqrt{\frac{2\Omega_0}{\pi}} T_{2n+1}\left(\frac{2\omega}{\Omega_0}\right)}{\sqrt[4]{\frac{\Omega_0^2}{4} - \omega^2}}, \tag{4.16}$$

where $T_k(\omega)$ is a kth order Chebyshev polynomial defined in Eq (B.14). For orthonormality the envelope is uniform over Ω_0 and is defined as

$$A(\omega) = \sqrt{\frac{2\pi}{\Omega_0}} \text{rect}\left(\frac{\omega}{\Omega_0}\right), \tag{4.17}$$

and the phase function of the kth symbol is defined as

$$\Phi_k(\omega) = \sum_{n=0}^{N-1} \sqrt{G_D} c_{kn} \int_\omega \frac{\sqrt{\frac{2\Omega_0}{\pi}} T_{2n+1}\left(\frac{2\omega}{\Omega_0}\right)}{\sqrt[4]{\frac{\Omega_0^2}{4} - \omega^2}} d\omega, \tag{4.18}$$

where c_{kn} is the nth element of the kth solution to the Hermit Problem. The synthesized Brown symbols are then

$$F_k(\omega) = \sqrt[4]{\frac{2\pi}{\Omega_0}} e^{\jmath\Phi_k(\omega)} \text{rect}\left(\frac{\omega}{\Omega_0}\right) \tag{4.19}$$

$$f_k(t) = \frac{1}{2\pi} \int_{-\frac{\Omega_0}{2}}^{\frac{\Omega_0}{2}} \sqrt[4]{\frac{2\pi}{\Omega_0}} e^{\jmath[\omega t + \Phi_k(\omega)]} d\omega \tag{4.20}$$

Again, a closed form solution to Eq (4.20) is unlikely to exist, however, a numerical approximation to this function provides a means of analysis.

These symbols are synthesized, as detailed in Section 4.2.3, for a code family of $N = 3$ symbols. A dB plot of the autocorrelation function, which is the same for each symbol, is displayed in Figure 4.14. The x-axis describes the time lag and the y-axis describes the amplitude, in decibels. The metrics described in Table 4.9 have been calculated from these crosscorrelation functions.

Figure 4.14.   Autocorrelation function for a Chebyshev basis with $N = 3$ and $G_D = 0$ dB.

Table 4.9.   Autocorrelation metrics for a Chebyshev basis with $N = 3$ and $G_D = 0$ dB.

$\rho_{lk}(t)$	PSL [dB]	ISL [dB]	σ_{kk}^2
$\rho_{00}(t)$	-13.267	-7.076	316.033
$\rho_{11}(t)$	-13.267	-7.076	316.033
$\rho_{22}(t)$	-13.267	-7.076	316.033

A dB plot of the crosscorrelation functions is displayed in Figure 4.15. The x-axis describes the time lag and the y-axis describes the amplitude, in decibels. The metrics described in Table 4.10 have been calculated from these crosscorrelation

Figure 4.15.   Crosscorrelation functions for a Chebyshev basis with $N = 3$ and $G_D = 0$ dB.

functions.

Table 4.10.   Crosscorrelation metrics for a Chebyshev basis with $N = 3$ and $G_D = 0$ dB.

$\rho_{lk}(t)$	PCCL [dB]	σ_{kl}^2
$\rho_{01}(t)$	-8.983	319.033
$\rho_{02}(t)$	-8.564	319.033
$\rho_{12}(t)$	-9.034	319.033

Although the Chebyshev basis provides worse autocorrelation compression, for the same dispersive gain the PCCLs are better than for the sinusoidal and polynomial bases. Notably, a the non-ideal envelope provides worse compression but better dispersion, normally this would lead to an envelope design trade-off between

dispersion and compression. However, the dispersive gain controls dispersion enough to accommodate for any trade-off that might otherwise have been necessary. Figures 4.16 and 4.17 illustrate the effect on the crosscorrelation functions of increasing G_D to 20 and 40 dB respectively. The metrics described in Tables 4.11 and 4.12
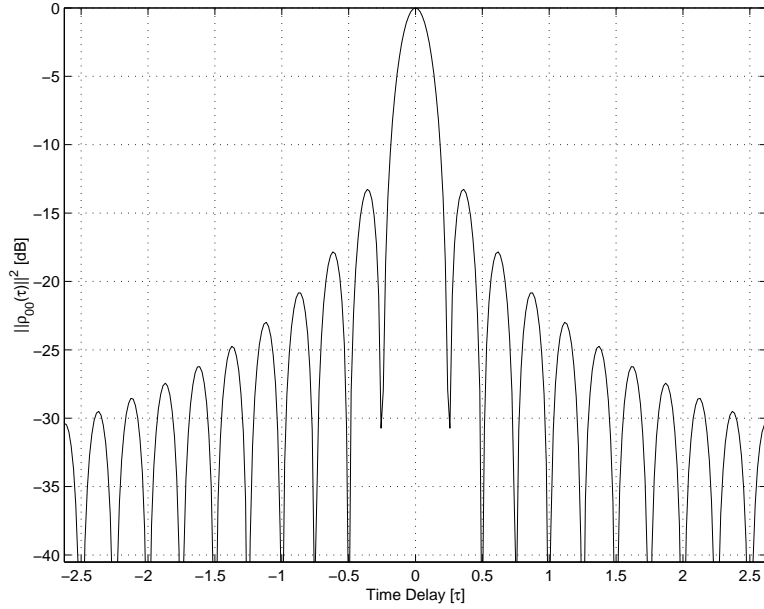

Figure 4.16. Crosscorrelation functions for a Chebyshev basis with $N = 3$ and $G_D = 20$ dB.

Table 4.11. Crosscorrelation metrics for a Chebyshev basis with $N = 3$ and $G_D = 20$ dB.

$\rho_{lk}(t)$	PCCL [dB]	σ_{kl}^2
$\rho_{01}(t)$	-16.066	616.029
$\rho_{02}(t)$	-15.617	616.029
$\rho_{12}(t)$	-16.830	616.029

have been calculated from these correlation functions shown in Figures 4.16 and 4.17 respectively.

As expected, the change in $A(\omega)$ to a non-ideal rectangular window results in worse performance of the autocorrelation function, *i.e.*, larger σ_{kk}^2, however mutual
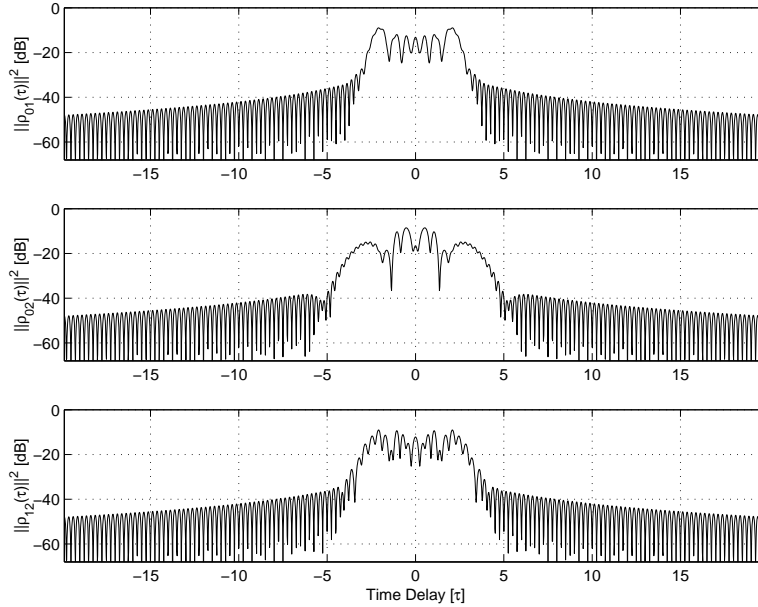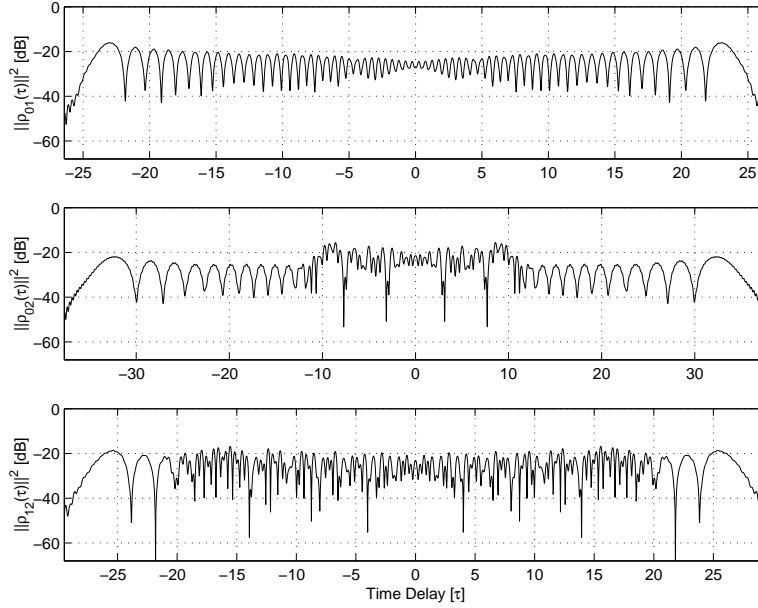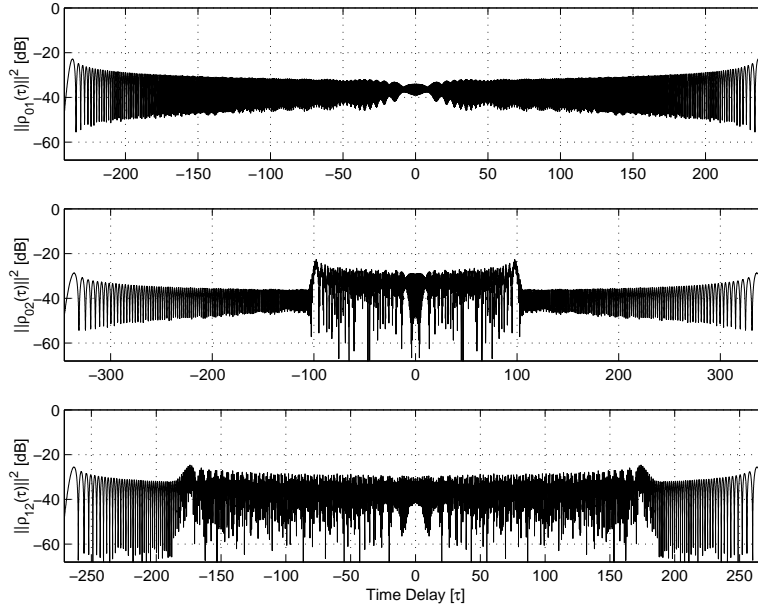
Figure 4.17.   Crosscorrelation functions for a Chebyshev basis with $N = 3$ and $G_D = 40$ dB.

Table 4.12.   Crosscorrelation metrics for a Chebyshev basis with $N = 3$ and $G_D = 40$ dB.

$\rho_{lk}(t)$	PCCL [dB]	σ_{kl}^2
$\rho_{01}(t)$	-22.780	30315.616
$\rho_{02}(t)$	-22.655	30315.616
$\rho_{12}(t)$	-24.680	30315.616

dispersion is exhibited due to orthonormality in the basis set. The control on dispersion offered by the dispersive gain accommodates any envelope design trade-off that might be made of worse compression for increased dispersion. This section analyzes the Chebyshev basis, for any size symbol family, showing that although the results are suboptimal the characteristics of the crosscorrelation functions are mutually dispersive and well suited to NLS.

4.3.4 Piecewise Continuous Basis. Appendix B.4 shows that a set of N orthonormal piecewise basis functions can be generated using the uniform taper applied previously for the Chebyshev case. The general form for each element in this set of basis functions is defined in Eq (B.19) as

$$
\varphi_n(\omega) \triangleq \frac{4\sqrt{3}\mathrm{a}_n}{\Omega_0} \left[(\omega + \Omega_0/2)\mathrm{rect}\!\left(\frac{\omega + \Omega_0/2 - \Omega_n/8}{\Omega_n/4}\right) \right.
$$
$$
+ \sum_{m=1}^{2\mathrm{a}_n - 1} (-1)^m (\omega + \omega_m)\mathrm{rect}\!\left(\frac{\omega - \omega_m}{\Omega_n/2}\right)
$$
$$
\left. + (\omega - \Omega_0/2)\mathrm{rect}\!\left(\frac{\omega - \Omega_0/2 + \Omega_n/8}{\Omega_n/4}\right) \right], \tag{4.21}
$$

therefore

$$
\Phi_k(\omega) = \sum_{n=0}^{N-1} \sqrt{G_D}\, c_{kn} \frac{4\sqrt{3}\mathrm{a}_n}{2\Omega_0} \left[(\omega^2 + \Omega_0\omega)\mathrm{rect}\!\left(\frac{\omega + \Omega_0/2 - \Omega_n/8}{\Omega_n/4}\right) \right.
$$
$$
+ \sum_{m=1}^{2\mathrm{a}_n - 1} (-1)^m (\omega^2 + 2\omega_m\omega)\mathrm{rect}\!\left(\frac{\omega - \omega_m}{\Omega_n/2}\right)
$$
$$
\left. + (\omega^2 - \Omega_0\omega)\mathrm{rect}\!\left(\frac{\omega - \Omega_0/2 + \Omega_n/8}{\Omega_n/4}\right) \right], \tag{4.22}
$$

where c_{kn} is the nth element of the kth solution to the Hermit Problem. The synthesized Brown symbols are then of the form

$$
F_k(\omega) = \sqrt[4]{\frac{4\pi}{\Omega_0}} \cos^{\frac{1}{2}}\!\left(\frac{\pi\omega}{\Omega_0}\right) \mathrm{e}^{-\jmath\Phi_k(\omega)} \mathrm{rect}\!\left(\frac{\omega}{\Omega_0}\right) \tag{4.23}
$$

$$f_k(t) \;=\; \frac{1}{2\pi} \int_{-\frac{\Omega_0}{2}}^{\frac{\Omega_0}{2}} \sqrt[4]{\frac{4\pi}{\Omega_0}} \cos^{\frac{1}{2}}\left(\frac{\pi\omega}{\Omega_0}\right) e^{j[\omega t + \Phi_k(\omega)]} d\omega. \tag{4.24}$$

Again, a closed form solution to Eq (4.24) is unlikely to exist, so a numerical approximation to this function is considered.

These symbols are synthesized, as detailed in Section 4.2.3, for a code family of $N = 3$ symbols. A dB plot of the autocorrelation function, which is the same for each symbol, is displayed in Figure 4.18. The x-axis describes the time lag and the y-axis describes the amplitude, in decibels. The metrics described in Table 4.13
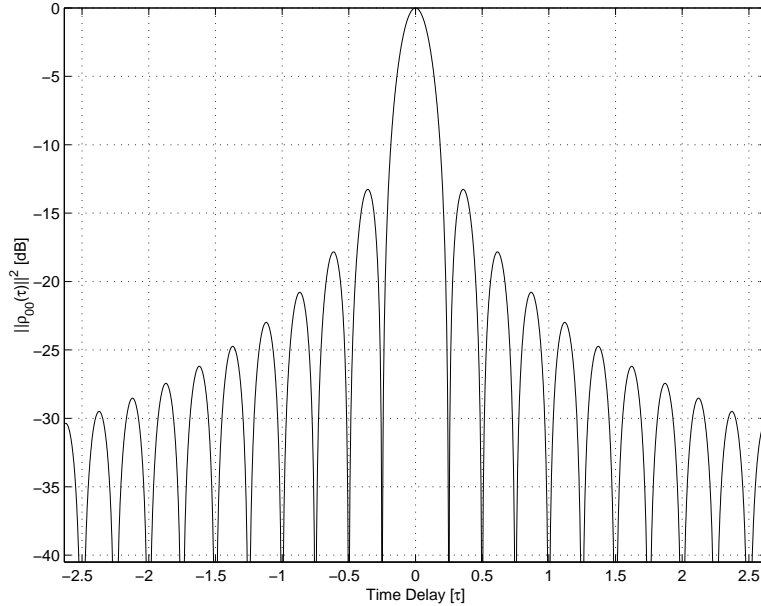
Figure 4.18.   Autocorrelation function for a piecewise basis with $N = 3$, $G_D = 0$ dB, and $\mathbf{a} = [1\ 2\ 4]^T$.

have been calculated from these crosscorrelation functions.

A dB plot of the crosscorrelation functions is displayed in Figure 4.19. The x-axis describes the time lag and the y-axis describes the amplitude, in decibels. The metrics described in Table 4.14 have been calculated from these crosscorrelation functions. The correlation plots exhibit similar characteristics to the Chebyshev basis, having less compression on the autocorrelation function and slightly better

Table 4.13.   Autocorrelation metrics for a piecewise basis with $N = 3$, $G_D = 0$ dB, and $\mathbf{a} = [1\ 2\ 4]^T$.

$\rho_{lk}(t)$	PSL [dB]	ISL [dB]	σ_{kk}^2
$\rho_{00}(t)$	-13.262	-7.109	63.203
$\rho_{11}(t)$	-13.262	-7.109	63.203
$\rho_{22}(t)$	-13.262	-7.109	63.203
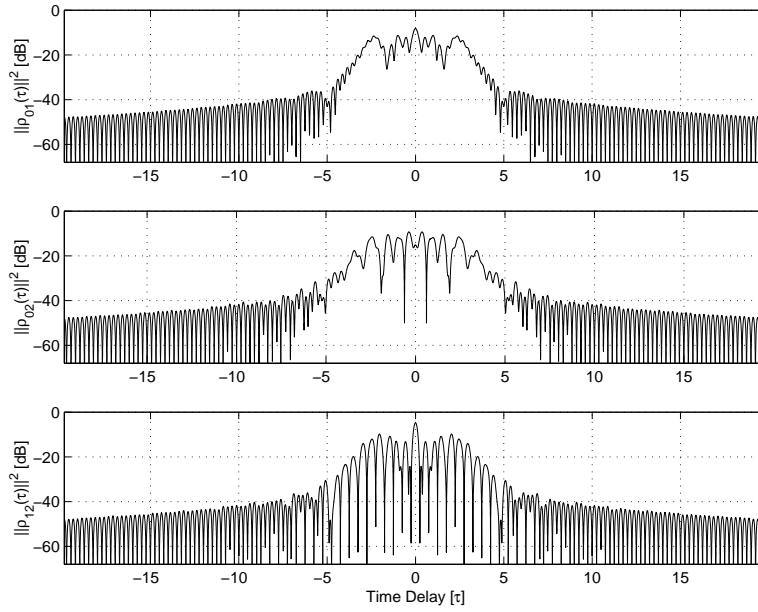
Figure 4.19.   Crosscorrelation functions for a piecewise basis with $N = 3$, $G_D = 0$ dB, and $\mathbf{a} = [1\ 2\ 4]^T$.

Table 4.14.   Crosscorrelation metrics for a piecewise basis with $N = 3$, $G_D = 0$ dB, and $\mathbf{a} = [1\ 2\ 4]^T$.

$\rho_{lk}(t)$	PCCL [dB]	σ_{kl}^2
$\rho_{01}(t)$	-8.187	66.203
$\rho_{02}(t)$	-9.307	66.203
$\rho_{12}(t)$	-4.788	66.203

dispersion on the crosscorrelation functions. The orthonormality in the basis provides the theoretical values for the dispersive term and the form of the correlation functions is suited to NLS, being similar to that of the Chebyshev and polynomial bases. Figures 4.20 and 4.21 illustrate the effect on the crosscorrelation functions of increasing G_D to 20 and 40 dB respectively. The metrics described in Tables 4.15
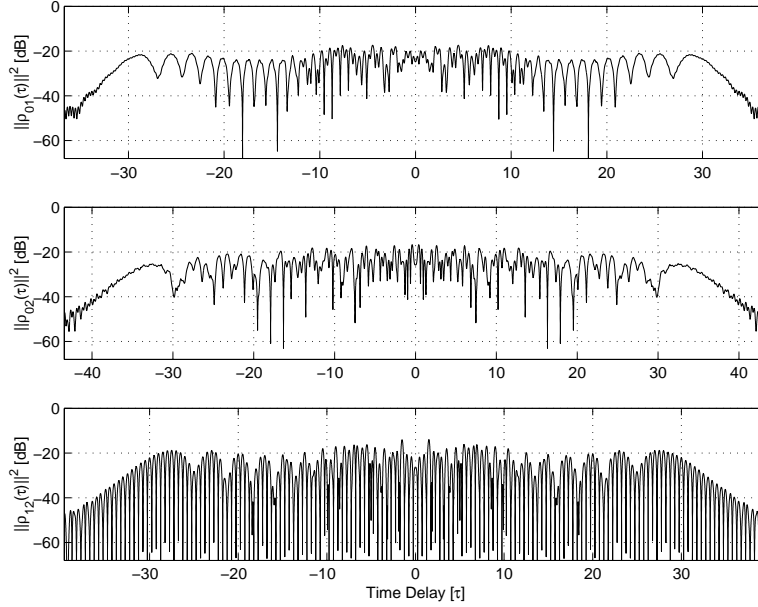
Figure 4.20.   Crosscorrelation functions for a piecewise basis with $N = 3$, $G_D = 20$ dB, and $\mathbf{a} = \begin{bmatrix} 1 \ 2 \ 4 \end{bmatrix}^T$.

Table 4.15.   Crosscorrelation metrics for a piecewise basis with $N = 3$, $G_D = 20$ dB, and $\mathbf{a} = \begin{bmatrix} 1 \ 2 \ 4 \end{bmatrix}^T$.

$\rho_{lk}(t)$	PCCL [dB]	σ_{kl}^2
$\rho_{01}(t)$	-17.394	363.182
$\rho_{02}(t)$	-16.711	363.182
$\rho_{12}(t)$	-14.061	363.182

and 4.16 have been calculated from these correlation functions shown in Figures 4.20 and 4.21 respectively.
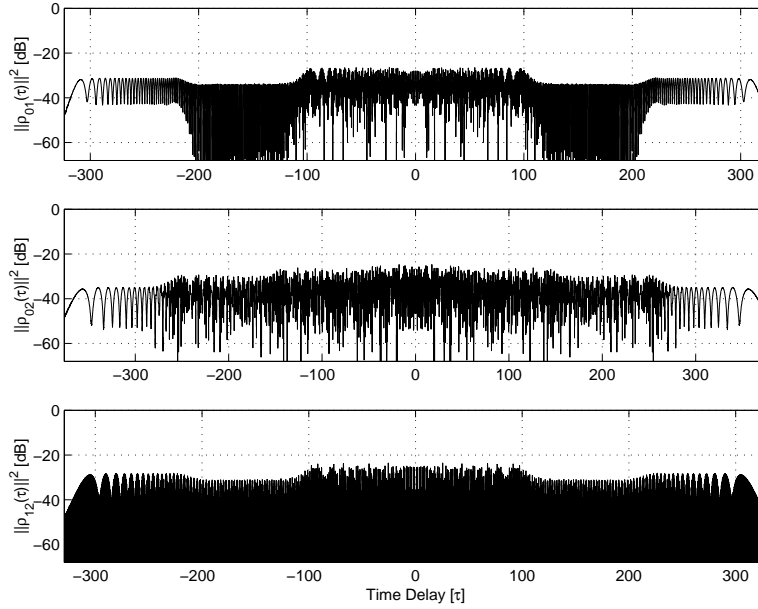
Figure 4.21.   Crosscorrelation functions for a piecewise basis with $N = 3$, $G_D = 40$ dB, and $\mathbf{a} = \begin{bmatrix} 1 & 2 & 4 \end{bmatrix}^T$.

Table 4.16.   Crosscorrelation metrics for a piecewise basis with $N = 3$, $G_D = 40$ dB, and $\mathbf{a} = \begin{bmatrix} 1 & 2 & 4 \end{bmatrix}^T$.

$\rho_{lk}(t)$	PCCL [dB]	σ_{kl}^2
$\rho_{01}(t)$	-26.603	30061.120
$\rho_{02}(t)$	-24.722	30061.120
$\rho_{12}(t)$	-23.631	30061.120

4-28

This section showed that the piecewise basis, for any size symbol family, is a valid basis. This basis provides slightly better performance than the Chebyshev basis.

4.4   Discrete Code Comparison

Spread spectrum multiple access schemes, such as Direct Sequence CDMA (DS-CDMA), require code families with dispersive crosscorrelation properties similar to those used in NLS. Unlike the Brown symbols described earlier, DS-CDMA utilizes discrete spreading codes. Gold codes were invented in 1967 specifically for use in multiple-access spread spectrum systems [30:135], and have been employed in a variety of applications including cellular DS-CDMA. Metrics for Gold codes and Simulated Annealing biphase codes are provided in this section contrasting the performance of Brown symbols.

The codes considered in this section are finite in time, unlike the finite bandwidth Brown symbols. The metrics, therefore, have been calculated for discrete symbols of equivalent signal energy and approximately equivalent bandwidth to the Brown symbols. The null-to-null bandwidth of a biphase signal is approximately $4\pi/\tau_b$, where τ_b is the bit duration; therefore by choosing $\tau_b = 4\pi/\Omega_0$ the bandwidth is approximately that of the Brown symbols. With the bit duration so defined, the amplitude of the biphase symbol is then chosen so that the energy of the biphase symbol is equal to that of a Brown symbol.

4.4.1   Gold and SA Biphase Codes.   PRN-sequences such as maximal-length codes and Gold codes are commonly employed in spread-spectrum communications systems [30:89]. Metrics for an $N = 3$ family of 31-bit and 127-bit Gold codes are illustrated in Tables 4.17 and 4.18 respectively.

Table 4.17.   Auto/Crosscorrelation metrics for a 31-bit Gold code family of $N = 3$.

$\rho_{lk}(t)$	PSL [dB]	ISL [dB]	PCCL [dB]	σ_{kk}^2	σ_{kl}^2
$\rho_{00}(t)$	-17.786	-7.227	x	13.857	x
$\rho_{11}(t)$	-17.786	-6.523	x	15.443	x
$\rho_{22}(t)$	-14.264	-3.742	x	16.078	x
$\rho_{01}(t)$	x	x	-9.827	x	44.600
$\rho_{02}(t)$	x	x	-8.999	x	48.393
$\rho_{12}(t)$	x	x	-10.742	x	36.230

Table 4.18.   Auto/Crosscorrelation metrics for a 127-bit Gold code family of $N = 3$.

$\rho_{lk}(t)$	PSL [dB]	ISL [dB]	PCCL [dB]	σ_{kk}^2	σ_{kl}^2
$\rho_{00}(t)$	-24.014	-6.023	x	267.233	x
$\rho_{11}(t)$	-22.991	-5.675	x	277.247	x
$\rho_{22}(t)$	-19.154	-2.240	x	325.511	x
$\rho_{01}(t)$	x	x	-14.842	x	818.573
$\rho_{02}(t)$	x	x	-15.228	x	701.845
$\rho_{12}(t)$	x	x	-15.228	x	666.453

Codes with controlled crosscorrelation properties have recently been devised using a Simulated Annealing approach [1:3-11]. Metrics for an $N = 3$ family of 31-bit and 127-bit SA codes are illustrated in Tables 4.19 and 4.20 respectively.

Table 4.19.   Auto/Crosscorrelation metrics for a 31-bit SA code family of $N = 3$.

$\rho_{lk}(t)$	PSL [dB]	ISL [dB]	PCCL [dB]	σ_{kk}^2	σ_{kl}^2
$\rho_{00}(t)$	-14.264	-3.106	x	19.472	x
$\rho_{11}(t)$	-14.264	-1.946	x	19.829	x
$\rho_{22}(t)$	-14.264	-2.820	x	18.038	x
$\rho_{01}(t)$	x	x	-11.765	x	41.693
$\rho_{02}(t)$	x	x	-11.765	x	46.396
$\rho_{12}(t)$	x	x	-11.765	x	51.002

Table 4.20.   Auto/Crosscorrelation metrics for a 127-bit SA code family of $N = 3$.

$\rho_{lk}(t)$	PSL [dB]	ISL [dB]	PCCL [dB]	σ_{kk}^2	σ_{kl}^2
$\rho_{00}(t)$	-19.154	-2.793	x	356.686	x
$\rho_{11}(t)$	-19.154	-1.844	x	321.849	x
$\rho_{22}(t)$	-19.154	-1.388	x	351.224	x
$\rho_{01}(t)$	x	x	-16.501	x	763.032
$\rho_{02}(t)$	x	x	-16.501	x	784.979
$\rho_{12}(t)$	x	x	-16.501	x	778.029

This section provided comparative results for biphase codes of equivalent signal energy and approximate bandwidth. Even 127-bit Gold and SA codes do not perform as well as Brown symbols in terms of PCCL and PSL indicating that Brown symbols are likely to be well suited to NLS applications.

4.5   Summary

This chapter synthesized and analyzed Brown symbols, using the process outlined in Section 3.7.2. The analytical approach described in Appendix B lead to

the construction and simulation of various Brown symbols in Matlab®. Section 4.2 considered the design of each of the components to a Brown symbol: the Hermit Problem solution, phase-rate basis function design, phase function calculation, and symbol synthesis. Section 4.3 provided results indicating the insensitivity of the performance of Brown symbols to the choice of phase-rate basis functions and envelope, and also considered physical realizability. These results support the claim that there is no sensitivity in rms time duration of the correlation functions to the choice of phase-rate basis functions, so long as the criteria of optimality and orthonormality are met. Finally, Section 4.4 contrasted the performance of Brown symbols with that of extant biphase symbols with Brown symbols showing superior performance in rms time duration characteristics of the correlation functions.

Tables 4.21 and 4.22 provide a summary of the comparative performance. As shown in Table 4.21, the autocorrelation function that provides the best overall performance corresponds to the Brown symbol family with the polynomial basis, which was derived with the optimal envelope. The lowest PCCL for each symbol family is extracted and displayed in Table 4.22. The Brown symbols derived from the non-ideal uniform taper, and Chebyshev and piecewise basis provide the best results. Notably, Brown symbols show greater mutual dispersion than 127-bit Gold and SA codes suggesting that they are better suited to NLS.

Table 4.21.　Autocorrelation metrics for various symbol/code families.

Symbol Basis/ Code	PSL [dB]	ISL [dB]	σ_{kk}^2
Sinusoidal	-23.000	-18.931	0.016
Polynomial	-23.048	**-18.975**	**0.016**
Chebyshev	-13.267	-7.076	316.033
Piecewise	-13.262	-7.109	63.203
31-bit Gold	-17.786	-7.227	13.857
127-bit Gold	**-24.014**	-6.023	267.233
31-bit SA	-14.264	-3.106	19.472
127-bit SA	-19.154	-2.793	356.6866

Table 4.22.　Crosscorrelation metrics for various symbol/code families with $N = 3$.

Symbol Basis/ Code	PCCL [dB]	σ_{kl}^2
Sinusoidal	-14.925	30000.016
Polynomial	-15.978	30000.016
Chebyshev	-22.655	**30315.616**
Piecewise	**-23.631**	30061.120
31-bit Gold	-8.999	48.393
127-bit Gold	-14.842	818.573
31-bit SA	-11.765	51.002
127-bit SA	-16.501	784.979

V. Conclusions and Recommendations

5.1 Restatement of Research Goal

As stated in Section 1.2, the goals of this research are to:

1. Explain the formulation of Brown's theorem [5] whilst introducing a simplified linear algebraic notation;

2. Describe a systematic process for designing Brown symbols through an analysis of Brown's work and by theoretical extension;

3. Provide a theoretical analysis for the digitization of Brown symbols;

4. Evaluate performance of Brown symbols, comprising dispersive gain, through simulation and numerical approximation; and

5. Compare the performance of various Brown symbols with discrete codes through simulation.

5.2 Conclusions

5.2.1 Brown Symbol Sensitivity. Optimal Brown symbols require phase rate functions to be described by a linear combination of basis functions that are orthonormal within the weighted inner product space incorporating $A^2(\omega)$, defined in Eq (3.17). Chapter IV considered two bases that meet this requirement, the sinusoidal basis described in Section 4.3.1 and the polynomial basis in Section 4.3.2. By relaxing the optimality requirement for envelope $A(\omega)$, two other bases were considered, the Chebyshev polynomials in Section 4.3.3 and piecewise continuous basis in Section 4.3.4.

The sinusoidal and polynomial bases provide a means of generating N optimally mutually dispersive symbols, with dispersive gain providing control over crosscorrelation dispersion. Both of these bases achieve the Brown theoretical autocorrelation and crosscorrelation performance in rms time duration, demonstrating

the validity of Brown's theorem. Notably, for unity dispersive gain, the form of the crosscorrelation functions vary despite having equivalent rms time durations. The sinusoidal basis produces crosscorrelation functions with a strong mainlobe and dominant sidelobes at approximately -18 dB, whereas the polynomial basis produces crosscorrelation functions with a broad mainlobe and no sidelobes. When the dispersive gain factor is increased, however, both bases produce crosscorrelation functions with extensive dispersion at approximately -20 dB. This result suggests that Brown symbols need only be considered for symbols with large dispersive gain, which also relates to large time-bandwidth products.

Brown symbols show insignificant degradation due to windowing, provided the window width T_w is selected according to dispersive gain as illustrated in Figure 4.7. This suggests that Brown symbols are suitable to radar applications. When compared to conjugate LFM, Brown symbols have superior autocorrelation statistics but produce crosscorrelation functions with a consistent 10 dB lower PCCL. Although the LFM pulse pair has better PCCL performance, Brown codes exhibit superior performance in terms of rms time duration. For example, the comparison of pulses with equivalent rms time duration, in Figure 4.9, showed that Brown codes exhibit greater compression. PCCL is an excellent indicator of a symbol families suitability for NLS, however, *any* two symbols will have only one crosscorrelation function and can claim justly to be mutually dispersive; this is not so for larger code families. LFM pulses have been shown to provide excellent performance in NLS but are of minimal benefit to NLS systems due to the severe limitation on symbol family size, $N = 2$. Conversely, Brown symbols are scalable to any sized family, they perform better in terms of rms time duration and are comparable to LFM in terms of PCCL.

When the constraint of envelope optimality is removed, and a uniform envelope applied, the properties of the autocorrelation function worsen. This is shown in Tables 4.9 and 4.13 with a significant increase in rms time duration and a 10 dB increase in PSL. The Chebyshev and piecewise bases, due to the increase in auto-

correlation dispersion, provide better crosscorrelation dispersion at unity gain than both the sinusoidal and polynomial bases. The dispersive gain can be increased to improve crosscorrelation dispersion, therefore, small differences in PCCL are easily accounted for in this way, negating the requirement to use a non-ideal envelope. The shape of the correlation plots is, however, significantly different. For lower dispersive gain, or time-bandwidth, the crosscorrelation functions resulting from these bases exhibit much flatter dispersive characteristics. A relaxing of the optimality constraint therefore effects both the autocorrelation and crosscorrelation statistics providing marginal improvements in PCCL and dispersion, potentially flatter crosscorrelation functions, but higher sidelobes.

5.2.2 Discrete Code Comparison. Section 4.4 provided a brief insight into the performance of extant waveforms that are suited to NLS. Gold codes and SA codes were considered in comparison to Brown symbols. Neither the 31- or 127-bit Gold or SA codes provide comparable performance to Brown symbols. Although the 127-bit Gold codes have comparable PSL values, both types of codes exhibit much worse compression and dispersion characteristics than Brown symbols. Also, these codes offer no means of controlling the degree of dispersion.

5.3 Significant Results of Research

NLS symbol families constructed from signals with desirable correlation properties, such as LFM symbols [28] and discrete Gold codes [2], have already been implemented. However, LFM pulse families are severely limited in size and the performance of Gold codes is constrained. Theoretically, Brown symbols can be easily tailored for utilization in NLS. The theorem claims that these symbols are optimally mutually dispersive, but has until now remained untested.

This research reintroduced Brown's theorem relating the system model assumptions and theory formulation. As a result of this research, a systematic method

for synthesizing Brown symbols is now defined and demonstrated. The synthesis and simulation process provides the theoretical background necessary to enable digitization of Brown symbols. The Brown symbols that were created and analyzed achieve theoretical performance and, for large dispersive gain, exhibit desirable correlation characteristics. The dispersive gain factor was introduced and integrated into the formulation and design of Brown symbols, thus providing a crosscorrelation dispersion control parameter. Subsequently, Brown symbols have been shown to be well-suited for physical implementation into pulse Doppler radar systems, exhibiting more desirable correlation statistics than comparable discrete codes. As such, the goals stated in Section 1.2 have been accomplished.

5.4   Recommendations for Future Research

Recommendations for future work center on expanding the complexity of the radar model and further demonstrating Brown symbol performance, robustness and sensitivity. The Brown theorem can also be expanded to image processing.

The radar model referenced in this research incorporated simplifying assumptions of a noiseless, distortion free environment with stationary single-point targets. To better understand the suitability of Brown symbols to pulse Doppler radar these assumptions should be altered to better reflect a real radar environment. As such, future work should consider the implementation of Brown symbols, with different generating bases, in the presence of noise. Also, Brown symbols appear reliant on the integrity of the phase functions, therefore, an analysis of the effect of Doppler and clutter on the properties of the correlation functions would be desirable.

Brown [5:13] has proposed a study of Brown symbols for implementation with functions of more than one variable, such as images. For example, future work could consider expanding the theory of mutually dispersive symbols to 2-dimensions and analyze the performance of signals generated in that way. A possible application identified by Brown is the coded-multiplexing of color television signals onto a single

channel. Other 2-dimensional research could include the expansion of the theory to facilitate the design of radially symmetric Brown surfaces.

The principle of stationary phase may be employed to approximate the inverse Fourier transform of the crosscorrelation functions. By considering this approach, an intuitive avenue of research becomes apparent, *i.e.*, the approximation to the cross-correlation function is a linear combination of complex sinusoids; their phases are determined by the stationary points of the phase-rate function. Periodic phase-rate functions, such as the sinusoidal basis, are therefore likely to generate crosscorrelation functions with constructive superposition leading to sidelobes. A random phase-rate process with uniform distribution would considerably alleviate this issue. An expansion to the theory provided in this thesis should consider constructing a framework for the use of random processes as basis functions. Initial work in this area shows crosscorrelation functions with excellent dispersive properties and PCCLs on the order of -32 dB.

Appendix A. Ambiguity Function Analysis

A.1 Ambiguity Surfaces

This appendix displays a series of ambiguity surfaces generated for various radar waveform types.

A.1.1 Single Pulse Waveform. The most basic pulsed radar consists of a single pulse modulated onto a carrier.

$$x(t) = \text{rect}\left(\frac{t}{T}\right) e^{j2\pi f_c t} \tag{A.1}$$

The ambiguity surface for this function, with $f_c = 0$, is determined from

$$\chi(\tau, \nu) = \int_{-\infty}^{\infty} \text{rect}\left(\frac{t}{T}\right) \text{rect}\left(\frac{t - \tau}{T}\right) e^{j2\pi\nu t} dt \tag{A.2}$$

and is illustrated in fig. A.1.

A.1.2 Pulse-Train Waveform. The next most advanced pulsed radar consists of a train of pulses modulated onto a carrier, used to improved detection and Doppler resolution. In practise an infinite pulse-train is not feasible, therefore in this analysis an N pulse train is considered.

$$x(t) = \sum_{n=-\infty}^{\infty} \text{rect}\left(\frac{t - nT_p}{T}\right) e^{j2\pi f_0 t} \tag{A.3}$$

The ambiguity surface for this function, with $f_c = 0$, is determined from

$$\chi(\tau, \nu) = \int_{-\infty}^{\infty} \sum_{n=0}^{N} \sum_{m=0}^{N} \text{rect}\left(\frac{t - nT_p}{T}\right) \text{rect}\left(\frac{t - mT_p - \tau}{T}\right) e^{j2\pi\nu t} dt \tag{A.4}$$

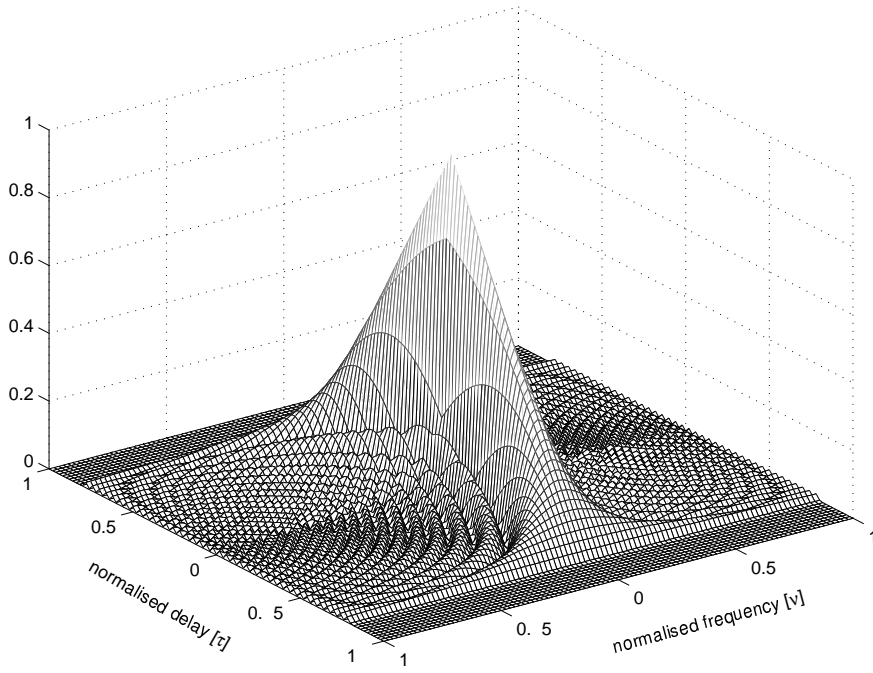and is illustrated in fig. A.2 for $N = 6$.

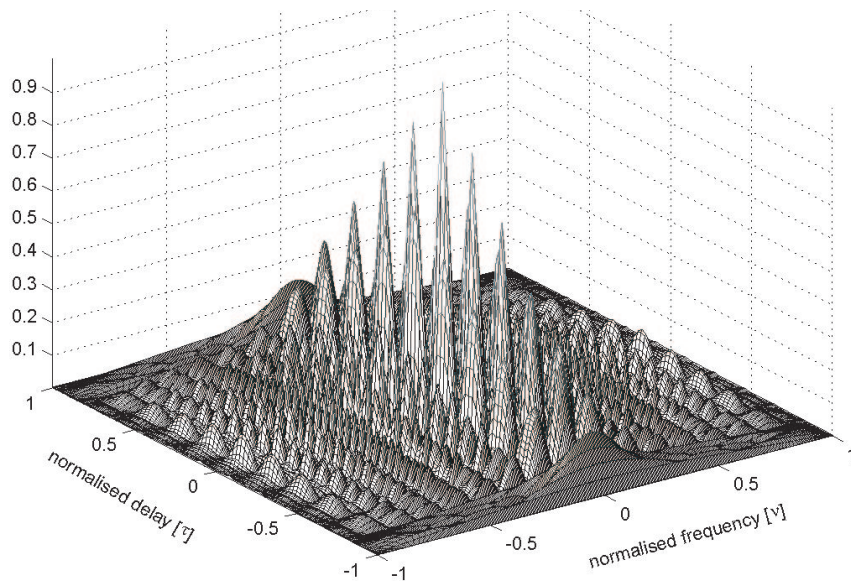Figure A.1.   Ambiguity surface of a single pulse radar waveform.

Figure A.2.   Ambiguity surface of a pulsed radar waveform.

A.1.3 Linear FM Waveform. The linear FM pulse also has interesting properties, as discussed in section 2.3.3.2. This signal sweeps a frequency range, Φ, and can be described by

$$x_{\text{LFM}}(t) = \text{rect}\left(\frac{t}{T}\right) e^{\jmath\pi k t^2}, \text{ where } k = \Phi/T \qquad (A.5)$$

The ambiguity surface for this function is determined from

$$\chi(\tau, \nu) = \int_{-\infty}^{\infty} \text{rect}\left(\frac{t}{T}\right) e^{\jmath\pi k t^2} \text{rect}\left(\frac{t-\tau}{T}\right) e^{-\jmath\pi k(t-\tau)^2} e^{\jmath 2\pi\nu t} dt \qquad (A.6)$$

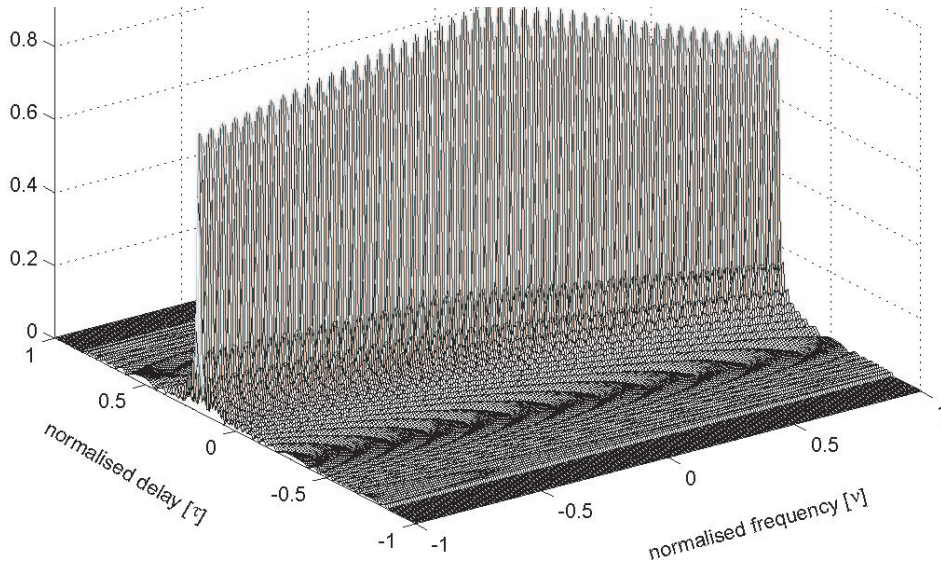and is illustrated in fig. A.3.

Figure A.3.   Ambiguity surface of a single pulse LFM waveform.

Appendix B. Basis Function Derivations

B.1 Sinusoidal Basis

The sinusoidal functions are an obvious choice to form a bases due to their orthogonality properties. With the optimal envelope for Brown symbols, however, the orthogonality must hold within the weighted inner product space, $(\vartheta_k, \vartheta_l)_{A^2}$. The weighted inner product of sinusoidal functions is defined such that

$$\vartheta_k(\omega) \overset{\triangle}{=} b\sin(\mathrm{a}_k\omega), \tag{B.1}$$

then

$$
\begin{aligned}
(\vartheta_k, \vartheta_l)_{A^2} &= \frac{1}{2\pi}\int_{-\infty}^{\infty}\vartheta_k(\omega)\vartheta_l(\omega)A^2(\omega)d\omega \\
&= \frac{1}{2\pi}\int_{\frac{-\Omega_0}{2}}^{\frac{\Omega_0}{2}} b\sin(\mathrm{a}_k\omega)b\sin(\mathrm{a}_l\omega)\frac{4\pi}{\Omega_0}\cos^2\left(\frac{\pi\omega}{\Omega_0}\right)d\omega \\
&= \frac{b^2}{\Omega_0}\int_{\frac{-\Omega_0}{2}}^{\frac{\Omega_0}{2}}\sin(\mathrm{a}_k\omega)\sin(\mathrm{a}_l\omega)d\omega + \frac{b^2}{\Omega_0}\int_{\frac{-\Omega_0}{2}}^{\frac{\Omega_0}{2}}\cos\left(\frac{2\pi\omega}{\Omega_0}\right)d\omega. \tag{B.2}
\end{aligned}
$$

While a_k are integers for all k, and $\mathrm{a}_k \neq \mathrm{a}_l$. Thus, the sinusoidal functions in the first term of Eq (B.2) are orthogonal when evaluated over an integer number of cycles. Subsequently, a sufficient constraint for orthogonality here is that $\Omega_0 = 2m\pi$, for any integer m. The weighted norm, $k = l$, reduces the first term as such

$$
\begin{aligned}
\frac{b^2}{\Omega_0}\int_{\frac{-\Omega_0}{2}}^{\frac{\Omega_0}{2}}\sin^2(\mathrm{a}_k\omega)d\omega &= \frac{b^2}{2\Omega_0}\left[\omega - \frac{\sin(\mathrm{a}_k\omega)}{\mathrm{a}_k}\right]_{\frac{-\Omega_0}{2}}^{\frac{\Omega_0}{2}} \\
&= \frac{b^2}{2}. \tag{B.3}
\end{aligned}
$$

The second term is simply an integral of a cosine function over one complete cycle, which will always be zero. Therefore the sinusoidal basis functions are orthogonal. By choosing b so that Eq (B.3) equals unity, an orthonormal basis is described.

Therefore an orthonormal sinusoidal basis is defined by

$$\vartheta_k(\omega) \overset{\triangle}{=} \sqrt{2}\sin(\mathrm{a}_k\omega), \tag{B.4}$$

where

$$\begin{aligned}
\Omega_0 &= 2m\pi \\
\mathrm{a}_k,\ m &\in \mathcal{Z} \\
\mathrm{a}_k &\neq \mathrm{a}_l,\ \forall\, k \neq l.
\end{aligned} \tag{B.5}$$

B.2 *Polynomial Basis*

There are a number of orthogonal polynomial bases such as Chebyshev functions, Legendre functions, Hermite functions and so on. The suitability of each of these alternate bases is dependent on them being odd functions that retain their orthogonality within the weighted inner product space, $(\vartheta_k, \vartheta_l)_{A^2}$. The search for a suitable basis begins by defining the kth basis element as a weighted set of odd polynomial functions of order $2p - 1$.

$$\vartheta_k(\omega) \overset{\triangle}{=} \sum_{n=0}^{p-1} \mathrm{b}_{kn}\omega^{2n+1}, \tag{B.6}$$

then

$$\begin{aligned}
(\vartheta_k, \vartheta_l)_{A^2} &= \frac{1}{2\pi}\int_{-\infty}^{\infty} \vartheta_k(\omega)\vartheta_l(\omega)A^2(\omega)d\omega \\
&= \frac{1}{2\pi}\int_{\frac{-\Omega_0}{2}}^{\frac{\Omega_0}{2}} \sum_{n=0}^{p-1}\mathrm{b}_{kn}\omega^{2n+1}\sum_{m=0}^{p-1}\mathrm{b}_{lm}\omega^{2m+1}\frac{4\pi}{\Omega_0}\cos^2\left(\frac{\pi\omega}{\Omega_0}\right)d\omega \\
&= \frac{2}{\Omega_0}\sum_{n=0}^{p-1}\sum_{m=0}^{p-1}\mathrm{b}_{kn}\mathrm{b}_{lm}\int_{\frac{-\Omega_0}{2}}^{\frac{\Omega_0}{2}}\omega^{2(n+m+1)}\cos^2\left(\frac{\pi\omega}{\Omega_0}\right)d\omega.
\end{aligned} \tag{B.7}$$

The resultant of the integral is a function only of m and n and is therefore redefined as

$$\mathrm{E}_{mn} = \frac{2}{\Omega_0} \int_{-\frac{\Omega_0}{2}}^{\frac{\Omega_0}{2}} \omega^{2(n+m+1)} \cos^2\left(\frac{\pi\omega}{\Omega_0}\right) d\omega, \tag{B.8}$$

which simplifies Eq (B.7) to

$$(\vartheta_k, \vartheta_l)_{A^2} = \sum_{n=0}^{p-1} \sum_{m=0}^{p-1} \mathrm{b}_{kn} \mathrm{b}_{lm} \mathrm{E}_{mn}. \tag{B.9}$$

Again this may be further simplified using linear algebraic notation as

$$(\vartheta_k, \vartheta_l)_{A^2} = \mathbf{b}_k^T \mathbf{E} \mathbf{b}_l. \tag{B.10}$$

Defining $\mathbf{B} = [\mathbf{b}_0\ \mathbf{b}_1\ \mathbf{b}_2\ \ldots\ \mathbf{b}_{N-1}]$ permits further simplification of Eq (B.10). Solving for orthonormality provides

$$\begin{aligned} (\boldsymbol{\vartheta}, \boldsymbol{\vartheta}^T)_{A^2} &= \mathbf{B}^T \mathbf{E} \mathbf{B} \\ &= \mathbf{I}_N. \end{aligned} \tag{B.11}$$

Therefore when $\mathbf{E}$ is invertible

$$\mathbf{B}\mathbf{B}^T = \mathbf{E}^{-1}, \tag{B.12}$$

or in other words with $\mathbf{B}^T$ as the Cholesky decomposition matrix to the inverse of $\mathbf{E}$ another orthonormal basis within the weighted inner product space is defined.

B.3 Chebyshev Functions

Changing the spectral envelope, $A(\omega)$, introduces a different weighted inner product space within which to design an orthonormal basis. An envelope that is uniform across the spectral bandwidth invites the use of Chebyshev polynomials. This is because any pair of Chebyshev polynomials exhibit the orthogonality prop-

erties described in Eq (B.13) [36:158]:

$$\int_{-1}^{1} \frac{T_m(\omega)T_n(\omega)}{\sqrt{1-\omega^2}}d\omega = \begin{cases} 0, & m \neq n \\ \pi, & m = n = 0 \\ \pi/2, & \text{otherwise} \end{cases} \qquad \text{(B.13)}$$

where $T_k(\omega)$ is an kth order Chebyshev polynomial. The odd Chebyshev functions can be defined as

$$\begin{aligned} T_{2m+1}(\omega) &= \cos[(2m+1)\cos^{-1}\omega] \\ &= \sum_{k=0}^{m}(-1)^k \binom{2m+1}{2k} \omega^{2m-2k+1}(1-\omega^2)^k. \end{aligned} \qquad \text{(B.14)}$$

With $A(\omega)$ defined as a uniform envelope on the interval $[-\Omega_0/2, \Omega_0/2]$ as in Eq (B.15), the Chebyshev functions are scaled to induce orthonormality within this inner product space as shown in Eq (B.16).

$$A(\omega) = \sqrt{\frac{2\pi}{\Omega_0}}\text{rect}\left(\frac{\omega}{\Omega_0}\right) \qquad \text{(B.15)}$$

$$\vartheta_n(\omega) = \frac{\sqrt{\frac{2\Omega_0}{\pi}}T_{2n+1}\left(\frac{2\omega}{\Omega_0}\right)}{\sqrt[4]{\frac{\Omega_0^2}{4}-\omega^2}}. \qquad \text{(B.16)}$$

Therefore the weighted inner product of any pair of basis functions is

$$\begin{aligned} (\vartheta_k, \vartheta_l)_{A^2} &= \frac{1}{2\pi}\int_{-\infty}^{\infty}\vartheta_k(\omega)\vartheta_l(\omega)A^2(\omega)d\omega \\ &= \frac{1}{2\pi}\int_{-\frac{\Omega_0}{2}}^{\frac{\Omega_0}{2}}\frac{\sqrt{\frac{2\Omega_0}{\pi}}T_{2k+1}\left(\frac{2\omega}{\Omega_0}\right)\sqrt{\frac{2\Omega_0}{\pi}}T_{2l+1}\left(\frac{2\omega}{\Omega_0}\right)\frac{2\pi}{\Omega_0}}{\sqrt{\frac{\Omega_0^2}{4}-\omega^2}}d\omega \\ &= \frac{2}{\pi}\int_{-\frac{\Omega_0}{2}}^{\frac{\Omega_0}{2}}\frac{T_{2k+1}\left(\frac{2\omega}{\Omega_0}\right)T_{2l+1}\left(\frac{2\omega}{\Omega_0}\right)}{\sqrt{\frac{\Omega_0^2}{4}-\omega^2}}d\omega. \end{aligned}$$

$$\text{(B.17)}$$

With a change of variable ($\gamma = 2\omega/\Omega_0$) the integral takes on the familiar form of Eq (B.13), where for all k, l,

$$\frac{2}{\pi} \int_{-1}^{1} \frac{T_{2k+1}(\gamma)T_{2l+1}(\gamma)}{\sqrt{1-\gamma^2}} d\gamma = \delta_{kl}. \tag{B.18}$$

Therefore the Chebyshev basis as defined in Eq (B.16) is orthonormal for a non-ideal uniform taper.

B.4   Piecewise Continuous Basis

LFM pulses were originally demonstrated in the early implementation of a NLS scheme. These pulses have linear phase-rate functions with spectral content that is approximately uniformly dispersed over a compact frequency bandwidth. The duality of the Fourier transform provides that functions of frequency having linear phase-rate functions will correspond to time signals that are uniformly dispersed and compactly supported. This is a desirable property of the crosscorrelation functions as the presence of sidelobes is expected to be significantly mitigated. This section explores the use of piecewise linear phase-rate functions, such as the saw-tooth waveform. To provide a means of analysis this basis utilizes the same uniform taper as the Chebyshev basis as described in B.15. As such, the function that describes the normalized basis is defined as

$$
\begin{aligned}
\vartheta_k(\omega) \quad &\triangleq \quad \frac{4\sqrt{3}a_k}{\Omega_0} \left[(\omega + \Omega_0/2)\mathrm{rect}\left(\frac{\omega + \Omega_0/2 - \Omega_k/8}{\Omega_k/4} \right) \right. \\
&+ \quad \sum_{n=1}^{2a_k-1} (-1)^n(\omega + \omega_n)\mathrm{rect}\left(\frac{\omega - \omega_n}{\Omega_k/2} \right) \\
&+ \quad \left. (\omega - \Omega_0/2)\mathrm{rect}\left(\frac{\omega - \Omega_0/2 + \Omega_k/8}{\Omega_k/4} \right) \right]
\end{aligned}
\tag{B.19}
$$

where

$$\Omega_k \quad = \quad \Omega_0/a_k$$

$$\omega_n = \frac{\Omega_0}{2}(n/a_k - 1).$$

That is, a_k is the number of cycles over Ω_0, Ω_k is the period, and ω_n are the zero crossings as illustrated in Figure B.4.
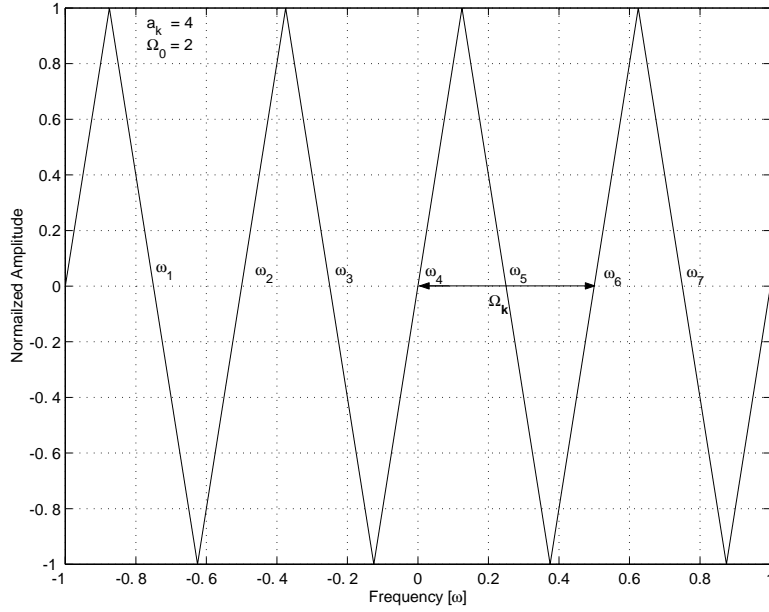

Figure B.1.   Saw-tooth basis function with $a_k = 4$ and $\Omega_0 = 2$.

The selection of a_k is constrained to ensure that $\vartheta_k(\omega)$ forms an orthonormal basis. This can be accomplished by ensuring that $\mathbf{max}\,\{a_k, a_l\}/\mathbf{min}\{a_k, a_l\}$ is radix 2 for all k, l. Figure B.4 illustrates that the product of two basis functions with $\mathbf{max}\,\{a_k, a_l\}/\mathbf{min}\{a_k, a_l\} = 2$ produce equivalent positive and negative areas.
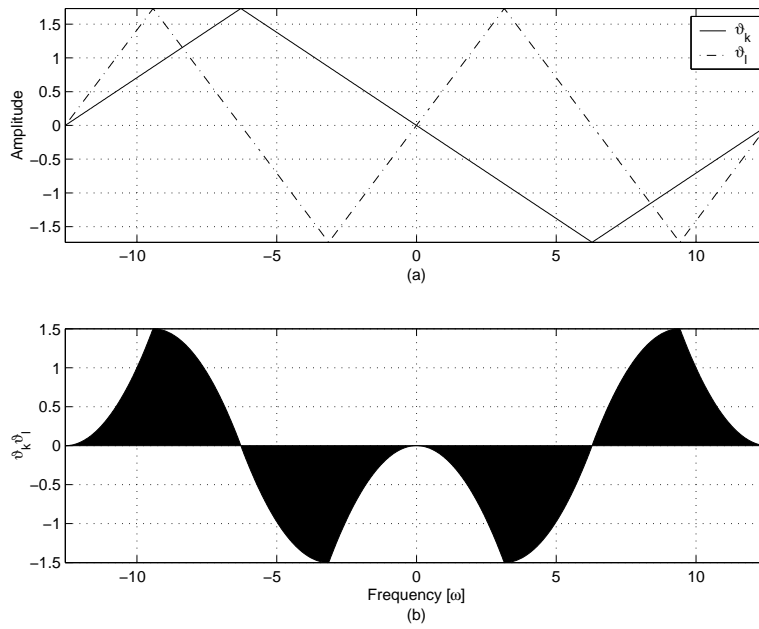
Figure B.2.   Orthogonal   piecewise   functions.
$\vartheta_k(\omega)$ and $\vartheta_l(\omega)$ selected   such   that
$\mathbf{max}\{a_k,\ a_l\}/\mathbf{min}\{a_k,\ a_l\} = 2$, (a), and
Area under $\vartheta_k(\omega)\vartheta_l(\omega)$, (b).

Bibliography

1. Anderson, J.M. *Nonlinear Suppression of Range Ambiguity in Pulse Doppler Radar*. PhD dissertation, Air Force Institute of Technology (AETC), 2001 (ADA397364).

2. Anderson, J.M., et al. "A Nonlinear Suppression Technique for Range Ambiguity Resolution in Pulse Doppler Radars," *Radar Conference, 2001. Proceedings of the 2001 IEEE*, 141 –146 (2001).

3. Barker, R.H. *Group Synchronizing of Binary Digital Systems*, 273–287. New York: Academic Press, 1953. in Communication Theory (W. Jackson, ed.).

4. Bedrosian, E. "A Product Theorem for Hilbert Transforms," *Proc. IEEE*, *vol. 51*:868–869 (1963).

5. Brown, Wm.M. "Mutually Dispersive Codes for Nonlinear Suppression of Ambiguities." Draft AFRL/SN Paper, August 2001.

6. Brown, Wm.M. and C.J. Palermo. *Random Processes, Communications and Radar*. United States: McGraw Hill, 1969.

7. Chen, C., et al. "Optimal Spread Spectrum Sequences - Constructed From Gold Codes," *Global Telecommunications Conference, 2000*, *vol. 2*:867 –871 (2000).

8. Costas, J.P. "A Study of a Class of Detection Waveforms Having Nearly Ideal Range-Doppler Ambiguity Properties," *IEEE Proceedings*, *vol. 72*(8):996–1009 (August 1984).

9. Ferrari, A., et al. "Doppler ambiguity resolution using multiple PRF," *IEEE Transactions on Aerospace and Electronics Systems*, *vol. 33*(3):738 –751 (July 1997).

10. Frank, R.L. "Polyphase codes with Good Nonperiodic Correlation Properties," *IEEE Transactions on Information Theory*, *IT-9*:43–45 (1963).

11. Franks, L. E. *Signal Theory*. United States: Dowden & Culver, 1981.

12. Gabor, D. "Theory of Communication," *J. Inst. Elec. Engrs. (London)*, *pt. III, vol. 93*:429–457 (1946).

13. Golumb, S.W. and H. Taylor. "Constructions and Properties of Costas Arrays," *IEEE Proceedings*, *74*:1143–1163 (1984).

14. Hamming, R.W. *Numerical Methods for Scientists and Engineers, 2nd Ed*. Ontario: Dover Publications, 1973.

15. Hansen, R.C. *Microwave Scanning Antennas, Vol. I*. New York: Academic Press, 1964.

16. Hlawatsch, F. *Time-Frequency Analysis and Synthesis of Linear Signal Spaces*. United States: Kluwer Academic Publishers, 1998.

17. Klauder, J.R., et al. "The Theory and Design of Chirp Radar," *The Bell System Technical Journal*, vol. *XXXIX*(4):745–808 (July 1960).

18. Larson, R.E. and B.H. Edwards. *Elementary Linear Algebra*. United States: D.C. Heath and Company, 1991.

19. Lei, W., et al. "Resolution of Range and Velocity Ambiguity for a Medium Pulse Doppler Radar," *Record of the IEEE 2000 International Radar Conference*, *IEEE AES* (2000).

20. Levanon, N. *Radar Principles*. New York: Wiley-Interscience, 1988.

21. Lewis, B.L. and F.F. Kretschmer. "A New Class of Polyphase Pulse Compression Codes and Techniques," *IEEE Transactions on Aerospace and Electronics Systems*, vol. *AES-17*(3):364–372 (May 1981).

22. Lewis, B.L. and F.F. Kretschmer. "Linear Frequency Modulation Derived Polyphase Pulse Compression Codes," *IEEE Transactions on Aerospace and Electronics Systems*, vol. *AES-18*(5):637–641 (September 1982).

23. MacWilliams, F.J. and N.J.A. Sloan. "Pseudorandom Sequences and Arrays," *IEEE Proceedings 64*, 1715–1729 (December 1976).

24. Morris, G. and L. Harkness. *Airborne Pulsed Doppler Radar, 2nd. Ed*. United States: Artech House, 1980.

25. Mullis, C.T. and R.A. Roberts. *Digital Signal Processing*. United States: Addison-Wesley, 1987.

26. Nathanson, F.E. *Radar Design Principles*. Mendham, NJ: SciTech, 1999.

27. Nevin, R.L. "Waveform trade-offs for medium PRF air-to-air radar," *IEEE National Radar Conference Proceedings*, 140–145 (1988).

28. Palermo, et al. "Ambiguity Suppression by Non-Linear Processing," *Record of the Eight Annual Radar Symposium* (June 1962).

29. Papoulis, A. *The Fourier Integral and its Applications*, chapter 7, 139–143. McGraw-Hill, 1962.

30. Peterson, R.L., et al. *Introduction to Spread-Spectrum Communications*. New Jersey: Prentice Hall, 1995.

31. Rihaczek, A.W. *Principles of High Resolution Radar*. New York: McGraw Hill, 1969.

32. Ruttenburg, K. and L. Chanzit. "High Range Resolution by Means of Pulse to Pulse Frequency Shifting," *EASCON Record*, vol. *III*:47–51 (1968).

33. Sarwate, D.V. and M.B. Pursely. "Crosscorrelation Properties of Pseudorandom and Related Sequences," *IEEE Proceedings*, *vol. 68*:593–619 (May 1968).

34. Scharf, L.L. *Statistical Signal Processing*. United States: Addison-Wesley, 1991.

35. Skolnik, M.I. *Introduction to Radar Systems 3rd Ed*. New York: McGraw Hill, 2001.

36. Spiegel, M.R. *Mathematical Handbook of Formulas and Tables*. New York: McGraw Hill, 1991.

37. Stark, H. and J.W. Woods. *Probability, Random Processes, and Estimation Theory for Engineers*. New Jersey: Prentice Hall, 1994.

38. Strang, G. *Linear Algebra and its Applications*. United States: Saunders, 1992.

39. Stremler, F.G. *Introduction to Communications Systems 3rd Ed*. United States: Addison-Wesley, 1992.

40. Ville, J. "Theory and Application of the Notation of the Complex Signal," *Câbles et Transmission*, *vol. 2*:67–74 (July 1948).

41. Woodward, P.M. *Probability and Information Theory, with Applications to Radar*. New York: Pergamon Press, 1953.

42. Xia, Xiang-Gen. "Doppler Ambiguity Resolution Using Optimal Multiple Pulse Repetition Frequencies," *IEEE Transaction on Aerospace and Electronics Systems*, *vol. 35*(1):371–379 (January 1999).

REPORT DOCUMENTATION PAGE

1. REPORT DATE (DD-MM-YYYY)	2. REPORT TYPE	3. DATES COVERED (From – To)
15-03-2002	**Master's Thesis**	Jun 2001 – Mar 2002

4. TITLE AND SUBTITLE	5a. CONTRACT NUMBER
AN ANALYSIS OF MUTUALLY DISPERSIVE BROWN SYMBOLS FOR NON-LINEAR AMBIGUITY SUPPRESSION	5b. GRANT NUMBER
	5c. PROGRAM ELEMENT NUMBER

6. AUTHOR(S)	5d. PROJECT NUMBER
Papaphotis, Matthew J., Flight Lieutenant, RAAF	If funded, enter ENR #
	5e. TASK NUMBER
	5f. WORK UNIT NUMBER

7. PERFORMING ORGANIZATION NAMES(S) AND ADDRESS(S)	8. PERFORMING ORGANIZATION REPORT NUMBER
Air Force Institute of Technology Graduate School of Engineering and Management (AFIT/EN) 2950 P Street, Building 640 WPAFB OH 45433-7765	AFIT/GE/ENG/M02-19

9. SPONSORING/MONITORING AGENCY NAME(S) AND ADDRESS(ES)	10. SPONSOR/MONITOR'S ACRONYM(S)
AFRL/SN Attn: Dr. William M. Brown 2241 Avionics Circle DSN: (937)-255-3627 WPAFB OH 45433-7765 e-mail: William.Brown3@wpafb.af.mil	11. SPONSOR/MONITOR'S REPORT NUMBER(S)

12. DISTRIBUTION/AVAILABILITY STATEMENT

APPROVED FOR PUBLIC RELEASE; DISTRIBUTION UNLIMITED.

13. SUPPLEMENTARY NOTES

14. ABSTRACT

This thesis significantly advances research towards the implementation of optimal Non-linear Ambiguity Suppression (NLS) waveforms by analyzing the Brown theorem. The Brown theorem is reintroduced with the use of simplified linear algebraic notation. A methodology for Brown symbol design and digitization is provided, and the concept of dispersive gain is introduced. Numerical methods are utilized to design, synthesize, and analyze Brown symbol performance. The theoretical performance in compression and dispersion of Brown symbols is demonstrated and is shown to exhibit significant improvement compared to discrete codes. As a result of this research a process is derived for the design of optimal mutually dispersive symbols for any sized family. In other words, the limitations imposed by conjugate linear frequency modulated (LFM) are overcome using NLS waveforms that provide an effective N-fold increase in radar unambiguous range.

This research effort has taken a theorem from its infancy, validated it analytically, simplified it algebraically, tested it for realizability, and now provides a means for the synthesis and digitization of pulse coded waveforms that generate an N-fold increase in radar effective unambiguous range. Peripherally, this effort has motivated many avenues of future research.

15. SUBJECT TERMS

Non-linear Ambiguity Suppression, Mutually Dispersive, Brown Theorem, Linear Algebra, Radar, Ambiguous Range, Digital Signal Processing, Ambiguous Doppler, The Hermit Problem, Orthonormalization, Monostatic Radar, Cosine Taper, Maximally Equidistant, Pulse Coding, Ambiguity Mitigation